EVENT CHARACTERISTICS OF INTRA-SEASONAL CLIMATE CIRCULATIONS

Warren James Tennant

Dissertation submitted to the Faculty of Science,

University of Cape Town

for the Degree Doctor of Philosophy

ABSTRACT

An analysis of rainfall characteristics over the summer rainfall areas of South Africa is done in order to find links between rainfall variability and the general circulation. Seasonal rainfall totals are clearly linked to significant rain days, indicating the importance of evaluating synoptic-scale event characteristics. Rank ordered rainfall characteristics reveal that normal rainfall may be considered as the middle three quintiles, with the outer quintiles representing wet and dry conditions.

The general circulation in terms of atmospheric state (humidity and temperature), moisture and heat transport, and energy exchange - with attention to tropical-extratropical cloud-bands, are central to wet seasons in South Africa. These are generally associated with deep convection that is driven by vertical instability. Transport of moisture into South Africa generally takes place from the east with the Indian Ocean being a major source of water vapour. Although important, fluctuations in moisture transport are not clearly associated with rainfall. This is because moisture is a necessary but not a sufficient condition for rainfall.

Atmospheric dynamics producing rainfall are a combination of disturbances of mid-latitude and tropical origin. These disturbances often initiate the tropical-temperate cloud-band where eddy available

potential energy, generated through surface heating over land, is converted to eddy kinetic energy. It is generally mid-latitude disturbances with stronger vertical shear that are associated with rainfall events. Increased baroclinic activity in the Southern Ocean south of South Africa, as such, is generally associated with dry seasons. During these seasons there is usually a greater amount of available potential energy which strengthens the southern branch of the Hadley Cell. The effect of this is to increase the strength of the subtropical jet through enhanced poleward flux of angular momentum. The resulting increase in baroclinicity in the South Atlantic Ocean then disrupts rainfall over South Africa through the advection of dry air from the west by the vertical-mean wind component.

General circulation models are shown to capture inter-annual variability such that forecasts of regional rainfall, of useful skill at a seasonal-scale, may be made. However, the skill level with regard to daily circulation, restricts their use to the large-scale circulation. Nonetheless, the analysis of rainfall and the links to large-scale circulation, discussed in the thesis, provide information to produce more skilful seasonal forecasts without having to model small-scale features directly. Such forecasts may also include additional information on rainfall characteristics, such as number of rain-days and length of dry spells.

I declare that this dissertation is my own, unaided work,

and that it has not been submitted previously

as a dissertation or thesis for any degree

at any other University.

University of Cape Town, 2002

To my family,

Melanie, Britney and Hannah.

Also in loving memory of my late mom and dad

PREFACE

The general circulation, defined as the time-averaged flow, exhibits a particular variability. Over the last century, many studies have concentrated on this type of variability. However, it is really the daily weather and its associated variability that impacts mankind. This naturally feeds back to the general circulation, altering the large-scale statistics, but characteristics of particular events can become masked when averaged over time. For this reason many studies are moving away from using time-averaged fields to using daily data.

Southern Africa is a region characterized by a high degree of climatic variability, but in recent years seasonal forecasts have not performed as well as expected. This is partly because the global forcing of the region's climate is not as strong as in other areas, such as around the Pacific Ocean. It is also partly because of a lack of understanding of the underlying causes of climate variability in the region.

This study attempts a renewed look into the atmospheric energy cycle and how the large-scale processes cascade down the space- and time-scales to impact South African summer rainfall.

Specifically, the objectives of the study are to:

(i) do a thorough analysis of rainfall characteristics at the daily time scale.

(ii) link these characteristics to various atmospheric states by using multi-variate, non-linear analysis techniques that classify daily fields into various scenarios. This will provide the basis for identifying key elements of the atmosphere system under different circulation modes.

(iii) apply an analysis of the atmospheric energy cycle and evolutionary aspects of the general circulation.

(iv) relate rainfall variability in southern Africa to the general circulation with particular attention to the onset and demise of specific rainfall events.

(v) evaluate the energy cycle of general circulation model simulations to identify the utility of these models in providing skilful seasonal forecast information.

The dissertation is divided into six chapters. **Chapter One** introduces the need for intra-seasonal forecast products and a better understanding of the forcing role of the general circulation on rainfall variability. **Chapter Two** discusses rainfall characteristics and their importance to the seasonal forecasting problem. In **Chapter Three** static associations between the general circulation and seasonal rainfall characteristics are explored. **Chapter Four** continues with the energy cycle, and studies the evolutionary aspects related to wet and dry spells. An evaluation of actual general circulation model forecasts is done in **Chapter Five**, ending with a summary and conclusions in **Chapter Six.**

Sections of Chapters Two and Three describing rainfall characteristics and their relation to the general circulation has been accepted for publication in the *International Journal of Climatology* (Tennant and Hewitson, 2002). The evolutionary aspects of the general circulation, from Chapter four, were presented[1] at the annual conference of the *South African Society of Atmospheric Sciences*[2] in Cape Town, 2001 (Tennant, 2001).

The thesis uses data from the NCEP reanalysis dataset[3], and rainfall observation data from the SA Weather Service database[4]. The General Circulation Model (GCM) output discussed in Chapter Five was obtained from simulations performed for the Department of Arts, Science, Culture and Technology (DACST)

---

[1] Received the award for the most outstanding presentation

[2] http://www.egs.uct.ac.za/sasas/conference2001/

[3] http://wesley.wwb.noaa.gov/reanlysis.html

[4] http://www.weathersa.co.za/climat/historic.html

sponsored innovative project[5] on seasonal forecasting[6]. The GCMs used in this project include the COLA T30 GCM (Kirtman *et al.*, 1997, Tennant, 1999), run on the SA Weather Service Cray-J90 supercomputer, and the Hadley Centre atmospheric model HADAM3 (Pope *et al.*, 2000), run at the University of Cape Town (UCT) on Dec-Alpha desktop supercomputers. Special thanks go to the DACST project team, particularly Mark Tadross, for their support and guidance. Finally, I would like to thank Professor Bruce Hewitson for being an endless source of inspiration and supply of knowledge and ideas. Most importantly, I would like to thank him for his invaluable supervision of this thesis.

[5] http://www.dacst.gov.za/science_technology/innovation/innov_home.htm

[6] http://www.dacst.gov.za/science_technology/innovation/proj23204.htm

CONTENTS

Chapter One

Background

Introduction

Climate variability in southern Africa places a large burden on vulnerable communities whose livelihood is governed by weather conditions. It is estimated that the drought associated with the 1982/83 El Niño event caused damages worldwide of approximately US$8.65 billion (Lamb, 1988, p195). Variability in climate is manifest through fluctuations in rainfall, which is arguably the meteorological phenomenon that has the greatest impact on human activity (Vogel, 2000). However, rainfall variability remains one of the most elusive characteristics of the climate system to predict.

Advances in numerical weather prediction models and available computing power have resulted in a steady improvement of short-range forecasts since 1950 (Haltiner and Williams, 1975; Kalnay *et al.*, 1998). However, skill of seasonal rainfall predictions has lagged somewhat in relation to that of short-range predictions. This is largely because the weather prediction problem has been addressed in order of increasing complexity. Short-range forecasting deals with atmospheric motions dependent on initial conditions while seasonal forecasting is the reverse, where atmospheric motion is determined by lower boundary conditions and is largely independent of initial conditions (Pfeffer, 1960, p9). The main barrier to extended-

range prediction is the fact that the predictability of the instantaneous state of the atmosphere is limited to about two weeks (Lorenz, 1963; Palmer, 1993). It was not until Shukla (1981) showed that time-averaged fields in the ocean-atmosphere system are indeed predictable up to a year that research in the field of seasonal rainfall forecasting began in earnest (e.g., Barnett and Preisendorfer, 1987; Barnston and Ropelewski, 1992; Shukla *et al.*, 2000).

Any successful prediction technique requires two things. First, knowing the characteristics of the predictand, i.e. rainfall in this case. If rainfall and how it varies in both space and time are poorly understood the predictions thereof would be undoubtedly hampered. Second, the processes that cause rainfall variability must be understood. In southern Africa key links between rainfall and various aspects of the general circulation are known, but the reasons for these links are less well understood.

The atmospheric general circulation and subsequent weather are primarily driven by large-scale energy exchanges (Lorenz, 1955). This study approaches the question of possible contributors to climate variability in southern Africa through an analysis of static and evolutionary associations between rainfall and the general circulation.

The primary motivation behind the study is to provide insight that will ultimately benefit the field of seasonal forecasting. With users of seasonal forecasts in mind, the focus of the thesis is on the summer season in the central and northern interior regions of South Africa. This is where the greatest concentration of users of

long-term forecast information in South Africa are found (Klopper, 1999). The area is characterised by summer rainfall and is where most of the country's grain and wheat crops are produced, much of which is exported when agricultural conditions are suitable for sufficiently high crop yields. Maize yields, for example, vary between seasons from less than 1 metric ton per hectare to more than 4 tons per hectare (Levey and Jury, 1996).

Another region of great importance is the southwestern Cape, a winter rainfall area. This region is home to fruit orchards, vineyards and wheat fields, which make up a large part of the produce export market. The area is also a premium international tourist destination. An analysis of climate variability in this region falls beyond the scope of this study, but techniques applied here could be used in future work to analyse rainfall variability in the region.

This chapter introduces the atmospheric data used in this thesis, along with various caveats in using the data. This is followed by a description of the fundamental aspects of the techniques used to analysis the data. Finally, the hypotheses to be tested in this thesis are listed at the end of the chapter.

NCEP Re-analysis Data

The National Centers for Environmental Prediction (NCEP) in association with the National Center for Atmospheric Research (NCAR) have produced a global analysis dataset from 1958 to the present (Kalnay *et al.*, 1996). The major advantage

of these analyses is that the data assimilation process is constant throughout the period. This provides, for the first time, a relatively homogeneous dataset that may be used in analyses, such as in this thesis. The temporal resolution of the data is six-hourly and the spatial resolution 2.5° in latitude and longitude. Parameters include all fields contained in the equations governing atmospheric motion, *viz.* the gas law, thermodynamic, momentum and continuity equations, and various diagnostic fields derived from these equations and generated directly by the GCM.

These data are, unfortunately, not perfect and some concerns, particularly relevant to the southern hemisphere, have been documented. The first is an error in the placement of the Australian Bureau of Meteorology PAOB surface pressure observations for the period 1979 to 1992 over the Southern Ocean[1]. These were shifted by 180° in the analysis. Fortunately, most of the observations were rejected by the quality control routines. The adverse effect of the remaining PAOB observations produced an error that is most notable in the winter season daily fields south of 50° to 60° S. It has been summarized as having doubled the intrinsic uncertainty in the daily fields south of 45°S. This study is concerned with summer season variables and over an area generally to the north of the affected latitudes, so the effect of the error on findings in this study is expected to be minimal. Furthermore, the study concentrates on motion-type (wind) pressure-level data in the mid- and upper-troposphere which are affected less by poor surface pressure observations.

[1] (see http://wesley.wwb.noaa.gov/paobs/paobs.html)

The second, and perhaps more critical, caveat of the re-analysis data involves the period of the data, which extends back to 1958. Before the advent of satellite observations in 1978, the Southern Hemisphere had a serious lack of upper troposphere observations. The main reason for this is that the southern hemisphere has for more extensive oceanic areas relative to the northern hemisphere limiting ground-based vertical soundings. Consequently, the data assimilation system, prior to 1979, had few observations to steer the analyses toward the real atmosphere so the analyses generally drifted toward the model climate.

Once more observation data became available in 1978 the model drift would be reduced. However, Marshall and Harangozo (2000) pointed out that the introduction of new data into a data sparse area can produce a climate jump, thus counteracting the benefit of using a fixed data assimilation scheme. Evidence of this can be found by applying a filter to the reanalysis data using an adaptive filter technique (Zurbenko *et al.*, 1996), and plotting the variance of discontinuities in the filtered data. This is illustrated for a time-series of 300 hPa temperatures averaged over the southern hemisphere (Fig 1.1). A distinct jump in this field around the time when satellite observations were introduced into the assimilation system is clearly apparent. Kistler *et al.* (2001) give a recent summary and review of the various caveats in using the NCEP re-analysis data, with particular reference to the southern hemisphere prior to 1979. Following this evidence, the study has been restricted to the period from December 1979 onwards.

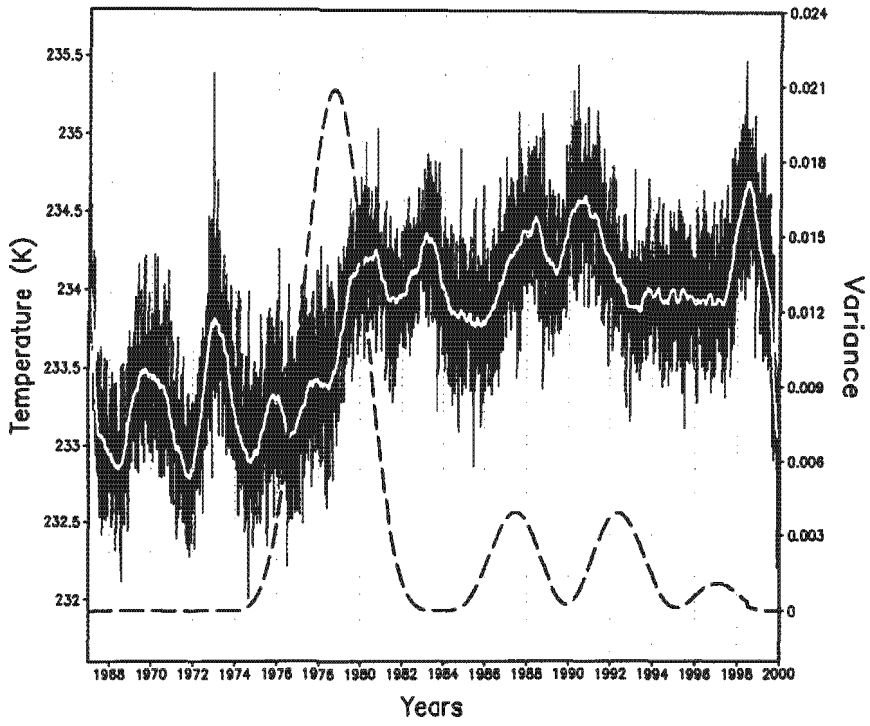

Figure 1.1: Daily series of 300-hPa temperature averaged over the southern Hemisphere from the NCEP reanalysis data. The thick white curve is the time-filtered values and the grey dashed line the variance of discontinuities in the data series.

Techniques Introduced in this Study

Self Organizing Maps (SOM), a technique for reducing the degrees of freedom in atmospheric data by forming arch-types, is used extensively as an analysis tool in this thesis. A comprehensive explanation and discussion of this technique follow.

Initially developed by Kohonen (Kohonen, 1995) at the Helsinki University of Technology[2], SOMs are now used in a broad range of applications. SOMs are a powerful technique to identify dominant modes within the span of a data set, and provides a mechanism for visualizing an array of atmospheric states. The use of this technique for atmospheric applications is somewhat in its infancy but examples of applications of SOMs to meteorology are documented (e.g. Eckert *et al.*, 1996). In other disciplines SOMs have widespread application[3] (e.g. automatic speech recognition, analysis of electrical signals from the brain, and analysis and visualization of large collections of statistical data). A review of SOMs and the application to synoptic climatology is described in detail by Hewitson and Crane (2002).

Essentially the SOM seeks to identify a number of nodes within the given data space such that the distribution of the nodes represent the observed distribution - thus providing a generalisation to few number of archetypes. One could describe the process as a non-linear projection of the probability density function of high-dimensional input data onto a two-dimensional array of nodes. The SOM technique is different from other cluster techniques in that representative points (nodes) are identified effectively spanning the data space. Individual data elements may then be associated with a node. In addition, it offers a powerful means of visualising the continuum of data space.

---

[2] http://www.cis.hut.fi/research/som-research/

[3] http://www.cis.hut.fi/research/som-bibl/

The process begins by initializing the reference vectors of the map using random numbers or in an orderly fashion along a two-dimensional subspace spanned by the two principal eigenvectors of the input data vectors. Upon investigation, it was found that both initialization methods were equally effective. The size of the map is subjective and is chosen according to the generalization that is required. Basically, number of nodes is analogous to the number of clusters in traditional methodologies. Typical sizes range from a rectangular array of 2 by 3 nodes to one of 6 by 8 nodes.

The next stage consists of a two-phase iterative training process where the weight vectors on a node are adjusted toward the training vectors, such that they effectively span the variance structure of the data space. In the first phase the reference vectors of the map units converge to the dominant variance structure of the data. This phase develops the broad mapping of the SOM. The second phase then develops the finer aspects of the SOM array.

During the update process a data element is presented and a winning node identified by the minimum error between the node vector and data vector. The winning node vector is updated maximally and other nodes within the predefined radius of update are updated by an amount proportional to the distance away from the winning node. The learning rate (a measure of how much a node vector is adjusted around each input data sample on each iteration) is taken as the software default (0.05) and the radius of update is the smaller of the SOM array dimensions. During the second phase the learning rate is smaller and the radius of update covers nodes in the immediate vicinity, starting at three. In both phases the learning rate decreases to zero and the radius of update to unity. The result of the training stage

is a two-dimensional map of nodes whose weight vectors span the continuum of data space as represented by the input data.

In the last stage the trained map is now used for visualization of the input data. The program generates a list of coordinates for the best-matching node in the map for each sample in the input data and an associated error (measure of distance between the node in data space and the data sample). Each node's reference vector now represents a particular archetype of the original data, and the node vectors can be plotted as an array of maps. The mapping coordinates for each data element may be used to calculate frequencies of each archetype and the average error at each node used as a measure of the coherence around a node.

A two-dimensional image of the reference vectors (Sammon map) (Sammon, 1995), where the distances between the node image vectors approximate the Euclidean distances in data space, is useful in obtaining an estimate of the spread of the SOM across the data space. It is not desirable to have folds in this image as the physical interpretation of the SOM would become more complex. If the image is too distorted the SOM process may be repeated to obtain a projection of data more suited to visualization. Owing to the initialization procedure a trained SOM is not reproducible, but results are all equally valid.

The utility of SOMs is demonstrated using a step-by-step, practical example, applied to monthly-averaged sea-level pressure fields around southern Africa. The first step is to subjectively choose the number of nodes to represent the range of variability in monthly average sea-level pressure fields. In this example, each of the

four seasons may be supposed to contain three major monthly mean patterns over the course of 20 years (duration of NCEP record used), giving a total of twelve nodes. Next, the nodes were initialized and the monthly data over a 20-year period from 1979 to 1999 applied in the training procedure. The visualization stage followed with a mapping of the input data to the SOM nodes. Finally, a visual representation (sammon map) of the separation of the nodes in terms of data space was produced to ensure that there were no folds in data space and that the array of nodes were spread in a satisfactory fashion.

The SOM, from the example above, is shown in figure 1.2, with the average error associated with each node in figure 1.3 and the spread of nodes (sammon map) in figure 1.4. The SOM distinguishes between cyclonic (right-hand-side) and anticyclonic (left-hand-side) circulation over southern Africa, characteristic of summer and winter respectively. The centre of the SOM shows a set of bridging nodes between these two scenarios, typical of spring and autumn. The sammon map (Fig. 1.4) shows that we have a well-designed SOM with a slight elongation along the horizontal axis, representing the axis of largest variability. This indicates that the difference between summer and winter is greater than the variance within a season. The error map (Fig. 1.3) shows how the summer circulation exhibits a lower variability than the other seasons.

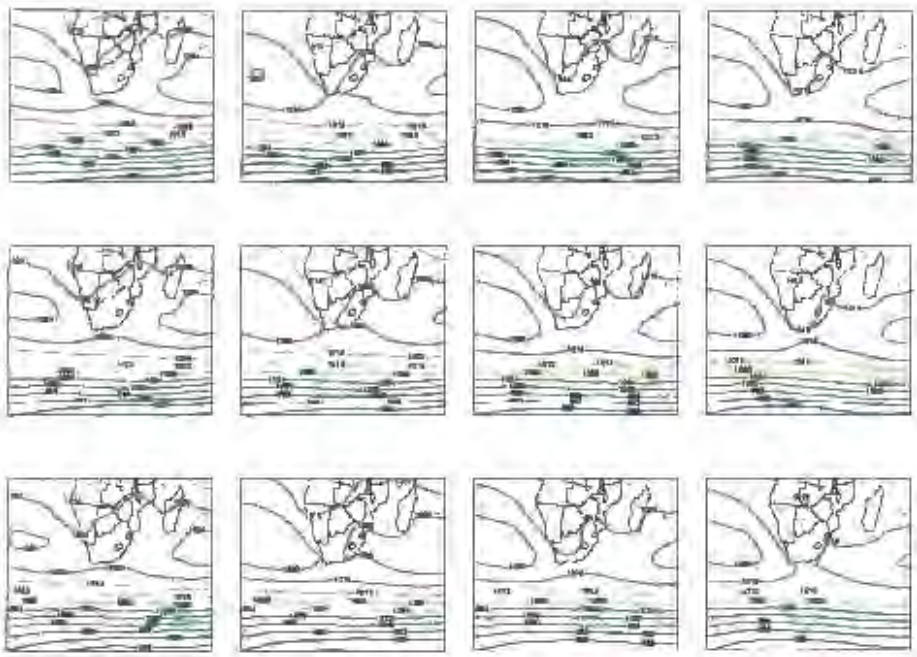

Figure 1.2: A 4x3-node self-organized map of monthly-mean sea-level pressure (hPa) from January 1979 to December 1999.

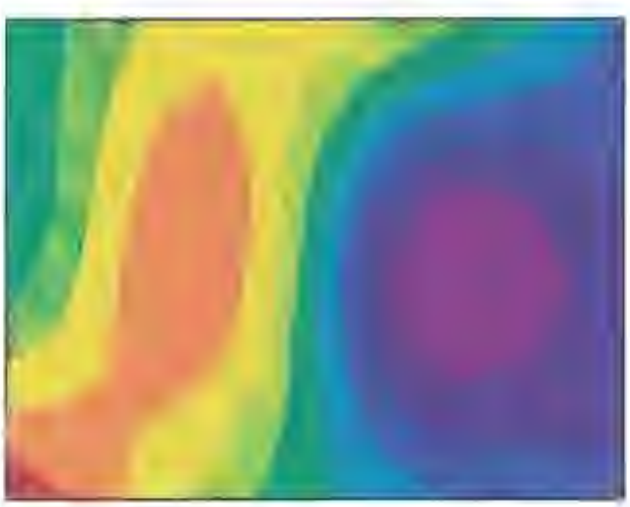

Figure 1.3: 2-Dimensional representation of the average error of the mapping of monthly sea-level pressure fields to the various nodes of the SOM. Red shading indicates large errors and purple shading small errors.

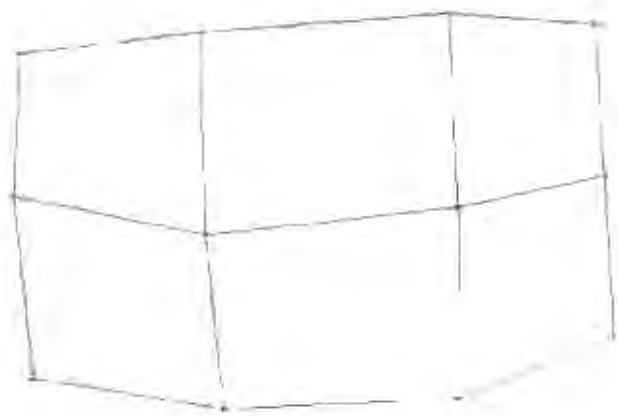

Figure 1.4: Sammon map representing the distances between the SOM nodes in data space.

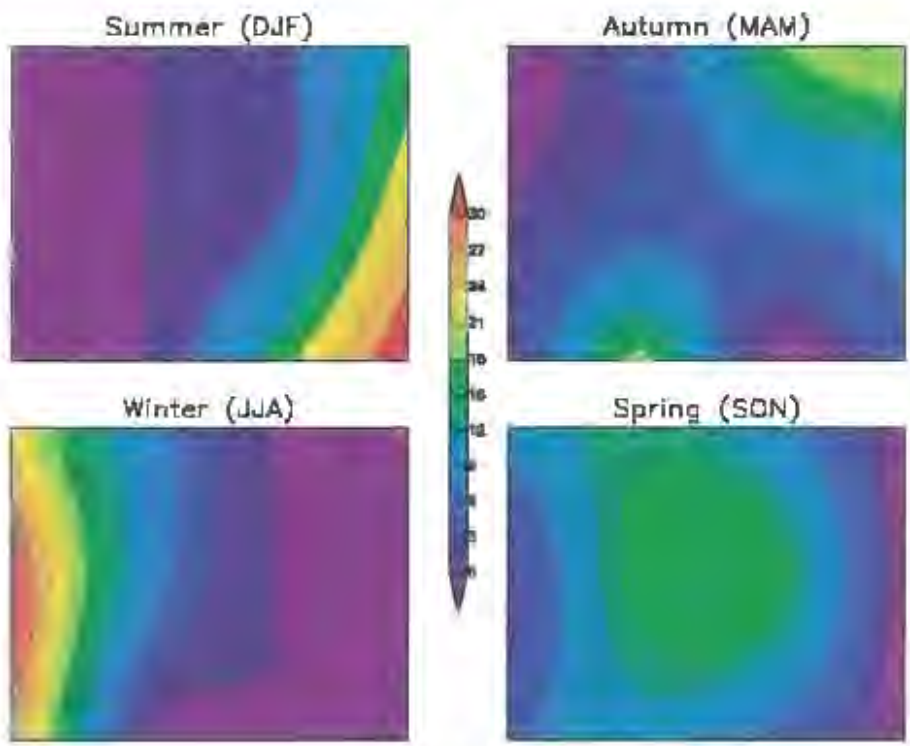

Figure 1.5: Frequency of mapping of monthly-mean sea-level pressure fields to SOM nodes during the four seasons.

A further useful aspect of a SOM analysis is to inspect the frequency of each node for different subsets of the period used in training the SOM, to determine what patterns are more prevalent under those circumstances. For example, the summer months map clearly to the right-hand-side of the SOM, winter to the left, spring to the centre and autumn, with a bi-modal tendency, towards the bottom-left and upper-right (Fig. 1.5). This technique will be applied to identify the types of circulation associated with seasons of different rainfall characteristics.

Hypotheses

The hypotheses to be tested in this thesis are:

(i) that to understand seasonal rainfall one needs to evaluate the sub-seasonal characteristics in addition to season rainfall total,

(ii) that concepts of wet and dry seasons need to be carefully defined within the context of the observed rainfall variability,

(iii) that seasons where rainfall characteristics deviate significantly from normal will be associated with altered frequencies of daily circulation states,

(iv) that the onset of and breaks in rainfall during the summer season in southern Africa are usually triggered by mid-latitude and/or tropical disturbances,

(v) that GCMs are effective in capturing intra-seasonal variability.

Chapter Two

Intra-Seasonal Rainfall Characteristics

Introduction

Predictability studies and forecast model development efforts have extensively sought links between large-scale phenomena, such as El Nino/Southern Oscillation (ENSO), and seasonal total rainfall anomalies in various regions, with South Africa prominent on this list (e.g., Lindesay *et al.*, 1986; Jury *et al.*, 1994; Mason, 1995; Mason, 1998; Jury *et al.*, 1999; Landman *et al.*, 2001). However, work to improve the understanding of the nature and characteristics of rainfall on an intra-seasonal time-scale, particularly down to daily scale, is lacking.

Notwithstanding, a number of studies have investigated intra-seasonal convective variability (Levey and Jury, 1996; Jury, 1999), monthly average rainfall patterns (Harrison, 1984a, 1984b; Taljaard, 1986) and characteristics of specific events (Lindesay and Jury, 1991). Recently, Todd and Washington (1999) have provided valuable insight into daily rainfall variability over southern Africa using satellite products. Their focus was on tropical temperature trough events during the austral summer. However, rainfall variability, particularly in the sub-tropics, is such that seasons with similar rainfall totals can have quite diverse rainfall characteristics. General circulation patterns and teleconnections associated with wet and dry seasons in South Africa are well documented (Mason and Tyson, 1992; D'Abreton and

Lindesay, 1993; D'Abreton and Tyson, 1995; Jury *et al.*, 1996; Mason and Jury, 1997; Tyson and Preston-Whyte, 2000, pp 328-335) but in order to probe more deeply into the mechanisms behind these inter- and intra-seasonal variations a closer look at rainfall characteristics becomes necessary.

Additionally, a study of rainfall characteristics will provide insight into rainfall variability and help improve the range of seasonal forecast products that can be made available. Surveys show that users of forecast information are not only concerned with rainfall totals for the season but would benefit from more detail in forecasts (Sonka *et al.*, 1992), particularly the spread of rainfall over time and space (Vogel, 2000). Levey and Jury (1996) also noted the importance of the temporal distribution and nature of wet and dry spells to agriculture in South Africa. Runoff of precipitation is important in the field of hydrology and this is dependent on a number of rainfall characteristics, *viz.* amount, intensity, concentration of rainfall season and persistence of rain-days (Schulze, 1997). The best way to provide this information is by doing an in depth analysis of rainfall to understand more clearly what one is trying to forecast.

The objectives of this chapter are to perform an analysis of daily rainfall characteristics within the summer season and to show that such an analysis is necessary when seeking a physical meaning for the cause of rainfall variability.

Data and Methodologies

Atmospheric modes

Before calculating and analysing rainfall characteristics it is necessary to determine which months should be used in the analysis. As the focus of the study is on the summer rainfall in the central and northeastern interior of South Africa those months where the atmospheric circulation falls into a particular seasonal mode are sought. A useful way of determining this is to classify daily low-level circulation into a Self-Organizing Map (SOM) and study the frequencies of the various arch-typical states (nodes) month by month. The SOM technique is discussed in detail in Chapter One.

A 7x5-node SOM of twice-daily (00Z and 12Z) instantaneous 925 hPa geopotential heights from 1979 to 1999 was created (Fig. 2.1a) using NCEP reanalysis data. A relatively large SOM, analogous in effect to clustering to 35 cluster groups, was chosen to capture the high level of variability in daily fields. This is comparable to synoptic classification studies in the literature (e.g. Yarnal, 1993). The 925 hPa level was chosen as a compromise between sea-level pressure and 850 hPa heights so that patterns over the oceans remain predominantly characteristic of the marine boundary layer, while over land they are nearer the surface of the inland plateau of southern Africa. The plateau varies from 1000 m in the west to 2000 m in the east and sub-surface parameters such as sea-level pressure are subject to errors of extrapolation. The fewer number of 925 hPa height points over land, relative to 1000 hPa heights, that are affected by extrapolation should have a reduced impact on the pattern of the nodes in the SOM.

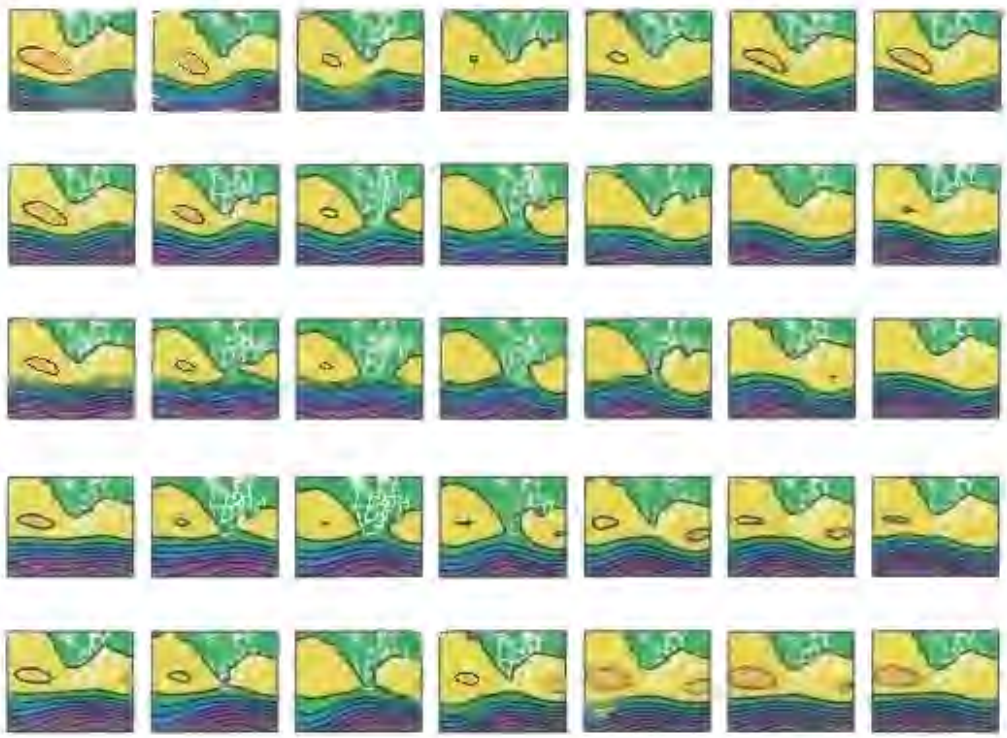

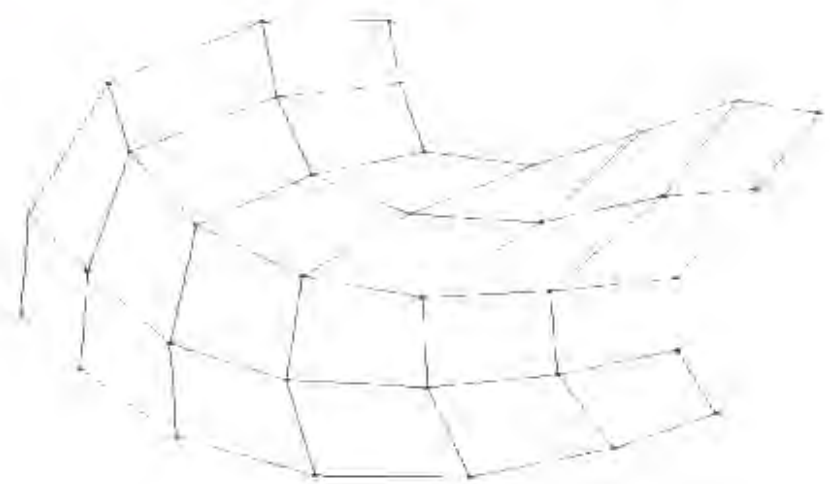

Figure 2.1a: a) Self-organizing-map (SOM) of daily 925 hPa heights from 1979 to 1999 (Top); b) Two-dimensional portrayal of the distances between the SOM nodes (Bottom).

The 35 nodes in the SOM allow for a large number of distinct circulations, however, it must be remembered that the technique is primarily aimed at spanning the continuum of data space, or a low-dimensional representation, rather than trying to cluster groups. Figure 2.1b provides a 2-dimensional representation of the inter-node distances across the N-dimensional data space, showing how the SOM has concentrated nodes in some regions of data space to capture variance structures. These nodes are not equidistant from each other in data space, as their relative distance from one another is still in terms of data space dimensionality, but the figure demonstrates the continuum nature of the SOM nodes. Thus, the frequency of synoptic events associated with the archetype represented by a node may be determined, and contoured across the node surface (bearing in mind the contour map would have the distortion of figure 2.1b underlying it).

The percentage of observations that mapped to each node during the months of October to March from 1979 to 1999 is shown in figure 2.2. It is clear that from December to February a particular type of circulation, located in the left-hand side of the SOM, is dominant. In December there is a residual of systems found predominantly in spring but these disappear from January. From March there is a bifurcation of the type of systems prevalent and again the rainfall can be attributed to systems of different origin and characteristics. To obtain a clear link between weather systems and rainfall characteristics it is best to consider the data for the period from December to February (DJF) when circulation around South Africa has the highest level of homogeneity.

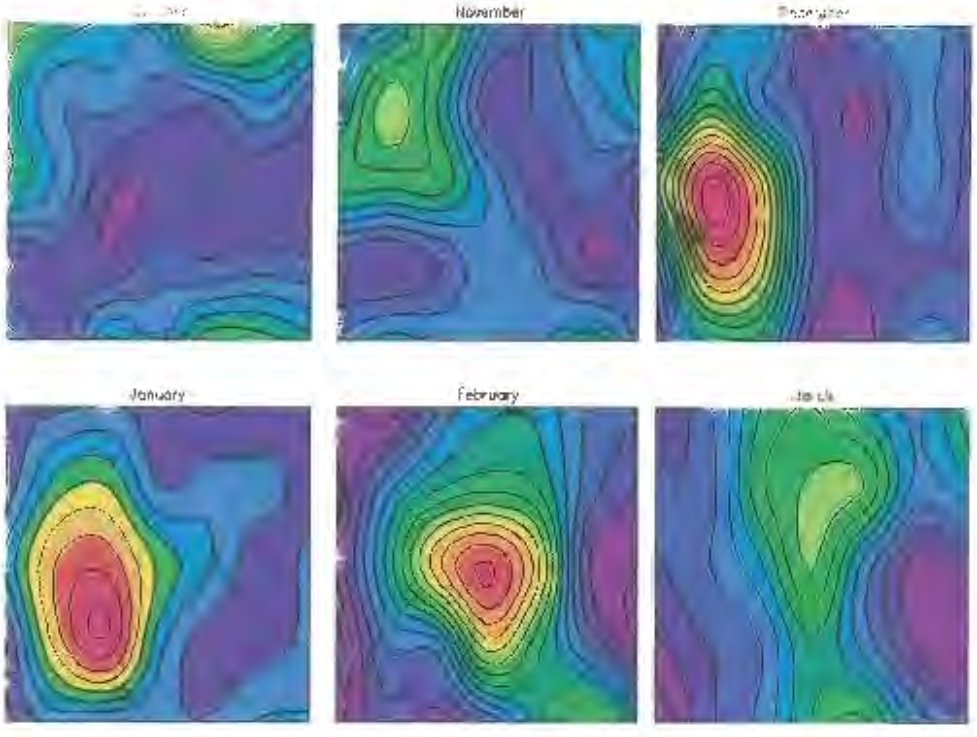

Figure 2.2: Frequency occurrence of each node of the SOM in figure 2.1 for specified months.

Rainfall regions

Rainfall is measured in a number of ways. The most common is using a rain-gauge which measures the accumulated rain that falls at a particular point. These instruments provide readings accurate to 0.1 mm, usually accumulated over 24 hours. The South African Weather Service maintains a rain-gauge network that has included up to 4000 stations during the 1980's. Currently the number is much less, but a set of 510 stations that have a continuous record for more than 60 years has been identified and daily data extracted from 1936 to 1999. The locations of these stations are shown in figure 2.3. There is a fairly even spread of rainfall stations across the country except in the arid northern parts of the Northern Cape Province bordering Namibia, and the Lowveld region in the extreme northeastern parts of the country. The focus of this study is on the central and northern interior regions of South Africa where rainfall station density is satisfactory. Thus, sparsity of station data will not have any undue adverse effects on results found here.

Other ways of measuring rainfall include the use of satellite (Huffman *et al.*, 1997) and radar (Doviak, 1983). These methods provide high-resolution data in both time and space. However, such data are only available for limited areas (in the case of radar data) and for a relatively short period of time (1970s onwards) and are unsuitable for this study which requires a longer period of data to accurately determine observed rainfall characteristics.

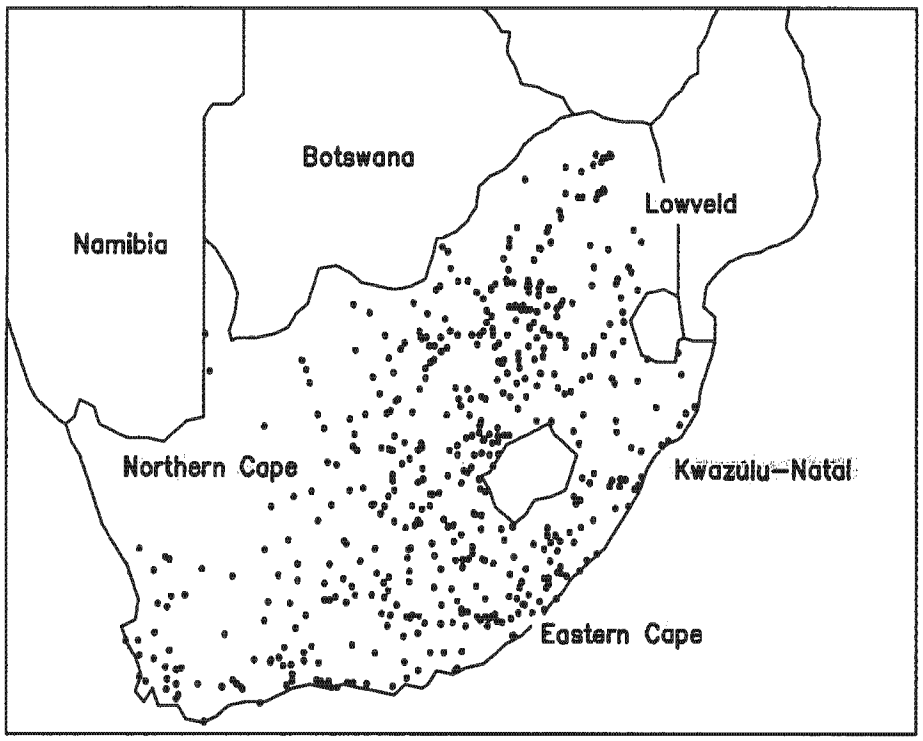

Figure 2.3: Locations of South African rainfall stations with a continuous daily record from 1936 to 1999.

Station rainfall data are only representative of some area of variable size and shape surrounding the rain gauge (Huffman et al., 1997). Such point measurements of a spatially variable parameter can be highly erratic relative to the rest of the area, and be a poor representation of the effect of the large-scale processes. This is particularly true of daily data. To overcome this problem, station data are combined into regions. Other studies have combined station data by creating gridded datasets (e.g. Xie and Arkin, 1996). However, for the purposes of this study where an analysis of rainfall characteristics are sought it is more useful to cluster the rainfall stations into near-homogeneous rainfall regions based on occurrence of rainfall events. In other words, stations that receive rain under similar synoptic weather conditions are

placed in the same region. A similar approach has been adopted by others in the field of seasonal forecasting in southern Africa. (Mason, 1998; Landman and Mason, 1999a). The main difference in the technique used in this study is that the clustering was done on daily rainfall data as opposed to monthly-total data. This is done to better capture the higher-order intra-seasonal variations in rainfall so that individual synoptic situations play a greater role in the clustering process rather than the average circulation for the whole season. Todd and Washington (1999) also noted the importance of a fine temporal resolution in rainfall data to capture associations between specific synoptic conditions and atmospheric circulation anomalies.

There are unavoidable gaps in the daily records of some of the 510 rainfall stations. These were filled using data from neighbouring stations that have the highest correlation to the station with missing data. The substitute rainfall amounts were multiplied by the ratio of the variance of the daily rainfall of the two stations. In this way the adjusted station retained its original climatological variance.

This study is concerned with disaggregating rainfall patterns in the summer rainfall area. First, those rainfall stations where the wettest month did not fall in the period from November to March were excluded, leaving 453 stations. These remaining stations were submitted to hierarchical clustering using Ward's method (Ward, 1963). The distance matrix was calculated using Euclidean distances. Ward's clustering method was chosen because it minimizes the within-group variance at each stage of merging and is based on optimizing an objective statistic. The method is widely used and performed best among the hierarchical methods reviewed by Gong and Richman (1995). The clustering tree (Fig 2.4) shows a clear distinction between

two major groups. The cluster on the left in the tree corresponds to stations in the western interior. These lie outside the area of interest, as described earlier, and were next to be eliminated from the list. The final data-set of summer rainfall stations, totalling 276, were then submitted to a separate cluster analysis (Fig 2.5). These data form four regions with a clear distinction between the coastal areas of the Eastern Cape and Kwazulu-Natal Provinces and the interior regions (Fig 2.6). There is also a sharp contrast between the central interior and the northeastern interior. This contrast will become more evident later.

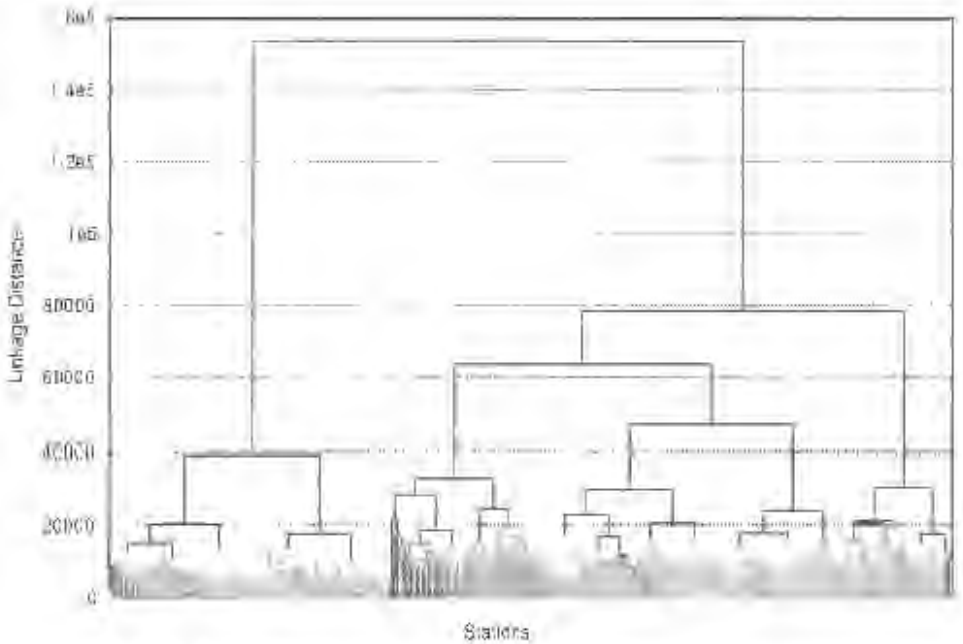

Figure 2.4: Clustering tree of 300 rainfall stations selected from those with the wettest month from November to March.

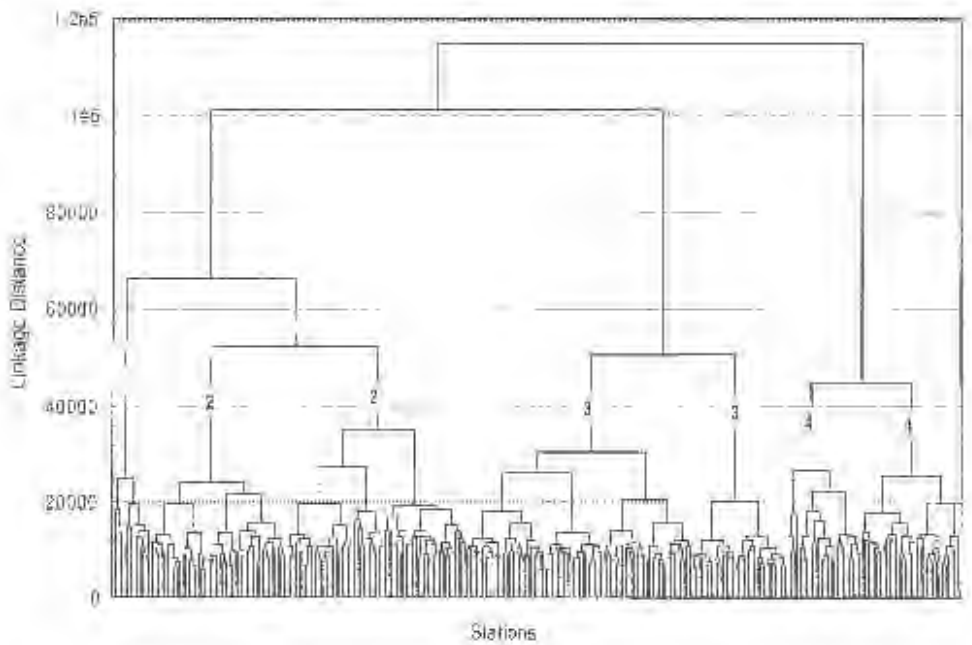

Figure 2.5: Clustering tree of 276 rainfall stations across northeastern South Africa. Numbers on branches correspond to regions in figure 2.6.

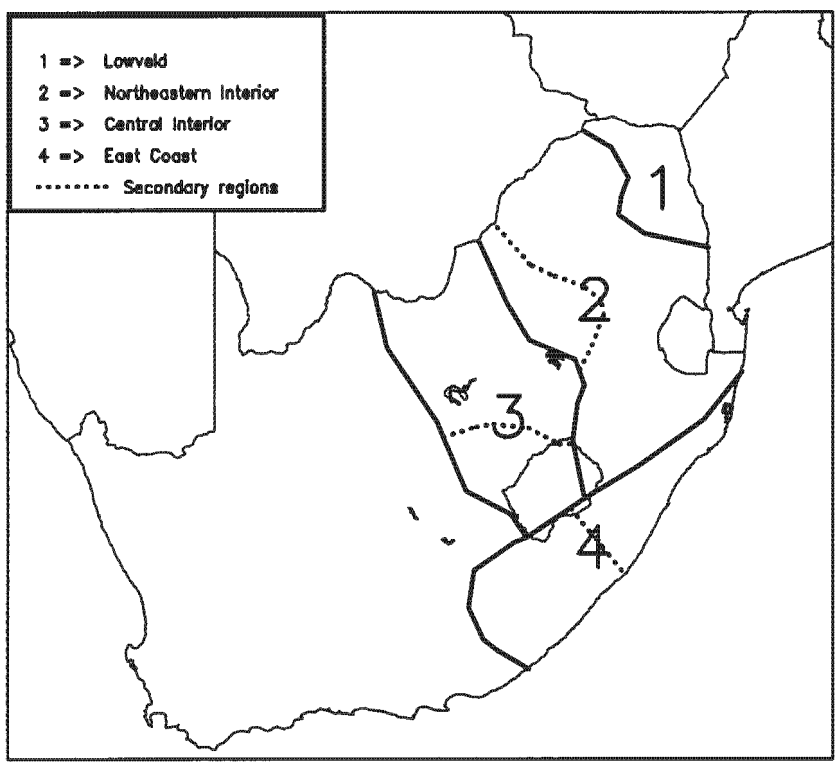

Figure 2.6: Homogeneous rainfall regions determined by cluster analysis of daily rainfall from 276 rainfall stations from 1936 to 1999.

Rainfall characteristics

The next step involves creating season rainfall characteristics for each region. The characteristics to be calculated were chosen to reflect common needs from users of seasonal forecasts. Specifically, nine characteristics for each season are used:

- Region-average seasonal rainfall total
- Region-average of station rain-days exceeding 1 mm and 20 mm
- Region-average of length of period between station rain-days of 1 mm and 20 mm (dry spells)
- Region-average of length of consecutive station rain-days exceeding 1 mm and 20 mm (wet spells)
- Correlation of daily rainfall between stations within each region
- Variance of station seasonal total anomalies within each region.

The figures of 1 mm and 20 mm were subjectively chosen to represent a measurable quantity of rain and a significant amount of rain, respectively. Regional values were calculated from a weighted mean of all station values in the region. The weights were determined from the cross-correlation matrix of the stations by finding the average correlation of each station, in turn, with all the other stations in the region. This process gives less weight to outlier stations and more weight to stations with similar trends, nudging the regional value towards a centroid value.

Station dry spell lengths are calculated as follows: Each day in the season is designated as wet or dry, using the thresholds of 1 mm and 20 mm respectively. Each

series of dry days is given a number equal to the length of the series. For example, three dry days in a row will each be assigned the number three. Wet days are given the value of zero. The sum of the values given to each day in the season is divided by the number of dry days to produce the seasonal average dry spell length. This process gives more weight to longer spells. However, it is justified in that the cumulative effect of a long dry spell and short dry spell is not equivalent to two equal length dry spells that have the same cumulative numerical value. When a dry spell straddles the season boundary only those days which fall in the season of interest are used in the calculation. Regional dry spells were determined from the station values in the same way as the rainfall totals. Dry spells are particularly crucial to agriculture as crops may be destroyed by a hot, dry period despite the seasonal total being favourable. Wet spell lengths are calculated in the same manner as dry spell lengths. Wet spells reflect different atmospheric modes compared to the number of rain-days, in that persistence of a rain-producing weather system is shown.

The eighth rainfall characteristic is the correlation of daily rainfall between stations in a region. First, the correlation of a time-series of daily rainfall between each station and all the other stations in the region is calculated, forming a cross-correlation matrix. This is done for the DJF portion of each year, in turn, over the 63-year period. The average of each correlation matrix produces a regional figure for each year which is used to determine inter-annual variability. This characteristic distinguishes between seasons where rain-bearing systems of large spatial extent (high figure) are predominant and those where rainfall consists mainly of localized showers (low figure).

The final characteristic is the variance of station seasonal total rainfall anomalies within a region. Station total rainfall for the DJF season of each year is first standardised over the full 63-year period. In this way dry seasons at a station will have a negative value and wet seasons a positive value. The variance of the standardised station values within a region is calculated for each year. Low values occur when stations throughout the region record a similar anomaly, e.g. all dry or all wet. If known a priori, this may provide a confidence indicator that can be attached to a forecast based on what proportion of the forecast area will likely experience the category that is forecast. The reliability of post-mortem verification may also be assessed using this characteristic, as station choice can significantly alter the outcome of the verification.

Discussion

In order to classify rainfall data into categories of magnitude and determine what could be considered normal, the time series of data for each rainfall characteristic are ranked by magnitude. One of the first striking features is that the rank ordered data for many of the rainfall characteristics form a s-shaped curve with a slow monotonic increase across the central portion and tails with increasing gradient toward the outer extremes. This is most evident for the seasonal total (thick solid line) (Fig. 2.7) and number of rain-days exceeding 1 mm (thick solid line) (Fig. 2.8) for the northeastern interior (Region 2). The nonlinear pattern in the sorted data suggests that an arbitrary definition of normal, without first studying the rainfall characteristics of a region, would not be suitable. Normal in this sense is used to

indicate a range of rainfall characteristics that do not deviate significantly from the average or median. The normal range is usually broad enough to include at least a third of all outcomes. In the case of Region 2, it appears that the normal category is broader than this and tends towards incorporating the central three quintiles.

Often seasonal forecasting methods are developed for predicting rainfall in equiprobable categories (e.g. Mason, 1998; Landman *et al.*, 2001). The popular tercile approach (three categories) is applied operationally by the Southern African Regional Climate Outlook Forum (SARCOF), and other fora, where consolidated seasonal rainfall and temperature forecasts are compiled using input from National Meteorological Services (NMS) and climate forecasters and is reviewed by Vogel (2000). In the tercile approach the assumption is made that normal conditions are expected about a third of the time and each category has an equal probability of being observed in any given year. However, figure 2.7 suggests that defining the normal category in this approach, results in a rather arbitrary separation of the rainfall data. Preferably, the process of defining rainfall categories should be optimized so that the relationship between rainfall and atmospheric circulation becomes clearer. In this way greater physical meaning can be inferred from the analysis about the cause of rainfall variability.

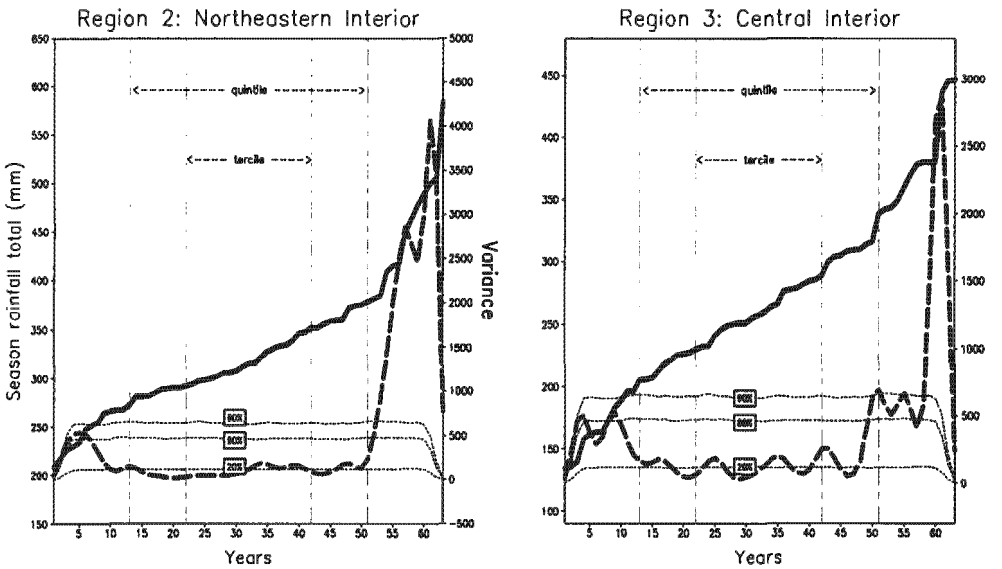

Figure 2.7: Sorted seasonal rainfall total (solid line), variance of discontinuity (dashed line) and significance of discontinuities (dotted line).

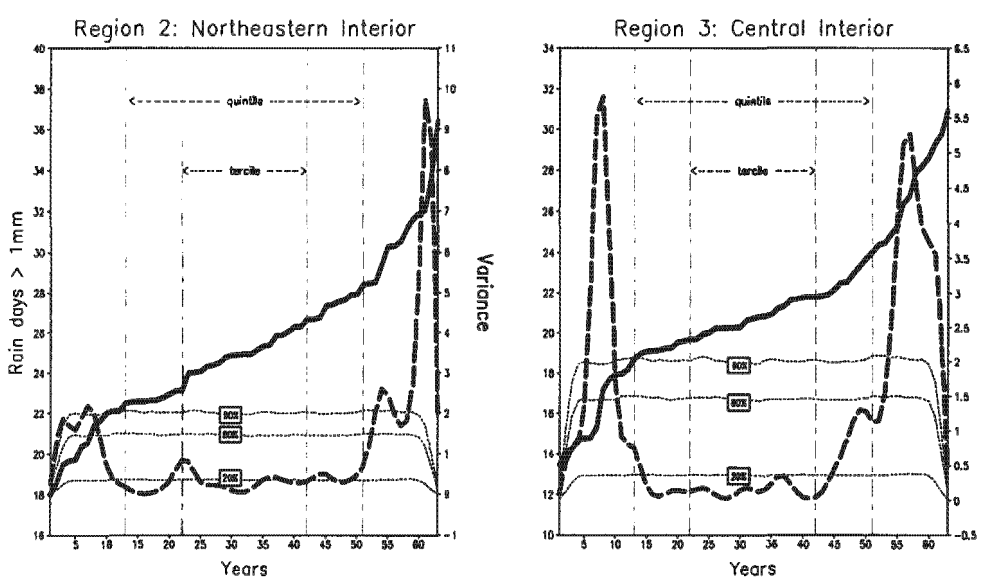

Figure 2.8: As per figure 2.7 but for number of rain-days > 1mm.

In order to test the hypothesis that the central three quintiles best categorize the sorted rainfall data into dry, normal and wet, a number of aspects are investigated. The first is to inspect the range of the DJF seasonal rainfall total for the different categories. In the Central Interior (Region 3), the regional average seasonal total has varied between 134 mm and 446 mm over the 63-year period from 1936 to 1999 (Fig. 2.7). The variation across the middle three quintiles is from 206 mm to 317 mm (35% of the total variation) while the middle tercile ranges from 230 mm to 300 mm (22% of the total variation). For this region and season the middle three quintiles correspond more closely to a third of the variation than the middle tercile does. In the more humid region to the north (Region 2) a similar pattern emerges. Seasonal rainfall totals have varied from 209 mm to 584 mm over the same 63 years. The middle tercile accounts for 18% of this variation and the middle three quintiles account for 32% of the variation.

A more robust method to test the hypothesis is to do an analysis of the discontinuities in the sorted data by using an adaptive filter technique (Zurbenko *et al.*, 1996). This technique has the advantage of being less affected by trend, such as seen in the sorted data. Clearly the largest discontinuities occur almost exclusively in the outer quintiles (dashed line) (Fig. 2.7, Fig. 2.8). The significance of these measures of discontinuity has been testing using a Monte Carlo method. A series of random data, within the same range for each parameter, was generated 10 000 times. A random linear distribution was chosen to simulate an expected linear curve. Discontinuities in the generated data were compared to those in the real sorted data to determine the significance of the observed steps. Discontinuities greater than the 90th percentile were found exclusively in the outer quintiles of both regions for

seasonal rainfall totals and the number of rain-days exceeding 1 mm. Furthermore, discontinuities across the central tercile and the middle three quintiles are constrained mostly below the 20th percentile.

This provides evidence needed to support the hypothesis of defining normal as events within the central three quintiles. The hypothesis is not necessarily true of other regions but a similar methodology, as the one above, could be used to identify the relevant separation of rainfall data for those regions. This approach should provide a more objective way of separating those years where the seasonal rainfall total has a significant deviation from normal. Identification of matching deviations in the ocean-atmosphere circulation system should follow more easily. Such an approach was suggested by Harrison (1983) in a study on the variations of South African rainfall.

Seasonal rainfall totals only form a part of the analysis of rainfall characteristics. In order to broaden the analysis each rainfall characteristic is stratified according to the other characteristics to investigate the relationship between the various rainfall characteristics. This is done by rank ordering each rainfall characteristic, noting the sequence of years, and sorting other characteristics in this order. If two characteristics are perfectly matched, the sequence of years will be identical. A perfect mismatch would reverse the sequence of years.

In order to quantify the level of agreement a score has been developed. The sorted data for each rainfall characteristic is first standardized and then the mean absolute difference between the sorted data and each stratification is calculated and

scaled between -1 and 1 (Table 1 and Table 2). Unity represents a perfect match and -1 a total reverse of the sequence of years. Values near zero indicate little or no relationship between the characteristics. The asymmetry in the matrix is a result of differences in the distribution patterns of each characteristic. The score when stratifying characteristic *a* according to characteristic *b* would be similar but not necessarily identical to the score when stratifying characteristic *b* according to *a*.

Generally the trend emerges where wetter seasons have more rain-days, shorter dry spells and longer wet spells. However, spread of rainfall across a region, both on a daily basis and as a station season total, bears little relationship to the region season total. This is because the spread of rainfall may be fairly uniform under both wet and dry conditions. Among the characteristics the closest relationship exists between seasonal rainfall total and the number of rain-days exceeding 20 mm. An increased number of rain-days exceeding 1 mm, i.e. all rain-days, are also characteristic of a wet season but to a lesser degree. This suggests that wet seasons are made up predominantly of heavier rainfall events rather than numerous light rain events. Harrison (1983) confirmed previous findings that rainfall in the area covered by Region 3 increases with both increasing numbers of rain-days and increasing rain per day.

Table 2.1: Mean absolute difference between each sorted characteristic and that characteristic stratified according to each other characteristic scaled from -1 to +1 for Region 2.

Region 2	Season total	Rain-days > 1mm	Rain-days > 20mm	Dry spells of 1mm	Dry spells of 20mm	Wet spells of 1mm	Wet spells of 20mm	Daily correlation	Season variance
Season total	1.00	0.54	0.84	0.26	0.41	0.49	0.18	-0.04	-0.19
Rain-days > 1mm	0.53	1.00	0.39	0.41	0.11	0.47	-0.01	-0.12	-0.28
Rain-days > 20mm	0.84	0.41	1.00	0.18	0.46	0.44	0.19	-0.07	-0.15
Dry spells of 1mm	0.20	0.29	0.14	1.00	0.16	0.06	-0.27	-0.41	-0.25
Dry spells of 20mm	0.31	0.02	0.41	0.12	1.00	0.07	0.06	-0.27	-0.01
Wet spells of 1mm	0.56	0.50	0.47	0.12	0.21	1.00	0.19	0.08	-0.27
Wet spells of 20mm	0.17	-0.01	0.19	-0.25	0.02	0.15	1.00	0.24	-0.40
Daily correlation	0.00	-0.15	-0.02	-0.39	-0.22	0.05	0.24	1.00	-0.36
Season variance	-0.13	-0.22	-0.07	-0.17	0.04	-0.28	-0.30	-0.34	1.00

Table 2.2: Mean absolute difference between each sorted characteristic and that characteristic stratified according to each other characteristic scaled from -1 to +1 for Region 3.

Region 3	Season total	Rain-days > 1mm	Rain-days > 20mm	Dry spells of 1mm	Dry spells of 20mm	Wet spells of 1mm	Wet spells of 20mm	Daily correlation	Season variance
Season total	1.00	0.68	0.88	0.31	0.30	0.37	0.30	-0.27	-0.09
Rain-days > 1mm	0.69	1.00	0.57	0.41	0.15	0.27	0.08	-0.41	-0.10
Rain-days > 20mm	0.88	0.57	1.00	0.25	0.35	0.38	0.35	-0.21	-0.09
Dry spells of 1mm	0.34	0.39	0.20	1.00	0.33	-0.08	-0.10	-0.46	-0.07
Dry spells of 20mm	0.36	0.15	0.24	0.38	1.00	0.00	0.17	-0.33	-0.09
Wet spells of 1mm	0.39	0.27	0.38	-0.13	-0.02	1.00	0.35	-0.13	-0.37
Wet spells of 20mm	0.26	0.10	0.31	-0.16	0.11	0.36	1.00	0.02	-0.29
Daily correlation	-0.25	-0.30	-0.22	-0.41	-0.25	-0.07	0.05	1.00	-0.45
Season variance	-0.06	-0.01	-0.10	-0.08	-0.12	-0.26	-0.23	-0.49	1.00

An interesting comparison can be drawn between the northeastern interior (Region 2) and the drier central interior (Region 3). The latter region is less affected by tropical air masses and associated weather systems. Wet seasons in Region 3 are more closely tied to an increase in the number of rain-days than in Region 2 (Table 2.1 & 2.2). Furthermore, the amount of rain-days exceeding 1 mm correspond more to the number of rain-days exceeding 20 mm in Region 3 than in Region 2. Whereas, the length of wet spells of at least 1 mm a day are slightly more important as a characteristic of a wet season in Region 2. These all suggest that rainfall in the drier region is heavier in nature, shorter-lived and that an increase in the number of rainfall events is more critical for a wet season in this region. The length of dry spells only shows a limited relationship to seasonal rainfall totals and number of rain-days.

There are several examples of wet seasons with abnormally long dry spells and also seasons with a high number of rain-days exceeding 20 mm with long dry spells. In 1974 Region 3 experienced the 10th wettest season (349.2 mm) but was the 16th driest in terms of length of dry spells (12.13 days) between rain-days of 1 mm. During 1971 the regional average for rain-days greater than 20 mm, of 6.075 days, was the 6th wettest out of 63 but the length of dry spells on average 11.96 days was the 17th driest. Variability of rainfall is thus not indicative of how wet a season is and conversely a wet season does not necessarily imply suitable rainfall conditions for agriculture. An extreme example of this is when most of the season's rain falls in one short-lived event. Dry spell lengths between 1 mm and 20 mm events also correlate poorly with each other, particularly in Region 2. The same is found with wet spell lengths of 1 mm and 20 mm. This provides evidence that light rainfall events for the region as a whole are not a good measure of heavy rainfall events. A low value for

daily rainfall in the region can also be a result of a poor spread of rainfall among the stations and does not necessarily imply that falls are light locally. In Region 2 there is almost a zero correlation between the number of rain-days exceeding 1 mm and daily station rainfall agreement across the region. These findings can be interpreted to mean that periods when thunderstorms are forced locally by convection are independent to times of organized rain-bearing systems that are forced by the large-scale circulation.

From this discussion it becomes clear that rainfall in the central interior of South Africa (Region 3) is governed to large degree by organized synoptic-scale weather systems which produce more uniformly-spread, heavier rainfall events with a median occurrence of about 21 days per season. Generally, the more these events occur the wetter the season. This is consistent with earlier work by Harrison (1984b) where cloud bands were found to be major individual contributors to the annual rainfall in the central parts of South Africa. Such cloud bands, common to South Africa (Tyson and Preston-Whyte, 2000, pp 212-217) and Australia (Nicholls, 1977; Kuhnel, 1990) are understood to link tropical and temperate disturbances while transporting moisture and momentum towards the pole. When studying the link between rainfall in this region and the general circulation it is best to pay closer attention to transient rain-producing systems.

The northeastern interior of South Africa (Region 2) has a less definite link to transient rainfall systems. Here local forcing appears to play a crucial role and a larger proportion of the seasonal rainfall can be attributed to situations where conditions are marginally favourable for localized development of convective rainfall.

Kelbe *et al.* (1983) noted the importance of topographical features and diurnal wind circulations in initiating deep convection. In regions such as this it becomes important to further separate the circulation classification to include mechanisms that might suppress rainfall. These can include large-scale phenomena such as Hadley cells and the proximity of the inter-tropical convergence zone (ITCZ). The greater disparity between station rainfall in this region is a factor to consider when searching for explanations of rainfall variability based on large-scale synoptic circulation. Conclusions drawn from pure season rainfall totals about global forcing may be contaminated by aspects of local forcing. The problem may be alleviated by first making a careful study of various other characteristics of the season's rainfall.

Cycles and trends in rainfall data, as such, have limited value in seasonal forecasting, but are useful for determining potential areas for further research into characteristics of rainfall. At a first glance there is a definite drying trend in the rainfall of northeastern South Africa during summer (Fig. 2.9). The regional average has dropped over 30 mm for the DJF season from 1936 to 1998. Rain-days have decreased by four from 27.5 days per season while dry spells have increased in length from 7.8 to 9.7 days. There is also a reduction in correlation between station rainfall on a daily basis indicating an increase in spatial variability. The trend in the seasonal total needs to be taken into account especially when working with only a subset of this period such as when training a statistical forecast model using rainfall as the predictand. The Central Interior does not have such a strong trend in the seasonal total. However, there is a lengthening of dry spells by about a day to 11.5 days (Fig. 2.10). The five-year running mean shows an 18-year cycle that is in close agreement with that described by Tyson and Preston-Whyte (2000, p 113). A qualitative

inspection of a spectral analysis of daily rainfall from 1936 to 1999 reveals peaks at 18 years, 10 years, 3.5 years and 2 years for the northeastern interior (Fig. 2.11). The highest peak is naturally at one year and a relatively short-range peak at 21 days. This seems to correspond to the 20-35 day oscillation in convection over southern Africa documented by Levey and Jury (1996). Similar peaks are found for the central interior but the period from 7 to 11 years appears as a broad region of increased frequency. The largest peaks in the sub-year range appear in the 6-25 day range which are used in Chapter Four as a basis for bandpass filtering in order to examine fluctuations in the general circulation with the goal of improving our understanding of the controls of weather and climate.

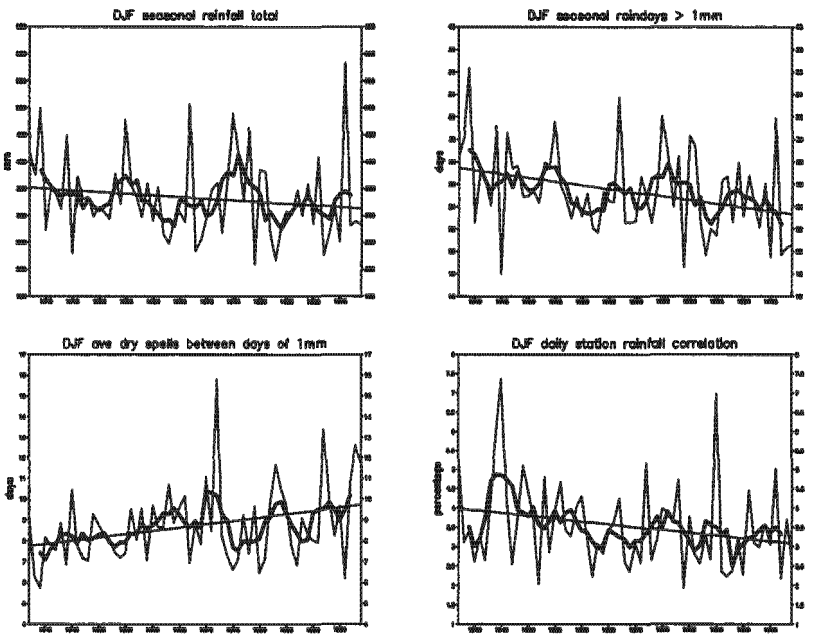

Figure 2.9: Trend of rainfall characteristics for the Northeastern Interior (Region 2) with 5-year running mean.

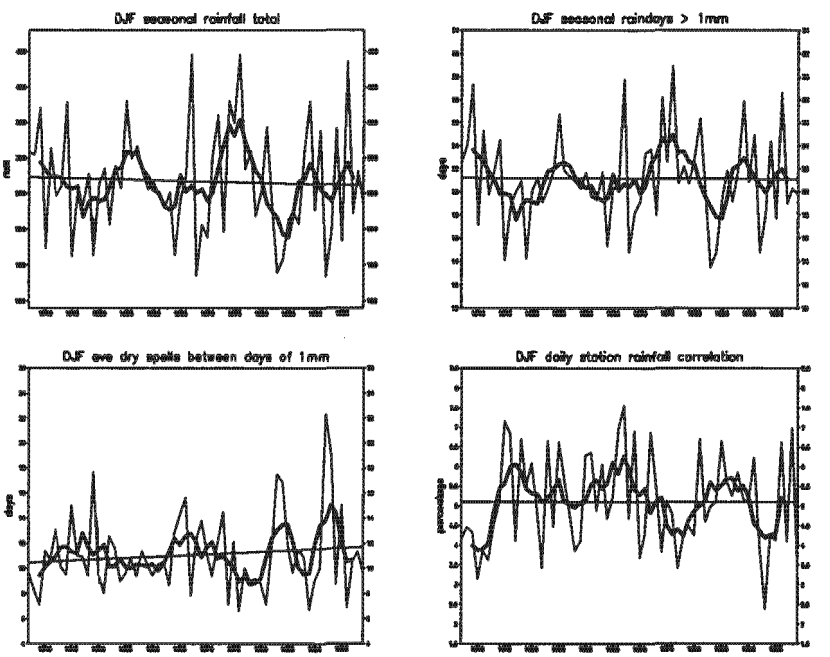

Figure 2.10: Trend of rainfall characteristics for the Central Interior (Region 3) with 5-year running mean.

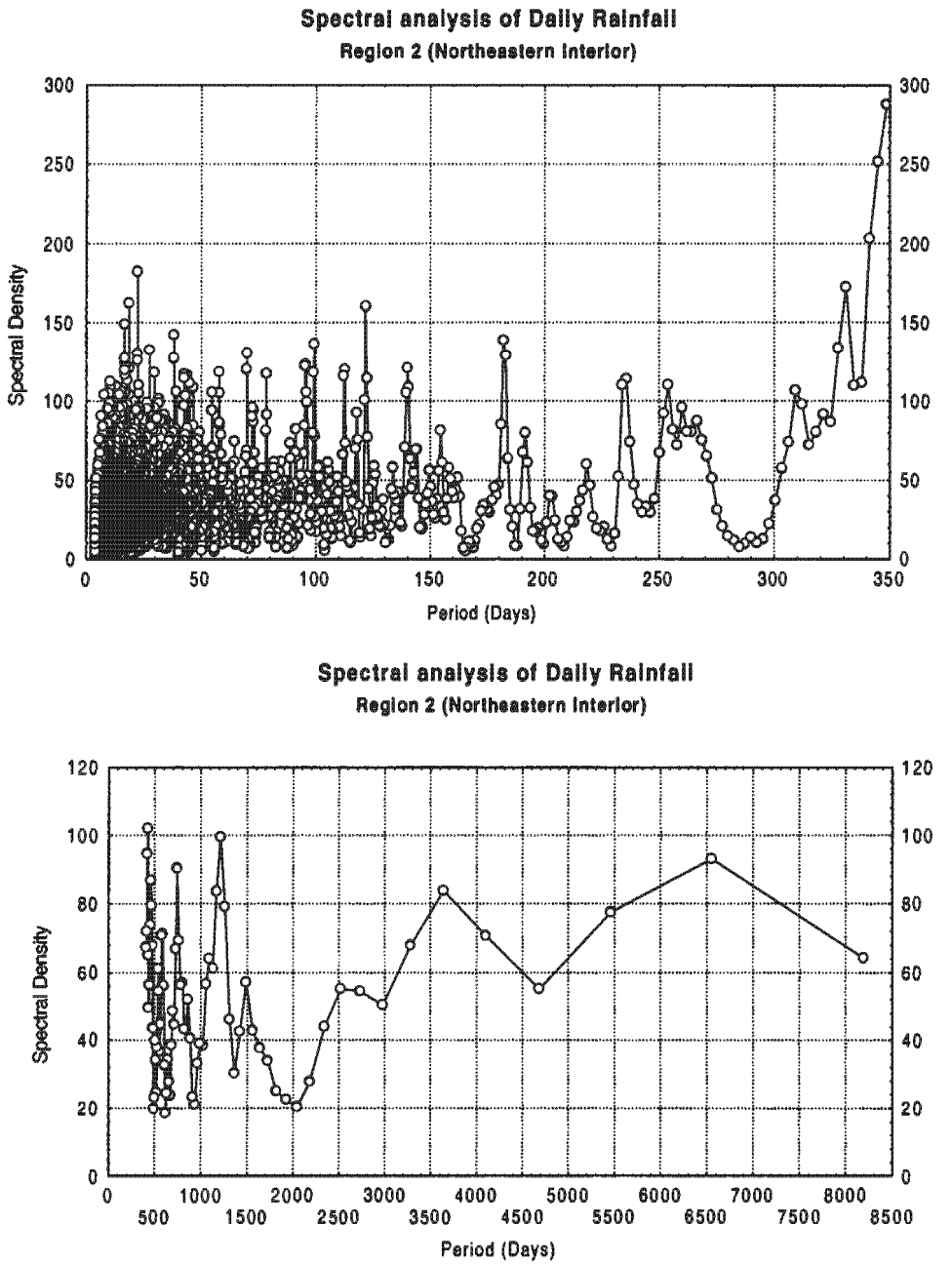

Figure 2.11: Spectral analysis of daily rainfall over 63 years from 1936 to 1999 for the Northeastern Interior (Region 2) 1 to 350 days (top) and 1 to 20 years (bottom).

Summary

The chapter has laid out a basis for delineating the summer rainfall season, and how daily station rainfall data is processed into regional data. Nine different seasonal characteristics have been calculated in order to better understand rainfall and its variability over the summer rainfall areas of South Africa. The change in the climate and synoptic forcing between the central and northeastern parts of the country is evident when comparing the rainfall characteristics of the two regions. It has also become apparent that defining a normal category requires careful attention, especially when attempting to link rainfall variability to the general circulation. In this application it was found that the middle three quintiles best describe normal for the rainfall regions discussed. Boundaries of this category coincide with discontinuities in sorted rainfall characteristics and statistics of the daily states, such that operational seasonal forecasts may include information about various seasonal rainfall characteristics.

Chapter Three

Static Associations between Rainfall and the General Circulation

Introduction

Relationships between synoptic scale atmospheric features and a relatively local scale response have a long history, and have become semi-formalised under the term "synoptic Climatology". Starting from Lamb's (1950) weather types, the methodological approach has become well developed, and is comprehensively reviewed by Yarnel (1993).

Analysis of atmospheric data containing a large number of variables commonly requires reducing or grouping the data into a smaller set of new variables that still represent the original data. Many useful techniques exist to do this. Foremost amongst these applied to atmospheric data are Empirical Orthogonal Functions (EOFs). Introduced in the 1950s (e.g. Lorenz, 1956; Kutzbach, 1967), EOFs have become popular in the atmospheric sciences. A review of the early work and the physical interpretation of EOFs is given in North (1984) and Richman (1986). Practically, when dealing with empirical meteorological data the concept of EOFs is the same as Principal Component Analysis and eigenvectors of a covariance matrix (Rinne and Karhila, 1979).

Classification of synoptic or circulation types has also being done in numerous studies since the 1950s. For example, Streten and Pike (1980) used circulation indices to study monthly patterns of southern hemisphere surface circulation during the First Global Atmospheric Research Programme (GARP) Global Experiment (December 1978 to November 1979). Huth (2001) used the classification of circulation patterns to study trends in climatic elements over Europe. More recently, artificial neural networks have also emerged as a powerful method in data analysis. Initially applied to other disciplines, its popularity in climatology has escalated (Hewitson and Crane, 1996).

The previous chapter highlighted the importance of rainfall characteristics, in addition to the simple season total rainfall, when studying the relationship between rainfall and the larger-scale circulation. The complex non-linear interaction between the various scales of motion and various meteorological parameters, such as temperature and moisture, make the detection and understanding of the controls of rainfall a non-trivial task. For this reason it is felt that the Self Organizing Maps (SOMs) method (Hewitson and Crane, 2002) is ideal for determining independent modes (or archetypes) within daily meteorological data. SOMs have the advantage over other techniques in forming nodes that closely resemble reality while spanning the full continuum of data space. One of the greatest assets of SOMs is the powerful means it offers in visualization of data. The method was introduced and discussed in Chapter One.

The objective of this chapter is to link identified modes within the atmospheric circulation, at a daily scale, to rainfall characteristics. Emphasis is placed on seasons

of marked rainfall deviation from normal. SOMs of various meteorological parameters including distribution of moisture, vertical temperature profiles and transport of heat, moisture and momentum, relevant to southern Africa rainfall are calculated and analysed. These are tied together with a discussion of seasonal-mean composites of the same.

Data and Methodology

The availability of the 6-hourly NCEP reanalysis data essentially provides a mammoth list of parameters and combinations thereof that can be input to the SOM analysis. However, the selected parameters must represent the concepts of atmospheric state and transport in an objective way. In this study the distribution of moisture, in the form of relative humidity and precipitable water, and vertical stability are used to represent atmospheric state. Vertically integrated transport of moisture, momentum, and heat is also considered.

The Helmholtz theorem states that the horizontal wind vector V can be split into non-divergent and irrotational components (Shukla and Saha, 1974) as follows:

$$\mathbf{V} = \mathbf{V}_\psi + \mathbf{V}_\chi = \mathbf{k}\times\nabla\psi + \nabla\chi \qquad (3.1)$$

With the vertical component of the relative vorticity ζ and horizontal divergence D calculated from the reanalysis data, the stream function ψ and velocity potential χ are obtained by solving the Poisson-type equations:

$$\nabla^2 \psi = \zeta \text{ and } \nabla^2 \chi = D \tag{3.2}$$

An advantage of the stream-function and velocity potential is that the same weight is given to perturbations in the wind fields and kinetic energy at any latitude (Kidson, 1999), whereas geopotential heights will be biased towards the mid-latitudes where gradients are an order greater. The stream-function may also be defined in the vertical plane to depict large-scale meridional circulations as a function of latitude (φ) and height (p). In this case it is defined as:

$$\Psi(\varphi, p) = \frac{2\pi a \cos(\varphi)}{g} \int_{p}^{p_s} [\bar{v}] dp \tag{3.3}$$

where $[\bar{v}]$ is the zonal average of the seasonal-mean meridional wind and $\mathbf{p_s}$ surface pressure.

Vertical levels used are the boundary layer ($\varphi = 0.995$) and above-ground pressure levels at 1000, 925, 850, 700, 600, 500, 400, 300, 200, 150 and 100 hPa. Calculations involving moisture are only done up to 300 hPa. Vertical integrals are calculated in the pressure coordinate system using the trapezoidal method (Ellis and Gulick, 1986),

$$X_{INT} = \frac{1}{g} \int_{p_s}^{p_t} X \, dp \tag{3.4}$$

where **X** is any scalar variable, **p** the pressure, $\mathbf{p_t}$ 100 hPa and $\mathbf{p_s}$ surface pressure.

Horizontal transport of moisture, integrated vertically over two layers *viz.* surface to 700 hPa (low level) and 700 hPa to 300 hPa (upper level), and moist static energy (MSE), integrated vertically from the surface to 100 hPa, are calculated using:

$$\mathbf{Q}_{u,v} = g^{-1} \int q \,.\mathbf{V}\, dp \tag{3.5}$$

$$\mathbf{M}_{u,v} = g^{-1} \int MSE \,.\mathbf{V}\, dp \tag{3.6}$$

$$MSE = (gZ + c_pT) + Lq \tag{3.7}$$

where q is specific humidity, MSE is moist static energy, Z geopotential height, g the gravitational acceleration, T the air temperature, L latent heat of condensation, c_p specific heat of dry air at constant pressure and **V** the horizontal vector wind. MSE is the sum of enthalpy (sensible heat), potential energy and latent energy and has been used in several studies on atmospheric energy transport (e.g. Masuda, 1988; Kann *et al.*, 1994). The first two terms on the right-hand side of (3.7) form the dry static energy and the third term the latent heat energy.

The reanalysis data have been interpolated from the model sigma levels to pressure levels (except the surface layer at sigma=0.995). In the flux calculations this can introduce an artificial mass divergence across the latitude circles (Trenberth, 1991). It is corrected at each time-step by subtracting the divergent component of the vertically integrated wind from the horizontal wind at each level. The same correction method was used by Masuda (1988). Trenberth (1991) suggests using the same method but only for vertically integrated mass flux calculations and not for level-specific calculations.

The vertically integrated mean flow V_m is defined by:

$$V_m = \frac{1}{p_s - p_t} \int_{p_s}^{p_t} V\,dp \tag{3.8}$$

where **V** is the vector wind, **p** the pressure, p_t 100hPa and p_s surface pressure. Following from this definition the wind components at any level can be written as:

$$U = U_m + U''; \quad V = V_m + V'' \tag{3.9}$$

where the double prime denotes the deviation from the vertical mean at each level. The vertically integrated kinetic energy of the mean and shear portions of the horizontal wind are defined as:

$$K_{mean} = 0.5 \times g^{-1} \int V_m \bullet V_m \, dp \tag{3.10}$$

$$K_{shear} = 0.5 \times g^{-1} \int V'' \bullet V'' \, dp \tag{3.11}$$

Where the discussion refers to wet and dry seasons in general, such seasons are defined in Table 3.1. In all cases the seasonal total rainfall for the region lies in the relevant outermost quintile (1 for dry and 5 for wet). Other rainfall characteristics including the number of rain days > 1mm and length of period between rain days > 1mm also lie in the outer quintiles in Region 3. In Region 2 some of these lie in the adjacent quintile, but never with a greater separation.

Table 3.1 Selection of Wet (Shade filled) and Dry DJF seasons (Clear) and associated quintile values of seasonal rainfall total, number of rain days exceeding 1 mm and length of period between 1 mm rain days. Highest quintile = 5 and lowest = 1.

Region 2				Region 3			
Year	Total	Rain Days	Dry Period	Year	Total	Rain Days	Dry Period
1979/80	5	5	1	1980/81	5	5	1
1986/87	5	5	1	1988/89	5	5	1
1990/91	5	4	2	1993/94	5	5	1
1995/96	5	5	1	1995/96	5	5	1
1981/82	1	2	4	1982/83	1	1	5
1982/83	1	1	5	1983/84	1	1	5
1991/92	1	2	5	1991/92	1	1	5
1992/93	1	1	5	1992/93	1	1	5
1994/95	1	1	4	1994/95	1	1	5

Distribution of Moisture

Relative humidity is a variable closely tied to rainfall because it is a function of both water vapour content and temperature of the air. It is an indicator of condensation, which usually leads to precipitation. Summer rainfall over the northeastern interior of South Africa is mostly a result of condensation through deep convection (Harrison, 1984a; Taljaard, 1986). In order to analyse this convection the vertically integrated mean of relative humidity from the surface to 300 hPa was calculated at 12Z for December to February (DJF) from 1979 to 1999. Data for 00Z was omitted to prevent the strong diurnal cycle present in relative humidity from

influencing the analysis. Owing to the highly variable nature of relative humidity a relatively large SOM of 5 x 4 nodes was created using the humidity data. The area chosen covers continental southern Africa from 10°S to 40°S. This latitude range includes synoptic weather systems of both tropical and mid-latitude origin. The longitudinal coverage is from 10°E to 50°E to encompass processes in the oceans around the sub-continent.

The SOM (Fig. 3.1) captures various positions and intensities of the well-documented tropical-extratropical cloud-band (Harrison, 1984b; Todd and Washington, 1999; Tyson and Preston-Whyte, 2000, pp 212-217). This is found in nodes towards the right-hand-side of the SOM. Nodes towards the left represent dry conditions over much of southern Africa. Further distinctions between the top and the bottom are evident on the right-hand-side of the SOM. At the bottom the cloud-band is clearly linked to a west-wind disturbance south of the continent, while at the top the cloud-band is truncated over land (see Tyson and Preston-Whyte, 2000, pp 212-217). The Inter-Tropical Convergence Zone (ITCZ), another important climatological feature, is stronger and displaced further south towards the right-hand-side of the SOM.

Each day used in creating the SOM maps to a single node. This mapping may be used to calculate the frequency of occurrence of each node in the SOM. For example, the node in the bottom left-hand corner has 108 out of 1805 (6%) days mapped to it while the adjacent node to the right had 71 (4%) of the days mapped to it. When only specific seasons, based on the rainfall characteristics described in Chapter 2, are considered the statistics of node frequency can change. Here, the

relative frequencies of each node for the selected periods are compared to the relative frequencies of the same nodes for the full period. In this way those modes that are associated with particular rainfall characteristics can be identified. This technique can be applied to a SOM of any atmospheric variable and is used throughout this thesis. An example of this technique applied to monthly-mean sea-level pressure data when selecting different seasons is shown in figure 1.5.

Seasons where the number of rain days exceeding 20 mm in the northeastern interior (Region 2) lay in the fifth quintile, are associated with an increase of between 3% and 7% in the relative frequency of the nodes in the right-hand column of the relative humidity SOM. During these two DJF seasons (1990/91 and 1995/96) the daily circulation was skewed towards the pattern of a well-defined cloud-band across northeastern South Africa. Similar investigation of the other rainfall characteristics reveals that seasons with above normal seasonal total rainfall, more rain days, longer wet spells and shorter dry spells in Region 3 are all associated with an increase in the occurrence of this cloud-band. However, in Region 2 the cloud-band is not as clearly associated with an increase in rain-days exceeding 1 mm or an above-normal seasonal total, despite the large increase in the number of rain-days exceeding 20 mm.

SOM node-13 (central column, second row from the bottom) is characterised by a strong gradient in the relative humidity over Regions 2 and 3, possibly linked to the dry-line. These areas of transition are favoured for convective development owing the proximity of both heat and moisture whereas areas to the west are too dry and areas to the east too cool for development (Rhea, 1966; Taljaard, 1996, pp 51-54). Consequently, this node which is present about 5% of the time is also associated with

wet seasons in Region 2 and 3, indicating the importance of the dry line in the summer rainfall over the interior of South Africa.

SOM nodes of precipitable water are not as clearly associated with rainfall characteristics, as is the case with vertically integrated relative humidity. However, there does appear to be a closer association between the SOM nodes of precipitable water (Fig. 3.2) and the SOM nodes of relative humidity (Fig. 3.1). This reveals interesting characteristics about the different types of cloud bands shown in figure 3.1. The truncated cloud-band nodes in the top-right of the relative humidity SOM are related almost exclusively to the right-hand three nodes on the precipitable water SOM. Physically, this means that a truncated cloud-band is associated with the highest levels of precipitable water along the Zambesi River basin. Precipitable water is characteristic of the lower level moisture of the atmosphere and is useful in identifying different air-masses. SOM nodes associated with the cloud-band that is linked to a mid-latitude system are more diverse but there is a clear maximum associated those nodes where a tongue of high precipitable water values extend southward over the Agulhas current (bottom centre of Fig. 3.2).

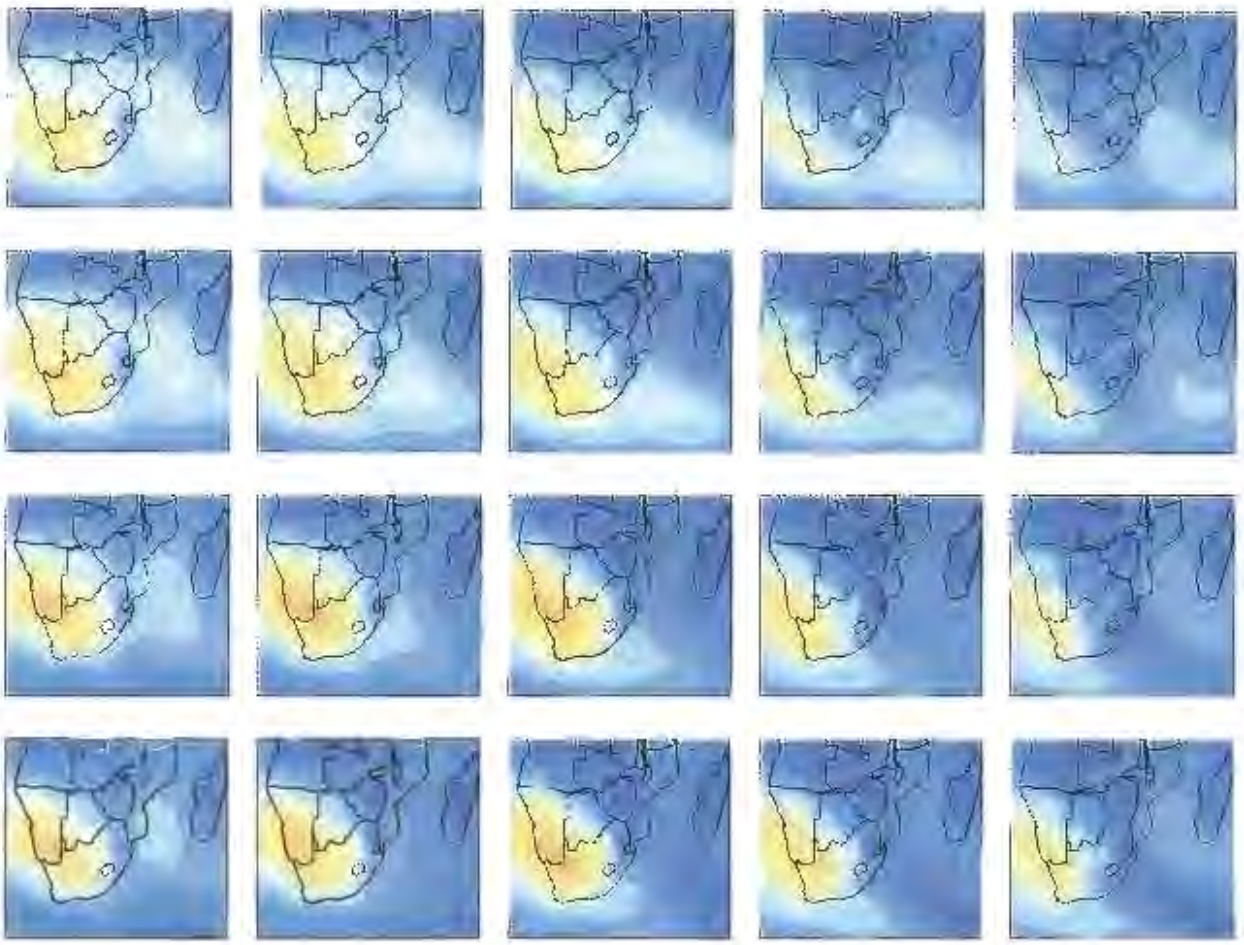

Figure 3.1: SOM of daily 12Z vertically averaged relative humidity. Darker blue colours indicate higher humidity values.

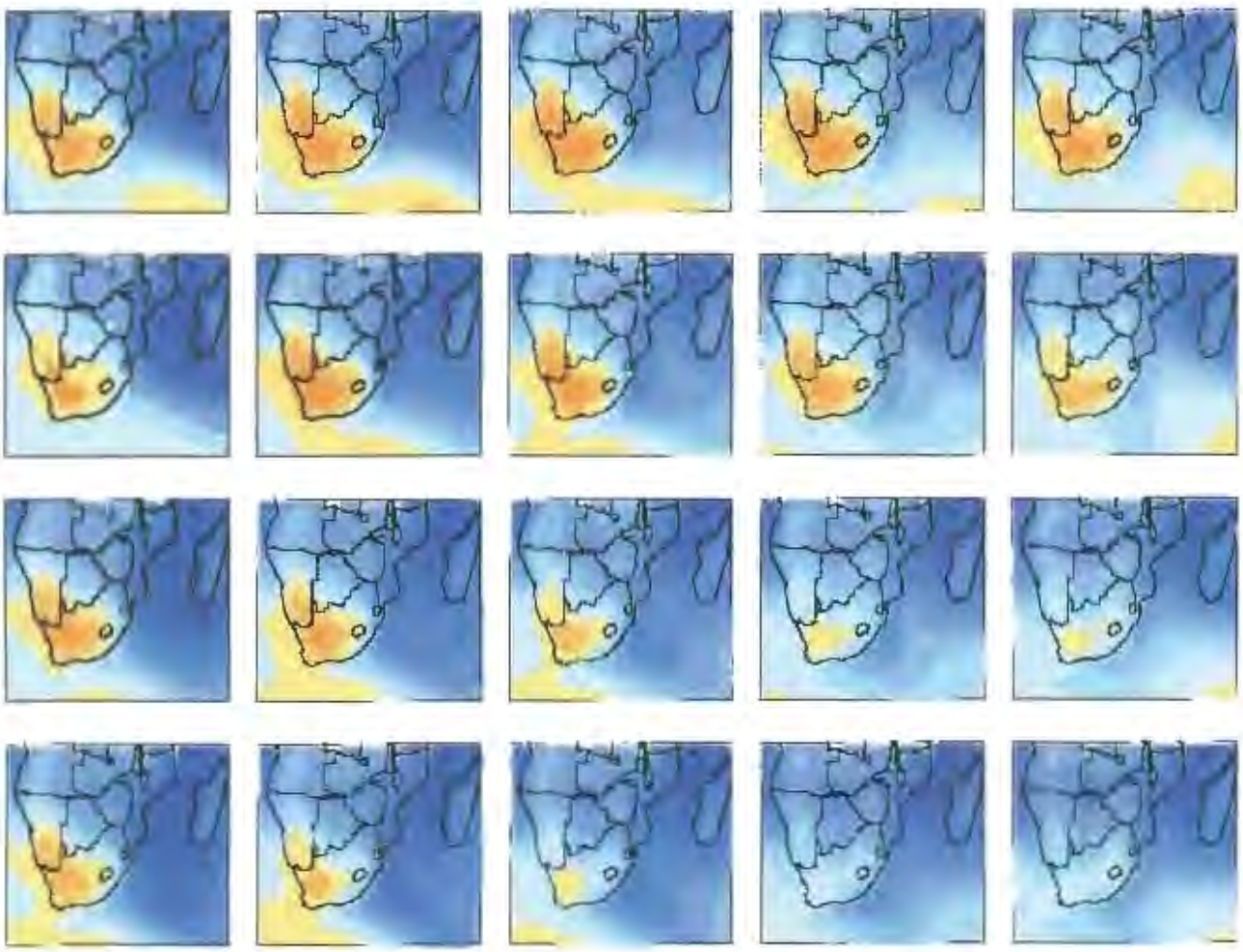

Figure 3.2: As for figure 3.1, but for precipitable water.

Vertical Stability

The role of convection in summer rainfall in South Africa may be investigated further by studying vertical temperature profiles of the atmosphere. Two grid points were chosen for this purpose. The one centred at 25°S 27.5°E to approximate conditions in Region 2 and the other at 27.5°S 25°E for Region 3. It is important to note that the model topography in a spectral numerical model is determined by the resolution of the model, and that the mean height over the grid-point area (Kanamitsu *et al.*, 1991) is represented in spectral form (Sela, 1980). Consequently, as the model resolution decreases the larger the difference between the model topography and that in the real world can become. However, the grid points chosen here lie over the vast interior plateau of South Africa (approximately 1200 metres altitude) such that the model topography, here, closely resembles reality. The error of the reanalysis model is less than 50 metres, so a model grid-point analysis is justified for these two points. The first data pressure level above the ground at both these grid points is 850 hPa.

Near surface ($\sigma = 0.995$) values of temperature and relative humidity were used to calculated the lifted parcel temperature at each pressure level above the ground (Wallace and Hobbs, 1977, p79-80). The dry adiabat (constant potential temperature) was followed to the lifting condensation level continuing with the wet adiabat (constant equivalent potential temperature) up to 300 hPa. The environment temperature was subtracted from the parcel temperature at each level and the 12Z daily profiles were submitted to a 4x3 SOM analysis (Fig. 3.3 & 3.4). A 12-node SOM, such as this, is typically used where only a broad categorization is required. The array of profiles ranges from stable to unstable conditions with various patterns

in-between of low-level or upper-level stability. In Region 2 a low-level inversion is apparent for about a quarter of the time. While low-level inversions are uncommon in Region 3, elevated inversions/stability at about 600 hPa dampen or cap the low-level instability for about half of the time.

Studying the changes in relative frequencies of each SOM node, as used for the relative humidity above, reveal that dry seasons in Region 2 have increased numbers of days with low-level stability. Wet seasons have more days with low-level instability. Prolonged wet spells are associated with the maximum deep instability (beyond 300 hPa). In Region 3 rainfall is clearly associated with deep instability, with wet seasons favouring days in the lower left of the SOM (Fig. 3.4) and dry seasons stable conditions on the right. It is interesting to note that days with the highest deep instability are stable at 850hPa, which is indicative of the dry surface conditions in that area as parcels cool at the dry adiabat until saturated. Furthermore, the relatively stable layer at 600 hPa found in the top left of the SOM is associated with dry seasons despite the profile being unstable in the upper troposphere. A question that arises concerning the stable layers is whether they play an important role in the transport of moisture across the continent. This will be investigated in the next section.

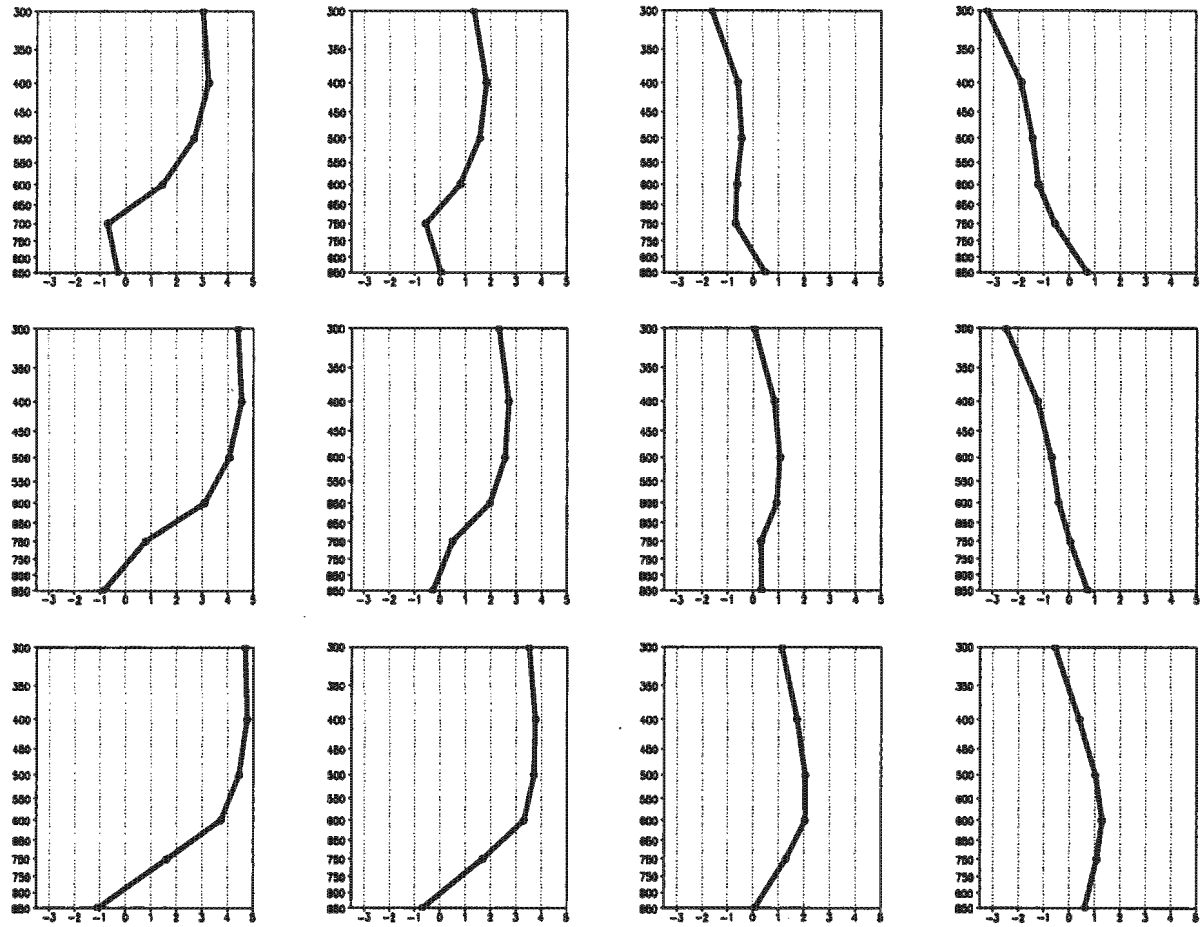

Figure 3.3: SOM of daily vertical profiles of the temperature difference between a parcel lifted from the surface to 300 hPa in Region 2.

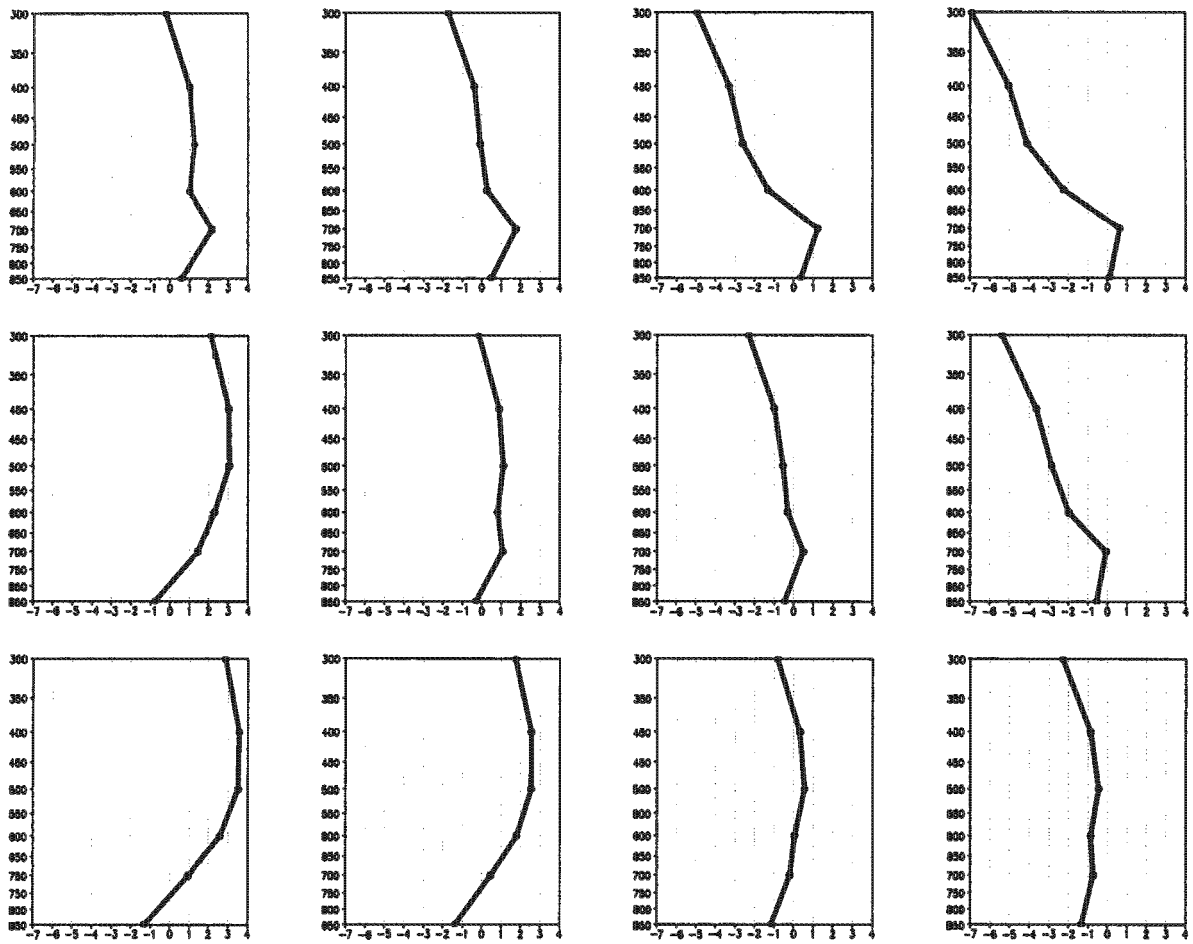

Figure 3.4: As for figure 3.3, but for Region 3.

Spatial maps of surface to 700 hPa instability (low-level instability) were also submitted to a 4x3 SOM analysis (Fig. 3.5) to determine the spatial patterns of instability related to rainfall. Clearly, low-level stability suppresses rainfall in Region 2. The maximum low-level instability in the bottom right of the SOM is associated with longer-lived wet spells and increased heavy rain-days which are fairly widespread. The tongue of instability spreading southward from the tropics, in the top right of the SOM, is associated with increased rain-days > 1mm and appears to have a greater correlation with seasons of above normal rainfall totals than the pattern in the lower right of the SOM. In Region 3 the relationship is simple, the greater the number of days with maximum low-level instability, the wetter the season.

Deep instability, surface to 300 hPa, shows a different array of patterns (Fig. 3.6). Conditions over South Africa during DJF are stable for a greater percentage of the time than for low-level instability. Poor mapping of SOM nodes in the upper right to wet seasons for Region 2 suggests that deep instability on its own is insufficient for above normal rainfall, but rather that normal conditions occur that are characterised by local showers with poor daily spatial coverage. In Region 3 deep instability in the form of a tongue (node in bottom right corner of figure 3.6) is best associated with wet seasons.

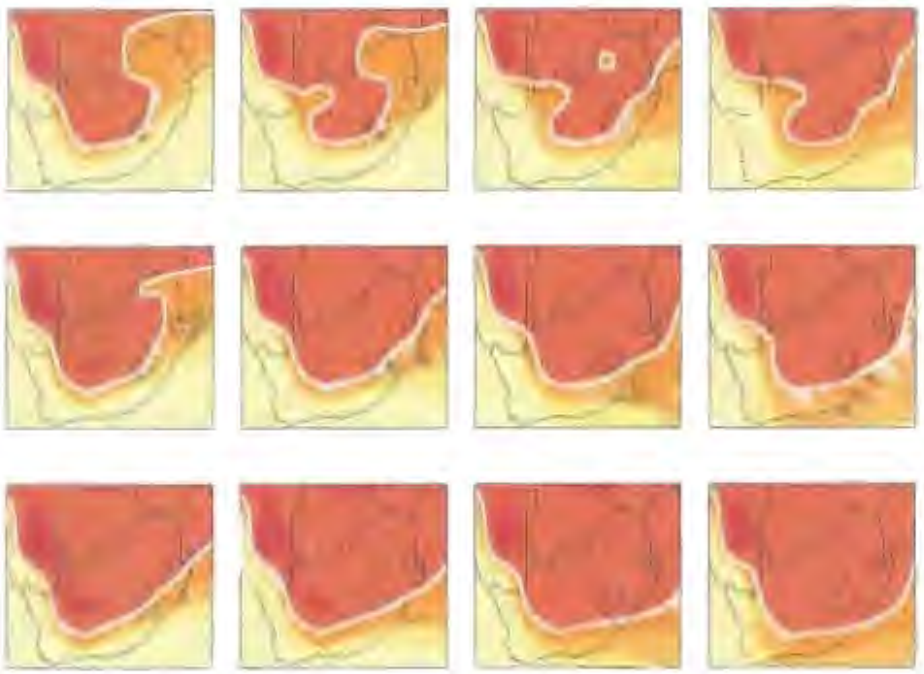

Figure 3.5: SOM of 700hPa stability (lifted from the surface). The thick white line denotes neutral stability and red shading increasing instability.

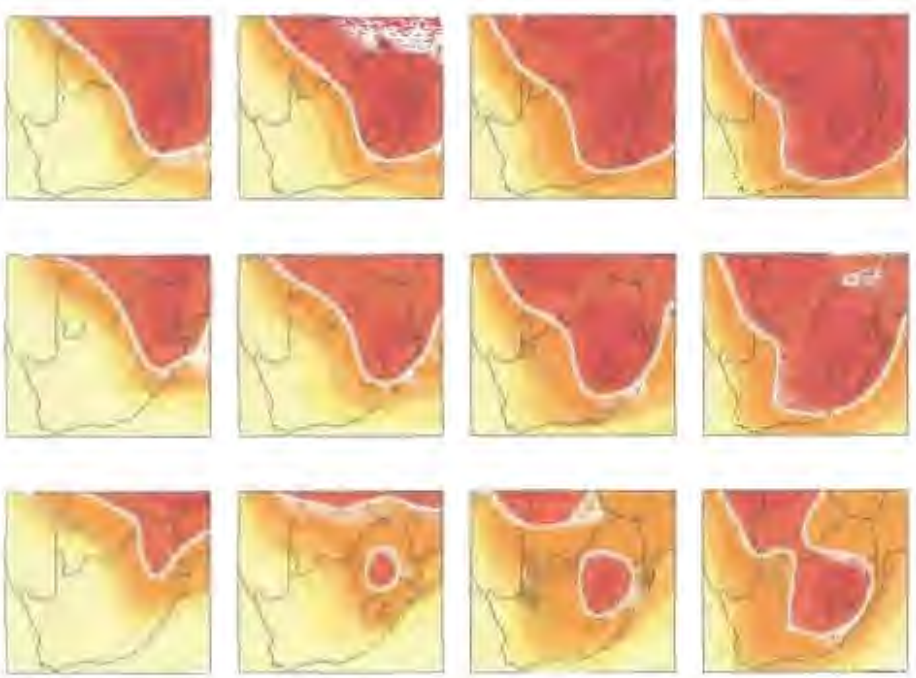

Figure 3.6: As for figure 3.5, but for surface to 300 hPa stability.

Large-scale Transport of Moisture, Heat and Momentum

It has long been recognized that water vapour flux is fundamental to the global hydrological cycle and that fluctuations in this flux can relate directly to droughts and floods (Rosen *et al.*, 1979a). Most of southern Africa is semi-arid and the moisture that contributes to precipitation in the region must be largely imported from elsewhere (D'Abreton and Lindesay, 1993). Potential sources of this water vapour have been identified as the southwest Indian Ocean (Lindesay and Jury, 1991; Levey and Jury, 1996), South Atlantic Ocean (Taljaard, 1986) and the tropical areas of continental Africa (D'Abreton and Lindesay, 1993). More recently, attention has been given to the influence of the Agulhas current on summer rainfall along the southeast coast of South Africa (Jury *et al.*, 1993; Mason, 1995) and over the sub-continent as a whole (Reason, 2001a). This narrow southward-flowing current hugs the east coast of South Africa as far south as Cape Agulhas before dissipating into eddies. A quantification of the importance of this warm current in supplying moisture to interior of southern Africa is still a matter of debate. However, significant positive correlations between SST anomalies in this region and summer rainfall have been established (Mason, 1995). Landman and Mason (1999b) also found a significant link between the sea-surface temperature in the Arabian sea and summer rainfall over southern Africa, particularly in the latter 1990s. This link is possibly manifest in fluctuations in the northeast monsoon, which is part of the northern Hadley Cell over East Africa, during the austral summer.

Twice-daily vectors of moisture flux, vertically integrated from the surface to 700 hPa, over the southern Africa area from the Greenwich meridian to 60°E and 45°S to the equator were submitted to a SOM analysis of 5x4 nodes (Fig. 3.7). In this case a larger SOM is required to capture sufficient features of this variable parameter. Each node depicts an archetype pattern of moisture flux. The arrows indicate the direction of the flux with the magnitude represented by the length of the arrow. Features of the low-level general circulation in this region are apparent in the figure. These include the South Atlantic anticyclone, mid-latitude westerlies with various positions of the transient waves, the Indian Ocean anticyclone and the northeast monsoon over Tanzania.

Areas of convergence and divergence, analogous to sinks and sources of atmospheric moisture, are shaded in blues and reds respectively. Predominantly, the sources of moisture lie over the oceans (red) while sinks of moisture are found over land and over the eastern side of transient mid-latitude troughs (blue). The values of moisture divergence over the Benguela Current appear unusually high for air over this cold ocean current. However, the southeasterly winds in this area are relatively strong which could account for enhanced evaporation and greater divergence of moisture. A second possible source of moisture in this low-level layer is from the upper boundary. Upper-level (700 to 300 hPa) moisture flux archetypes (Fig. 3.8) show a ubiquitous westward transport of moisture, sourced across central South Africa and Namibia, converging over the South Atlantic Ocean. As this air subsides over the Ocean, driven by a mid-tropospheric anticyclone, it could complement the moisture content of the air in the lower levels. In the tropics convergence of moisture extends higher into the troposphere as seen by the blue shading north of 20°S.

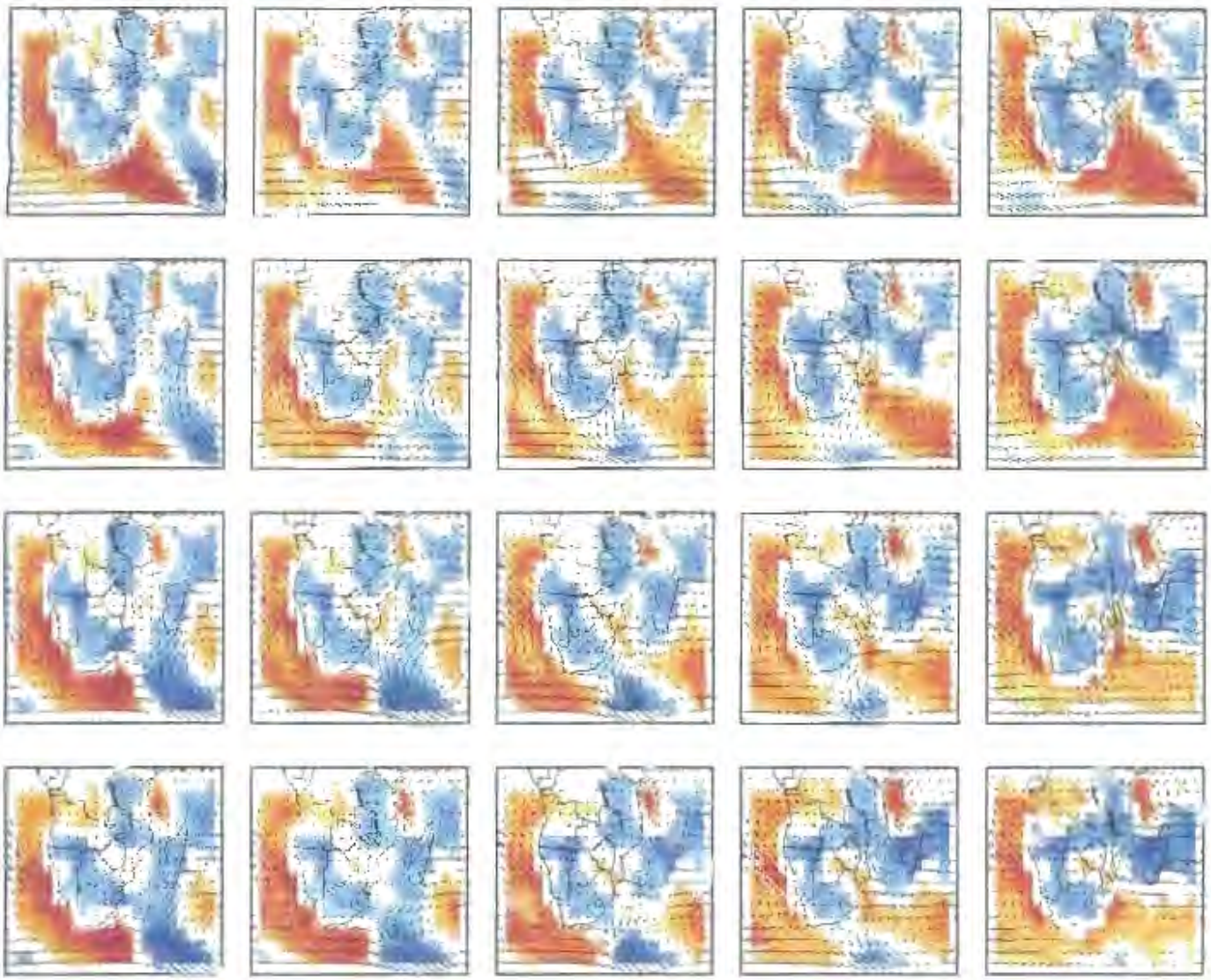

Figure 3.7: Moisture flux SOM sfc-700hPa, reds indicate divergence (atmospheric moisture source) and blues convergence (moisture sink).

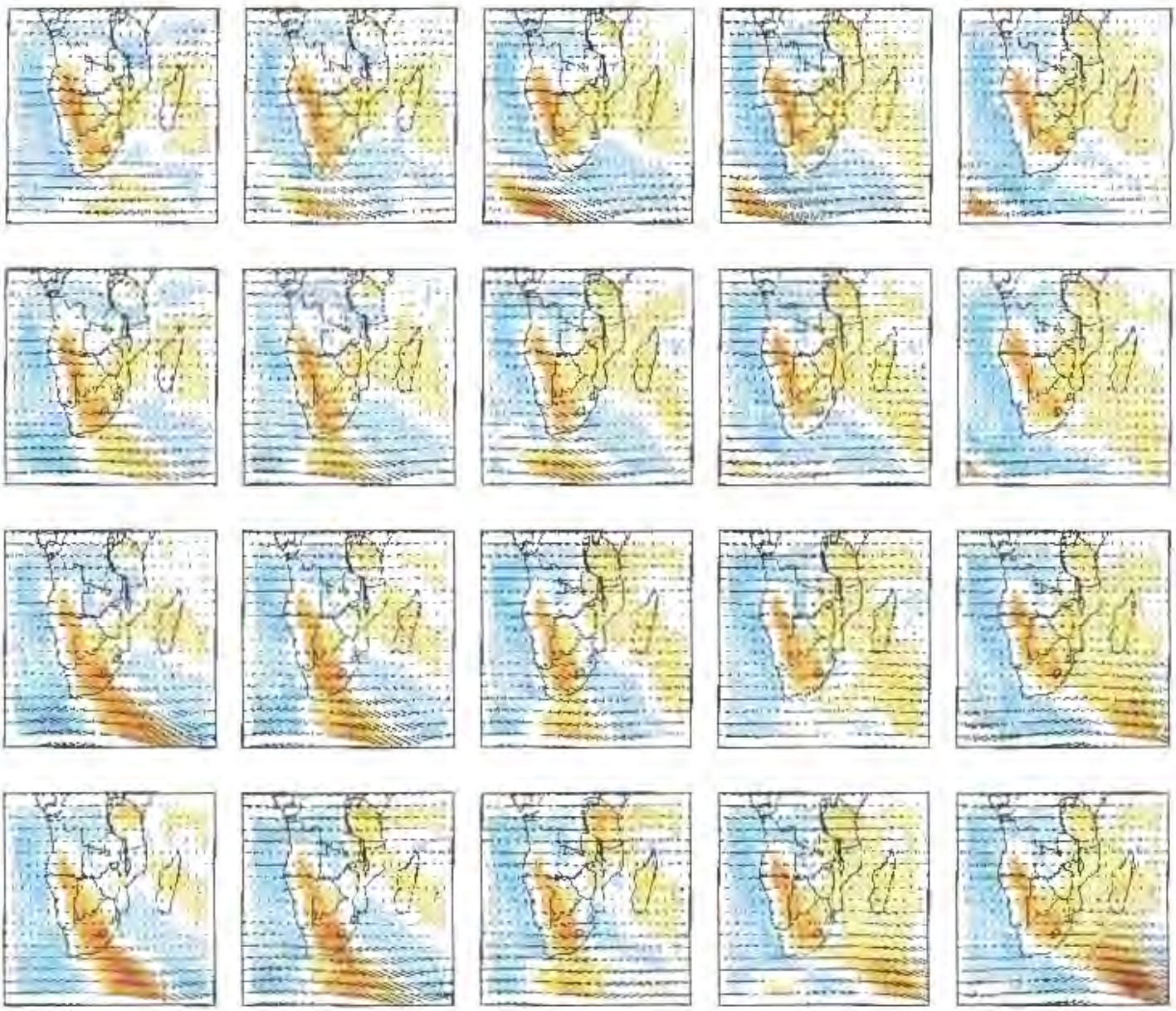

Figure 3.8: As for figure 3.7 but for 700-300 hPa layer

In the previous section the idea of low-level inversions over Region 2, in the northeast, providing conduits for moisture transport into the central interior was raised. Days when the low-level inversion was present on the lifted parcel SOM were related to the different nodes on the low-level moisture flux SOM. However, no definite link between the low-level inversion and low-level moisture flux could be found. In fact, westward flux of moisture over the northeastern parts of South Africa is the dominant circulation mode (about two-thirds of the time) and appears to be independent of inversion layers. This finding may possibly be related to biases in the NCEP reanalysis data, for example, the continental heat low may be too deep and be drawing in too much moisture. However, it is also possible that the perception of stronger moisture flux below the inversion has resulted from limited analysis of the inversion/ moisture flux relation. In both cases the actual moisture flux may be similar in magnitude. Furthermore, low-level easterlies that increase in strength during the evening over the northeastern highveld (Schulze, 1965, p 256) may also play an important role in westward moisture flux. These winds are a local climatological feature largely independent of inversion layers.

The effect of the Hadley Cell and mid-latitude wave activity on moisture flux can be seen in the meridional transport of latent heat (Fig. 3.9). These zonally integrated values for the DJF season are consistent with earlier work by Masuda (1988) and Michaud and Derome (1991). The patterns reflect the low-level circulation as this is where the highest quantities of atmospheric water-vapour are found (Rosen *et al.*, 1979b). In the tropics moisture is transported towards the ITCZ by the trade winds. These winds make up a large part of the time-mean meridional circulation. In the mid-latitudes moisture is transported towards the poles

predominantly by transient systems. The inter-annual variability of meridional moisture flux is demonstrated by showing dry seasons in the central interior (Region 3) in red and wet seasons in blue. On the hemispheric scale the northern branch of the Hadley Cell is stronger in dry years, while mid-latitude wave activity in the southern hemisphere is reduced slightly. Over the African longitudes (Fig. 3.9) the flux during dry years differs from wet years as follows. There is a clear increase in the poleward transport of moisture south of Africa and a strengthening of the low-level inflow of the southern branch of the Hadley Cell. The variations are nearly all associated with changes to the time-mean flow. Changes in the moisture flux north of the ITCZ in Africa appear unrelated to rainfall in central South Africa.

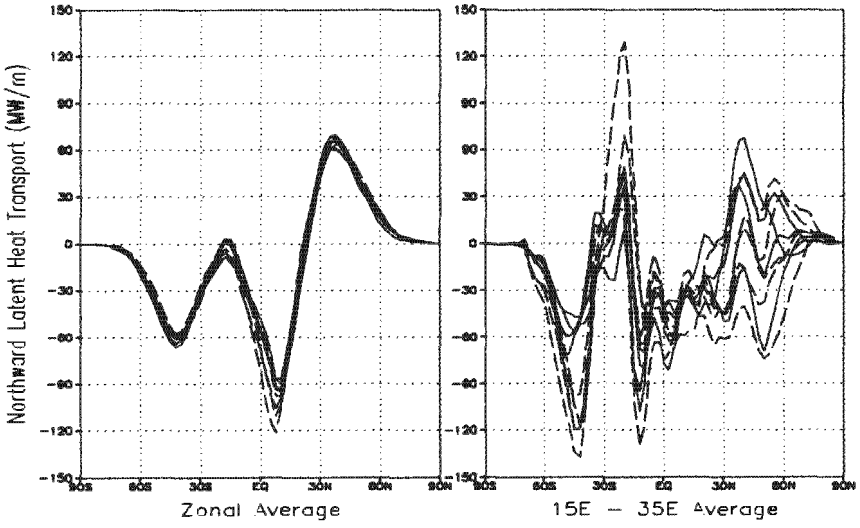

Figure 3.9: Meridional flux of latent heat, zonal average (left) and African Longitudes (right). Blue lines represent wet years and red lines dry years as define in table 3.1.

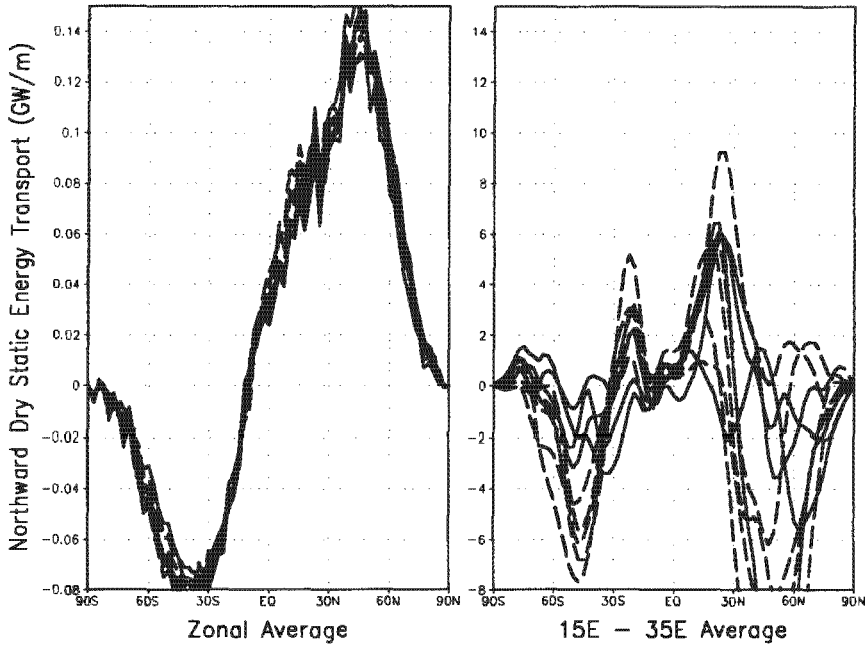

Figure 3.10: As for figure 3.9, but for Meridional flux of dry static energy.

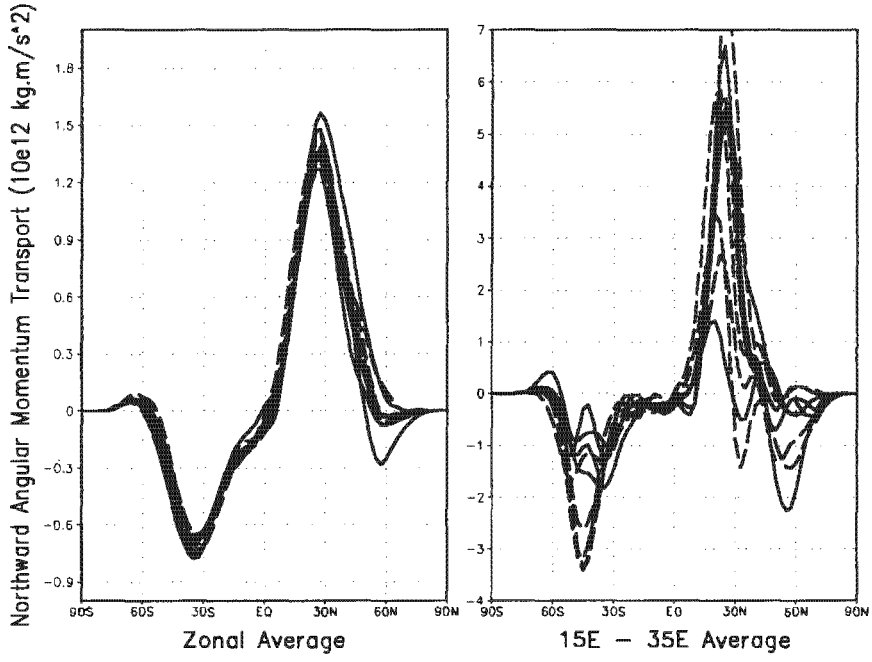

Figure 3.11: As for figure 3.9, but for Meridional flux of angular momentum.

Meridional flux of dry static energy (Fig. 3.10) confirms the increase in strength of the northern branch of the Hadley Cell during dry years, with enhanced northward transport of dry energy, particularly across the equator. In the African sector (15°E to 35°E) the climatological transport of dry static energy is northward between (30°S and 15°S) and southward south of 30°S (Fig. 3.10). In dry years these northward and southward transports are increased respectively. Again these variations are almost entirely due to changes in the time-mean flow. These relationships hold significant value for the climate impacts community and seasonal forecasting, as discussed later.

In order to maintain the westerlies of the mid-latitudes, angular momentum must be transported poleward (Lorenz, 1967, pp 93-96; Newell *et al.*,1972, pp 157-164). This may be understood in terms of the angular momentum budget, which is maintained as follows. The atmosphere gains angular momentum from the earth through the easterly trade winds in the tropics that drag against the rotation of the earth. The Hadley Cells transport this momentum away from the equator in the upper troposphere to the sub-tropics from where it is transport to the the mid-latitudes. The latter transport is achieved through a co-variance of the zonal and meridional components of the wind, where the trough-ridge pattern assumes a northwest-southeast (southwest-northeast) orientation in the southern (northern) hemisphere. Angular momentum is lost back to the earth through surface friction of the westerlies

Zonally integrated momentum flux calculated from the NCEP reanalysis data (Fig. 3.11) is poleward in both hemispheres, peaking at about the 30° latitude. During dry years in central South Africa the transient momentum flux in the southern

hemisphere shifts slightly northward and the time-mean momentum flux associated with the northern Hadley Cell shifts southward. Over the African sector (Fig. 3.11) there is a large increase in southward momentum transport at 45°S mostly in the time-mean circulation component.

Over South Africa itself there is no distinction in meridional momentum transport between wet and dry years. This is somewhat puzzling because wet years clearly have more tropical temperate troughs which have been shown to transport momentum poleward (Harrison, 1984b). In order to determine the underlying reason for this finding, daily fields of angular momentum transport where submitted to a SOM analysis (Fig. 3.12). Frequency of occurrence of each node was then stratified according the nodes of the relative humidity SOM (Fig. 3.1). The nodes of momentum transport are created around varying positions and intensities of the field. The stratification does reveal a clear link between the full tropical-temperate trough cloud-band and a strong southward transport of momentum aligned with the cloud band. It is interesting, however, that the truncated cloud band is not associated with a southward transport of momentum over South Africa. Rather southward transport occurs to the southwest of Cape Town. Seasons may comprise a combination of both types of cloud-band, thus offering an explanation why momentum transport at the seasonal scale does not necessarily relate to rainfall. For example, it may also be that a longitudinal shift in the cloud band will not affect the net momentum transfer over the region, but still have a strong impact on the region's rainfall.

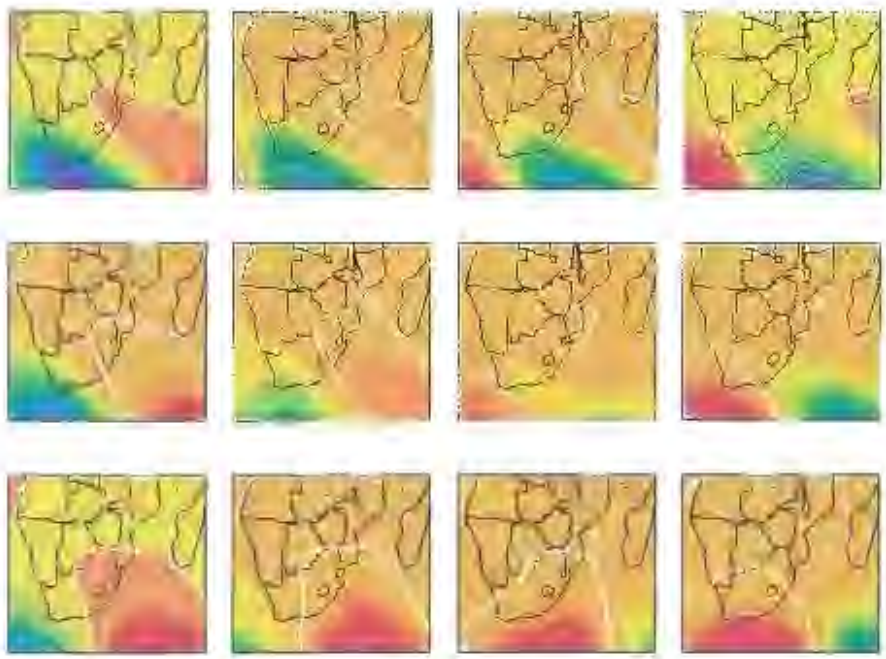

Figure 3.12: SOM of daily fields of vertically integrated angular momentum transport. Red colours indicate northward transport and green-blue colours southward transport. The zero value is indicated by a thick white line. Shading interval is $5x10^5$ $kg.m^2.s^{-1}$.

The results presented in this section on transport of moisture, heat and momentum raise a number of important issues and some new ideas about atmospheric processes in the region. These are re-examined, in context with other results, in the discussion section later in this chapter.

Energy States and Large-scale Circulation

Atmospheric motion is essentially driven by energy cascading from one form to another (Lorenz, 1955). Kinetic energy is the manifestation of these exchanges and is useful in determining different modes of atmospheric circulation. The DJF climatological vertically- integrated kinetic energy for the southern hemisphere from 1979-1999 (Fig. 3.13) reveals that the jet is strongest in the African sector. This suggests that energy conversions in this sector are important on a hemispheric scale and that possible influences of the weather of southern Africa are related to this field.

Eastin and Vincent (1998) used a method introduced by Wiin-Nielsen (1962) to partition the horizontal wind at each level into the vertical mean and shear to study the kinetic energy variability of the sub-tropical jet in the Australian region. Southern Africa is one of three preferred locations of continent-based tropical-extratropical cloud bands in the southern hemisphere (Todd and Washington, 1999; Cook, 2000). These cloud-bands are essentially convergence zones where energy is transported between the tropics and mid-latitudes and should impact these two components of the kinetic energy, perhaps in distinct ways. Wiin-Nielsen (1962), showed that this energy conversion will increase the shear kinetic energy which then maintains the mean flow against frictional dissipation.

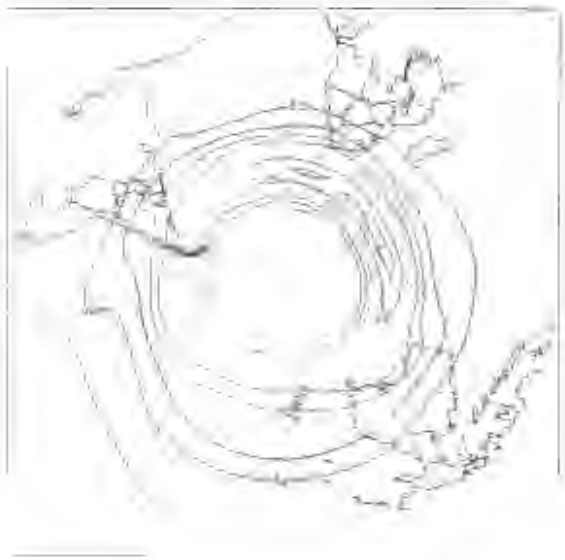

Figure 3.13: Climatological (1979-1999) Total Kinetic Energy of the Southern hemisphere in DJF (10^6 J.m^{-2}).

The kinetic energy of the vertical mean wind and vertically integrated kinetic energy of the shear wind were submitted to a 4x3 SOM analysis. The mean wind (Fig. 3.14) shows a repeating pattern of a subtropical jet between 40°S and 50°S. Each SOM node shows a slightly altered wave-structure to the jet and a longitudinal shift of the core. The strength of the core of the jet is similar to the Australian region (Eastin and Vincent, 1998). The SOM of the shear-component of the wind (Fig. 3.15) shows much greater variability in its structure. Towards the left of the SOM there is a bi-furcation of the shear component of the jet while toward the right there is a single jet. The northern section of the double-jet appears to originate over continental southern Africa.

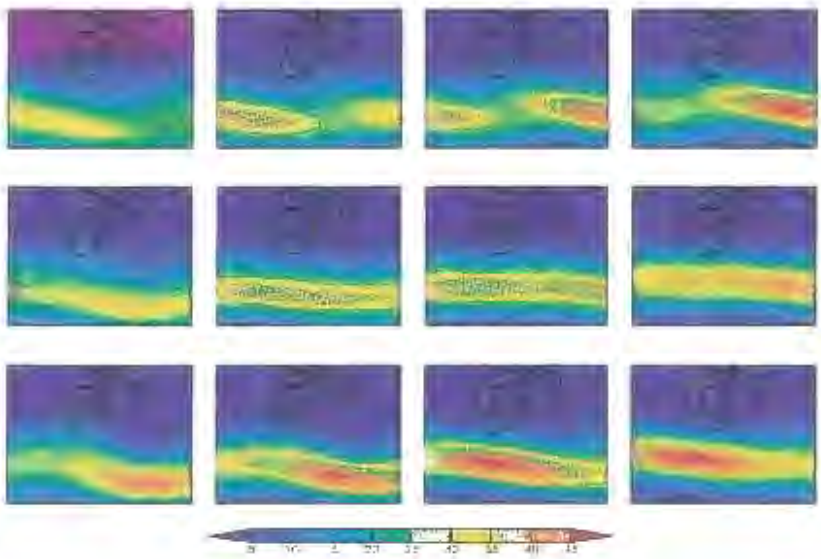

Figure 3.14: SOM of daily kinetic energy of the vertical mean component of Wind (10^5 J.m^{-2}).

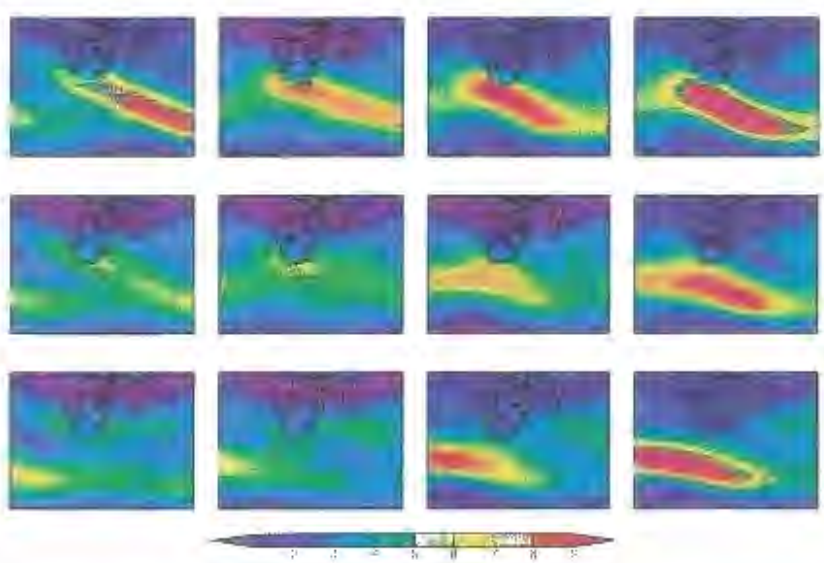

Figure 3.15: SOM of daily kinetic energy of the vertical shear component of Wind (10^5 J.m^{-2}).

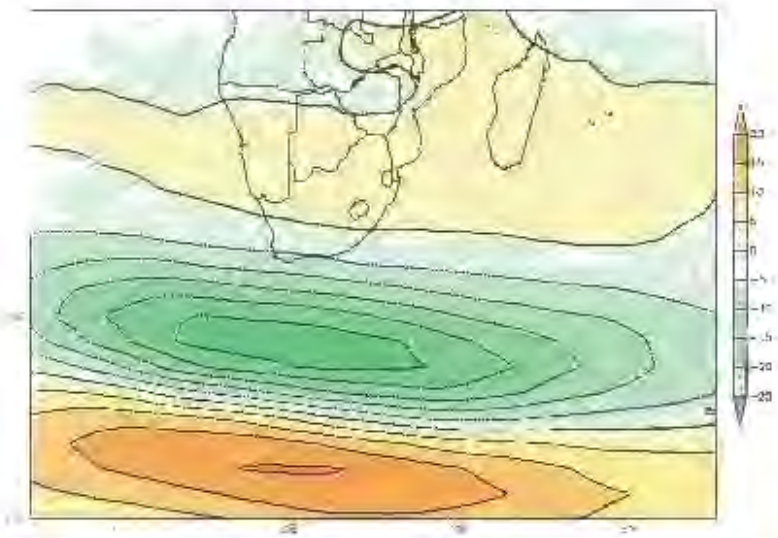

Figure 3.16: Difference of SOM nodes most associated with wet years minus that of dry years for the Vertical Mean component of Wind (10^6 J.m^{-2}).

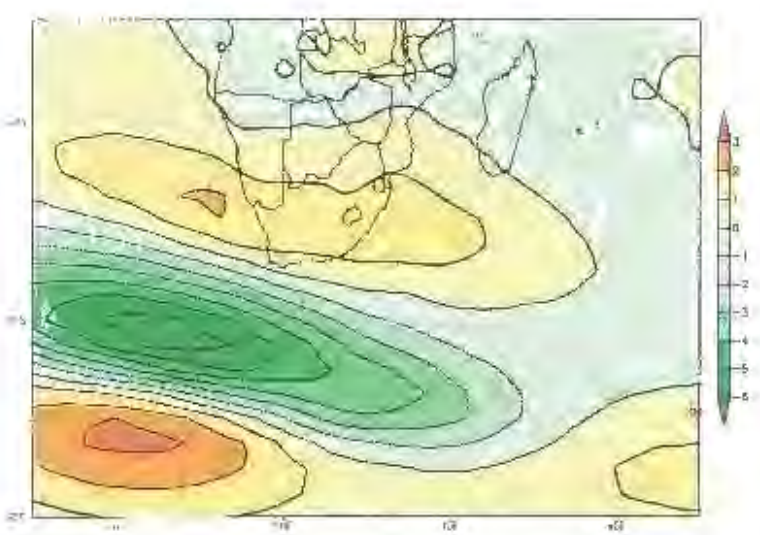

Figure 3.17: Difference of SOM nodes most associated with wet years minus that of dry years for the Shear component of Wind (10^3 J.m^{-2}).

Comparison of the jet during wet and dry seasons shows that the vertical-mean component of the jet weakens and shifts southward (Fig 3.16) while the shear component bifurcates and intensifies over South Africa (Fig. 3.17) when it is wet. Nodes on the upper right of the mean wind SOM (Fig. 3.14) are also associated with wet conditions, but only over Region 2. Here there is a strengthening of the jet to the east of southern Africa. Nodes of the shear component associated with this scenario, are found in the upper-central portion of the shear SOM (Fig. 3.15). However, there is no bifurcation of the jet as found with the nodes in the bottom left corner.

Kinetic energy fields demonstrate the characteristics of atmospheric motion while moist static energy (eqn. 3.7) provides a way of investigating energy states related to atmospheric waves. Moist static energy consists of the sum of geopotential energy, sensible and latent heat. The latent heat term is analogous to precipitable water, which was investigated earlier, leaving the remaining terms which comprise the dry static energy. High values of dry static energy can be associated with ridges or anticyclones in the mid-tropospheric circulation and low values with troughs and cyclones.

A 4x3 SOM of daily values of dry static energy show that wet seasons in both regions are associated with a two cell structure of above normal dry static energy in the southwest and below normal values in the southeast (Fig. 3.18). Generally the wetter seasons are associated with higher values of dry static energy in the mid-latitudes (top row of SOM). Dry seasons are associated with lower than normal dry static energy throughout the region or, alternatively, with a pattern of below normal values in the southwest and above normal values in the southeast.

These findings are consistent with the notion of rainfall over South Africa being associated with a mid-latitude trough accompanied by a stronger ridge of the South Atlantic anticyclone at the surface. Dry seasons are the reverse pattern with a ridge over the country and stronger baroclinic activity in the mid-latitudes. This relates back to the increased kinetic energy of the circulation south of South Africa during dry years. This is particularly true of the vertical-mean or barotropic component of the wind, which would also compare well to the dry static energy, as temperature and geopotential height waves are in phase in a barotropic atmosphere.

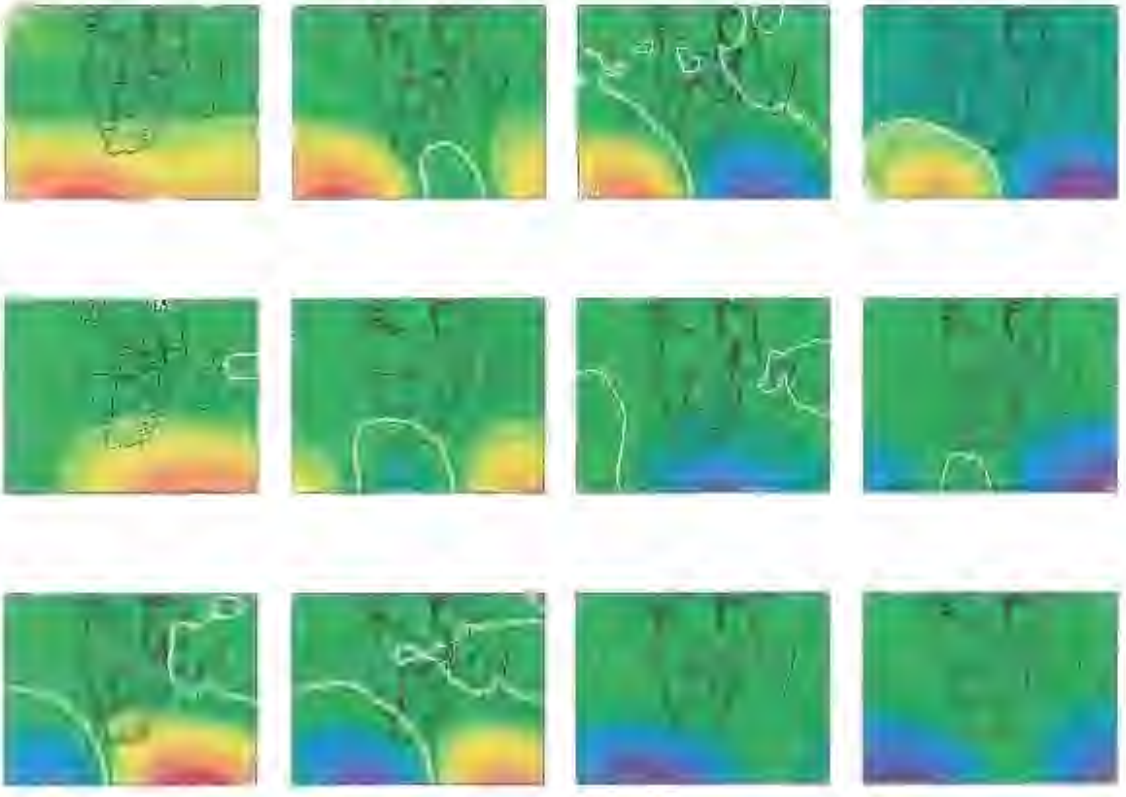

Figure 3.18: SOM of dry static energy anomalies. Thick white line denotes zero anomaly with red shading positive values. Shading interval is $5x10^6$ J.m^{-2}.

Discussion

When seeking causes of inter-annual variability, it is instructive to begin with the global fields of moisture flux and dry static energy flux. These are best viewed in the form of velocity potential anomalies. Such fields clearly show events such as ENSO (Fig 3.19). The characteristic two-cell pattern during the 1982/83 El Niño of enhanced moisture convergence (positive velocity potential anomaly) in the eastern Pacific Ocean and reduced moisture convergence across Indonesia (negative areas) is reflected in the surface to 700 hPa layer and in the 700 to 300 hPa layer. Over the far eastern Pacific Ocean anomalous divergence of moisture is evident in the upper layer while convergence remains in the lower layer. This is an indication of the smaller vertical extent of convection in this colder part of the Ocean. The dry static energy fields show the reverse pattern with anomalous divergence of heat over the warm sea surface temperature anomalies and anomalous convergence further west. The anomalous divergence of dry heat is probably related to the increased release of latent heat under conditions of enhanced convection. It is clear that the effect of the El Niño spreads across a large portion of the globe in the form of two cells of opposing sign.

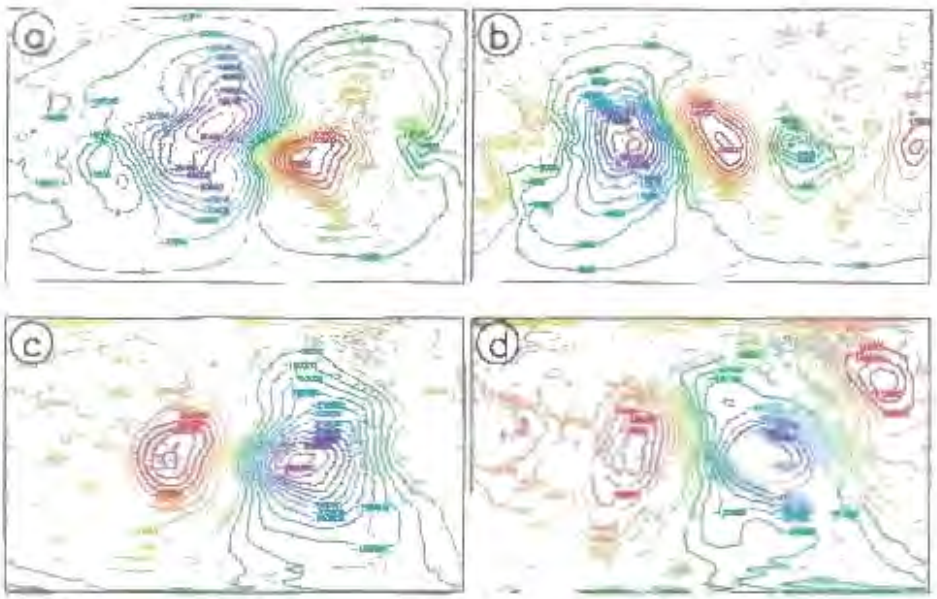

Figure 3.19: Velocity potential anomalies of horizontal flux of a) surface to 700 hPa moisture, b) 700 to 300 hPa moisture, vertically integrated (surface to 100 hPa) c) dry static energy and d) moist static energy for the 1982/83 season.

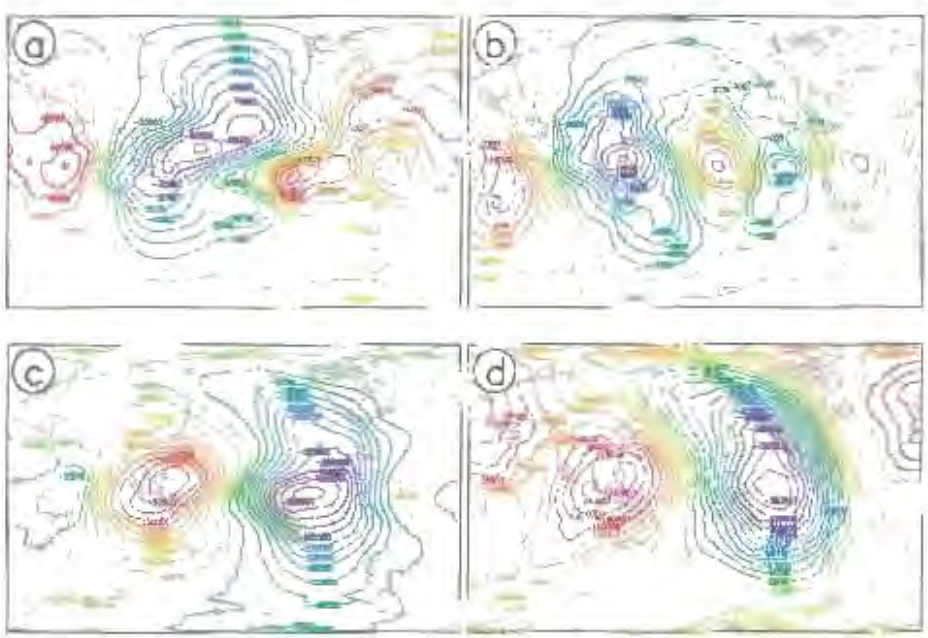

Figure 3.20: As for figure 3.19, but for the 1997/98 season.

The danger of oversimplifying the remote effect of these global events is illustrated by comparing the patterns of the 1982/83 El Niño with those of the 1997/98 El Niño (Fig. 3.20). Conditions in the Indo-Pacific region are generally the same, however over southern Africa conditions differ dramatically. During the 1982/83 event dry static energy was converging anomalously on southern Africa and moisture diverging. In contrast, during the 1997/98 event there was an anomalous convergence of moisture through both layers and dry heat was diverging from the area. Even during strong ENSO events, that raise the level of predictability in the areas surrounding the Pacific Ocean, predictability over southern Africa is not necessarily enhanced. The large two-cell pattern in the anomalies associated with ENSO events does not extend as far as southern Africa. In fact, the large anomalies seen in the velocity potential fields of energy flux over the Pacific and eastern Indian Oceans are seldom realised in the southern Africa region.

The remote effect of ENSO is usually manifest through modulations of the Walker circulation (Reason *et al.*, 2000). To inspect this the zonal component of the divergent moisture flux, which may be used as an indicator of the Walker-type circulation (Salstein *et al.*, 1980), is evaluated. The inter-annual east-west shift of the upward branch of the Walker Cell in the Pacific Ocean between 140°E and 150°W is clear in figure 3.21. El Niño events (red) are usually associated with eastward shifts and La Niña events (blue) with westward shifts. A second upward branch is evident over South America, but this branch shows remarkably little inter-annual variability. The third upward branch occurs over the central Indian Ocean and demonstrates a moderate variability of about 40° from 40°E to 80°E. Over Africa (30°E) there is nothing more than a local minimum in the surface divergent flux from the west. The

poleward extensions of these branches of the Walker Cells are the South Pacific Convergence Zone, the South Atlantic Convergence Zone and the South Indian Convergence Zone respectively. However the South Indian Convergence Zone is more intermittent than the others (Cook, 2000). This apparent lack of strong global forcing and observed erratic nature of the atmospheric circulation around southern Africa may offer a reason for the lower predictability in this region relative to the Pacific region, also implying that there must be other controls of the region's weather that need to be identified.

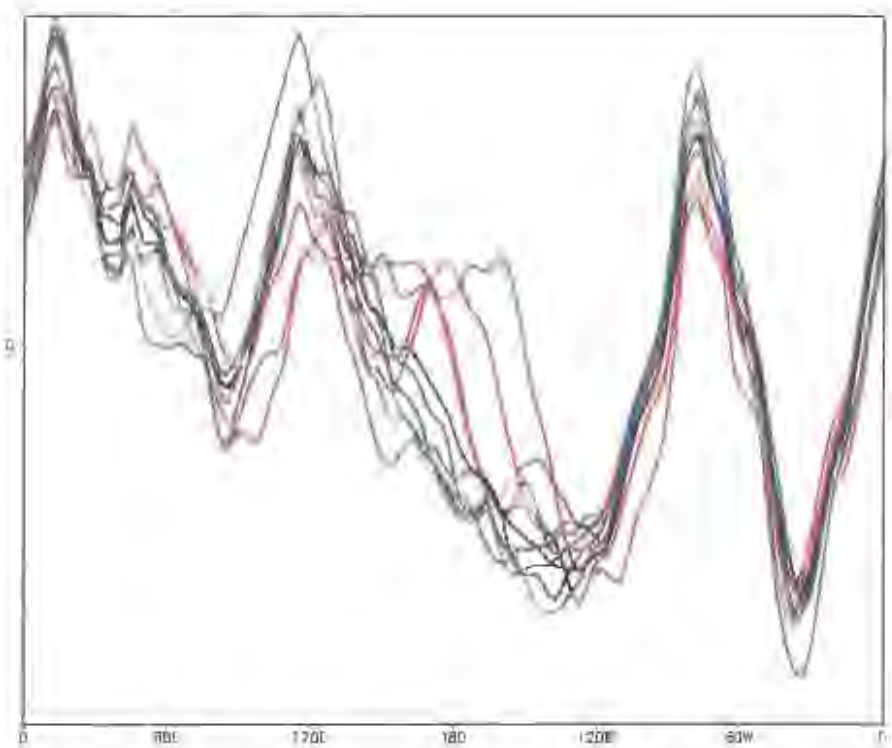

Figure 3.21: Zonal divergent moisture flux during DJF averaged from 30°S to the equator indicating the position of the Walker Cells. Blue lines represent wet years and red lines dry years (see table 3.1). The black line represents 1979-1999 DJF climatology.

Notwithstanding, clearly there are signals in the variability of rainfall in southern Africa brought about through teleconnections. Reason *et al.* (2000) propose a transport of the ENSO signal into the Indian Ocean at two distinct time-scales – quasi-biennial (2-2½ year) and low frequency (2½-7 year) bands. They point out that the superposition of the two bands masks any signal in SST and sea-level pressure anomalies. Peterson and White (1998) showed how changes in SST anomalies in the Pacific induce anomalies in the subtropical ocean through the Hadley Cell. They suggest that these anomalies propagate southward and around the southern hemisphere as the Antarctic Circumpolar Wave (ACW). Such signals alter the low-frequency eddies in the mid-latitudes which have a strong influence on the development of tropical-temperate-troughs (TTTs) (Todd and Washington, 1999). However, land-based convergence zones (and TTTs) (Cook, 2000) are also affected by the continental thermal low which in turn may be affected by signals such as those described by Reason *et al.* (2000).

As this thesis concentrates on intra-seasonal variability there is insufficient information to comment on the proposed functioning of these teleconnections. However, the fact that teleconnections play a role in controlling the weather in southern Africa cannot be denied. Basically the interaction between the tropical lows and mid-latitude disturbances, which is fundamental to understanding TTTs, pieces together a complex puzzle that may account for some of the rainfall variability in southern Africa. This still leaves a number of unanswered questions about what causes the remainder of the rainfall variability but this work is mentioned as it raises some interesting ideas about possible mechanisms behind climate variability which are explored later from the energy exchange perspective.

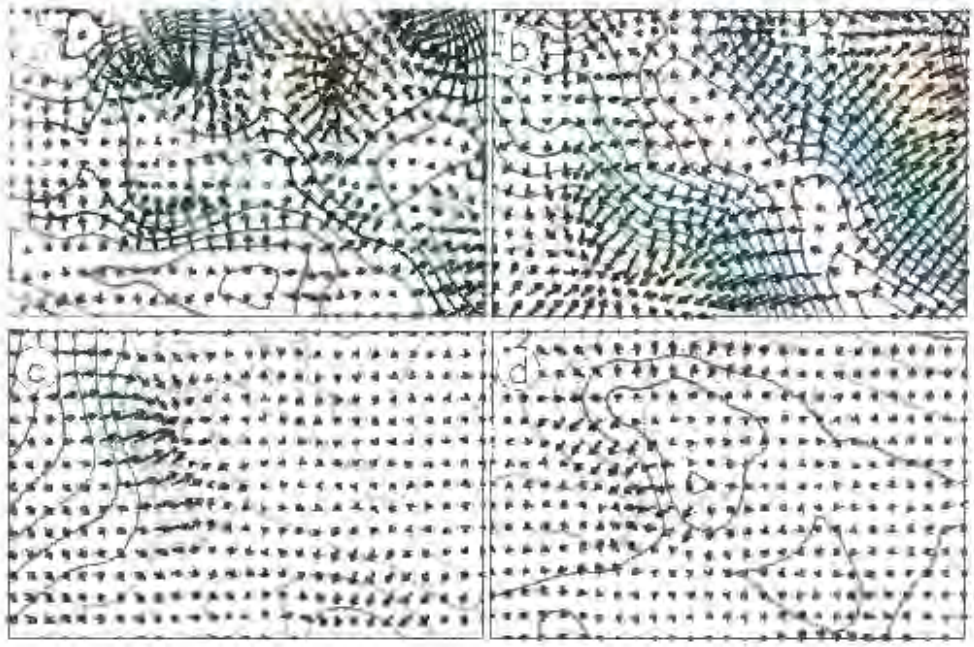

Figure 3.22: Anomalous divergent moisture flux in the surface to 700 hPa layer during a) wet and b) dry years, and in the 700 to 300 hPa layer during c) wet and d) dry years

As global forcing appears to play only a part in the rainfall variability of southern Africa, the next step is to zoom in over the region and consider forcing mechanisms of a local nature. Beginning with divergent moisture flux it is evident that the four wet seasons in the central Interior (Region 3) are all associated with an anomalous divergent flux of moisture from the northeast in both the surface to 700 hPa and 700 to 300 hPa layers. A composite of the seasons (Fig. 3.22) shows the net convergence of moisture over South Africa. The five dry seasons are more mixed but the anomalous divergent moisture flux in the 700 to 300 hPa layer is from the southeast during four of the years and from the northwest during the remaining year.

In the lower layer anomalies are more generally from the southwest. D'Abreton and Tyson (1995) interpreted these patterns to mean that wet seasons in central South Africa are the result of an influx of moisture from the northeast, with the moisture source in the Indian Ocean north of Madagascar. However, the SOM of daily low-level moisture flux (Fig. 3.7) show that this type of circulation is not one of the major modes. There is indeed a source of moisture on the coast of Tanzania but this is north of the ITCZ and the moisture flux generally terminates in this zone.

Furthermore, a SOM of daily moisture flux divergence (Fig. 3.23) shows that the major moisture sources around southern Africa are the Agulhas Current and the South Atlantic Ocean. Divergent moisture flux takes place towards the central Indian Ocean rather than away from it. This is supported by the climatological velocity potential of moisture flux that indicates the tropical Indian Ocean is a sink of moisture (Fig. 3.24). Apparent moisture sinks calculated by Yanai and Tomita (1998) reveal a similar picture of moisture sinks in the Indian Ocean north of 20°S and moisture sources in the Atlantic Ocean and, more importantly, in the Agulhas Current region.

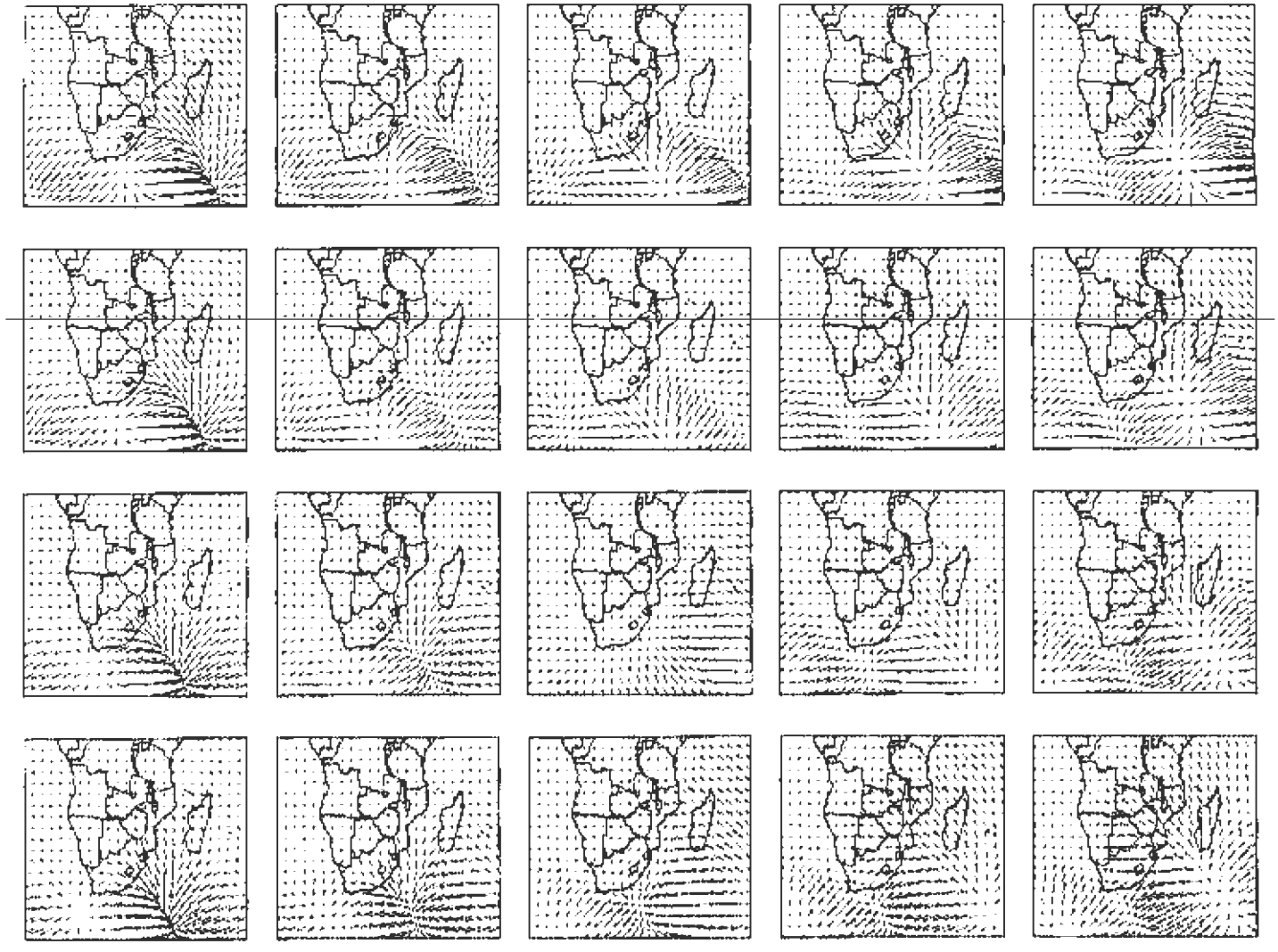

Figure 3.23: SOM of daily low-level divergent moisture flux.

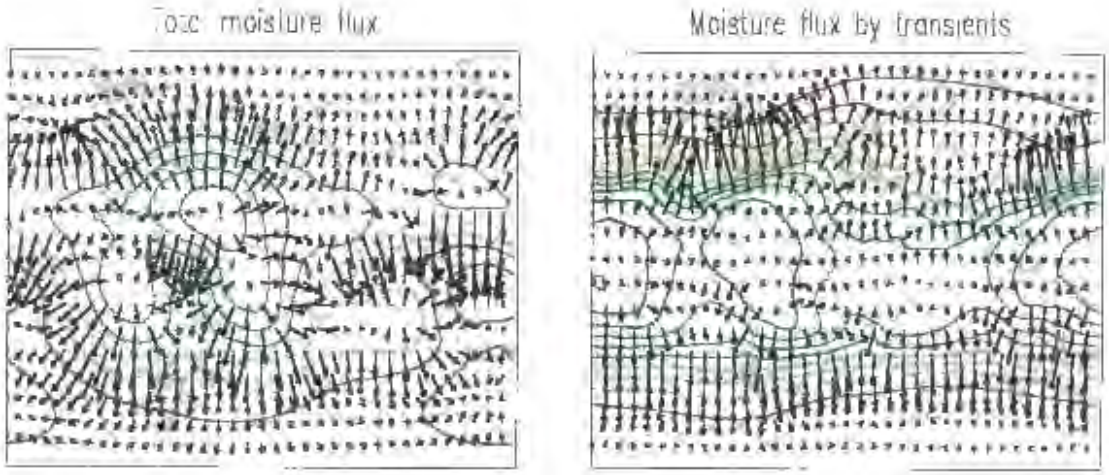

Figure 3.24: Global velocity potential and divergent moisture flux by the total wind and transient systems.

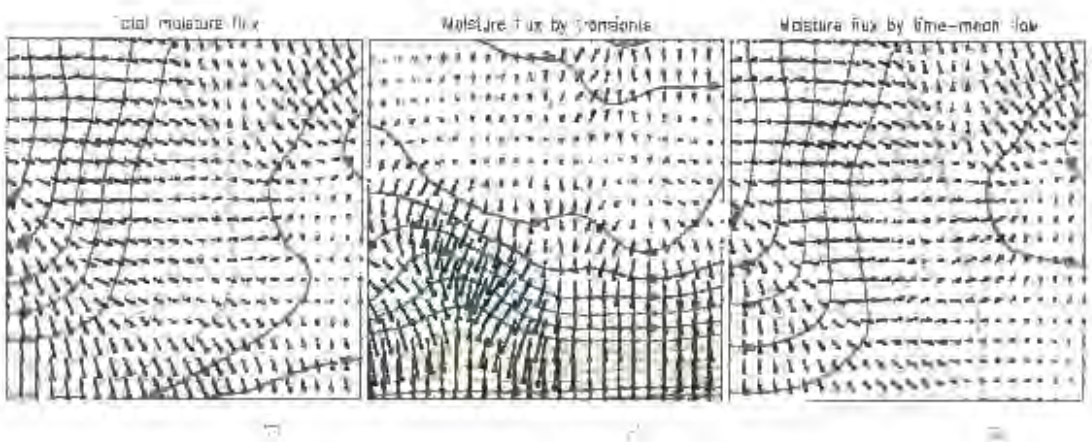

Figure 3.25: Local velocity potential and divergent moisture flux by the total wind, transient systems and time-mean wind.

Moisture flux may be analysed more closely by separating the flux field into time-mean and transient components. Moisture originating at the ITCZ, situated at roughly 15°S, is transported southward across southern Africa by transient activity (Fig. 3.25). Generally the magnitude of this flux is smaller than that by the time-mean flow, but over central South Africa and the Southern Ocean the fluxes are of a similar magnitude. It is worth noting that the direction of moisture flux by the transients takes place at right angles to that of the mean flow, also noted by D'Abreton and Tyson (1995). Rainfall events in South Africa are generally associated with a southward transport of moisture (Harrison, 1984b; D'Abreton and Lindesay, 1993; Taljaard, 1996), indicating that rainfall events in southern Africa occur when there is a disruption to the mean flow. This shows the importance of transient systems in transporting moisture polewards across South Africa. Oort (1971) found that the transient waves contributed to almost half the poleward moisture transport across the sub-tropics in the northern hemisphere. This is also seen in figure 3.24. In the southern hemisphere where standing waves are much weaker the effect of transient systems may be even greater.

The original notion that the Indian Ocean north of Madagascar is an important moisture remains plausible. Moisture transported into the ITCZ from the northeast may then reach South Africa in a two-step process: First, by the mean circulation into the ITCZ and second, southward into South Africa through the action of transient systems. However, findings from the SOM analysis of moisture flux suggests that the Agulhas Current region remains the major source of water vapour for South Africa and that this is achieved by moisture transport from the east around the Indian Ocean anticyclone. A recent study by Reason (2001b) supports this by

showing that above normal SSTs south of Madagascar lead to enhanced evaporation and that these are significantly correlated with summer rainfall over eastern South Africa.

Atmospheric processes are in reality 3-dimensional, highlighting the necessity to consider the vertical structures of the processes under investigation. In the previous section it was shown that rainfall variability is closely tied to the subtropical jet which in turn may be controlled by the Hadley Cell. The vertical structure of the large-scale meridional Hadley and Ferrel Cells is best shown through a two-dimensional stream function (see eq. 3.3) which may be interpreted as the flux of mass (Newell *et al.*, 1972, p 149-151). The values of $\Psi(\varphi,p)$, a function of latitude and the vertical pressure coordinate, may be used as an indication of the intensity of the circulations. Positive values denote circulation in a clockwise sense. On the hemispheric scale (Fig 3.26) these cells are clearly shown. In the tropics the northern and southern Hadley Cells meet between 10°S and 15°S, curving northward to 5°S at the surface. During the Austral summer the northern cell is much stronger. Adjacent to the Hadley Cells, in the mid-latitudes, the thermally indirect Ferrel Cells are found. These are followed by the thermally direct Polar Cells. Changes in moisture and heat fluxes between wet and dry years in central South Africa are evident in the vertical profile of mass flux. Overall there is an intensification of the thermally direct Hadley Cells and weakening the of the thermally indirect Ferrel Cells during dry years in central South Africa, with the northern Hadley Cell and southern Ferrel Cell showing the greatest change relative to wet years.

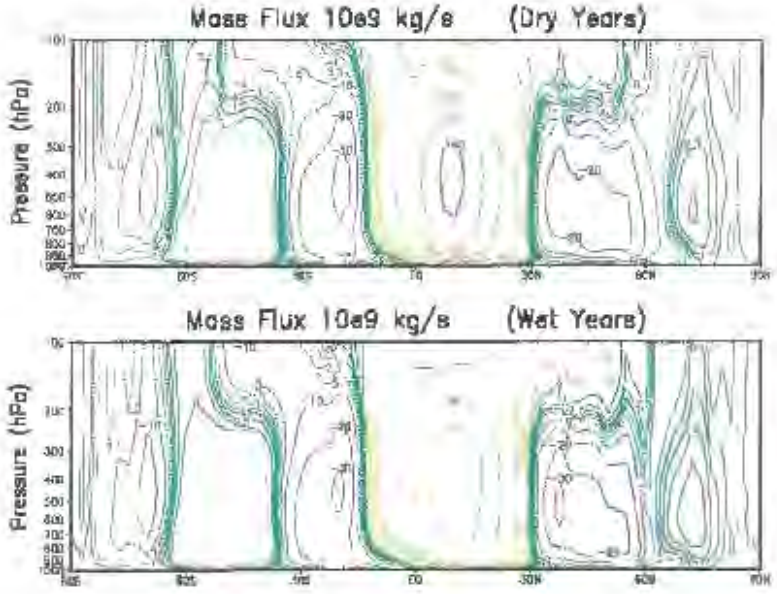

Figure 3.26: Vertical cross-section of the mass-flux streamfunction showing the zonally averaged Hadley Cells during dry years (top) and wet years (bottom).

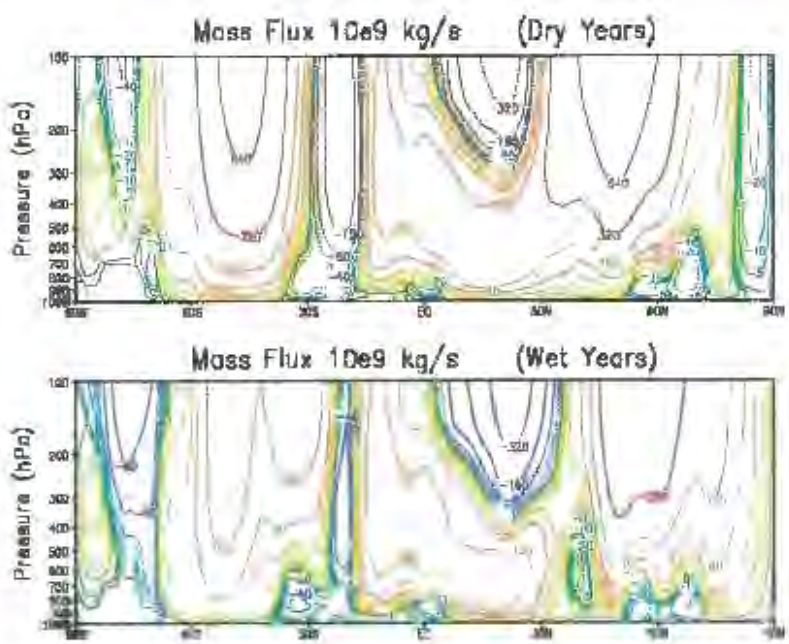

Figure 3.27: As for Fig 3.26 but for African longitudes (15E-35E).

Over the African longitudes (Fig 3.27) the meridional cell structure is not as clear owing to a net zonal mass divergence. Notwithstanding, some important features emerge. During dry years both the southern Hadley Cell and the southern Ferrel Cell strengthen considerably. The Ferrel Cell reduces in size and shifts slightly northward. Changes to the subtropical jet in the African sector (Fig. 3.28) confirm this, with an increase in speed throughout the column at about 45°S, shrinking in latitudinal extent and lowering of the core maximum from 250 hPa to 300 hPa. As mentioned earlier the westerly subtropical jet is necessary in areas of convergence of angular momentum. An increase in the transport of angular momentum by the Hadley Cell would be associated with an increase in the subtropical jet.

During wet years a mini thermally direct cell becomes evident at 30°S. Its vertical depth does not extend above 500 hPa. The southern Hadley Cell halves in intensity and shrinks in latitudinal extent, being replaced by a double-core Ferrel Cell with a quarter of the intensity found during dry years (Fig. 3.27). The subtropical jet weakens and shifts southward (Fig. 3.28) but there is a small increase in wind speed at 200 hPa between 30°S and the equator.

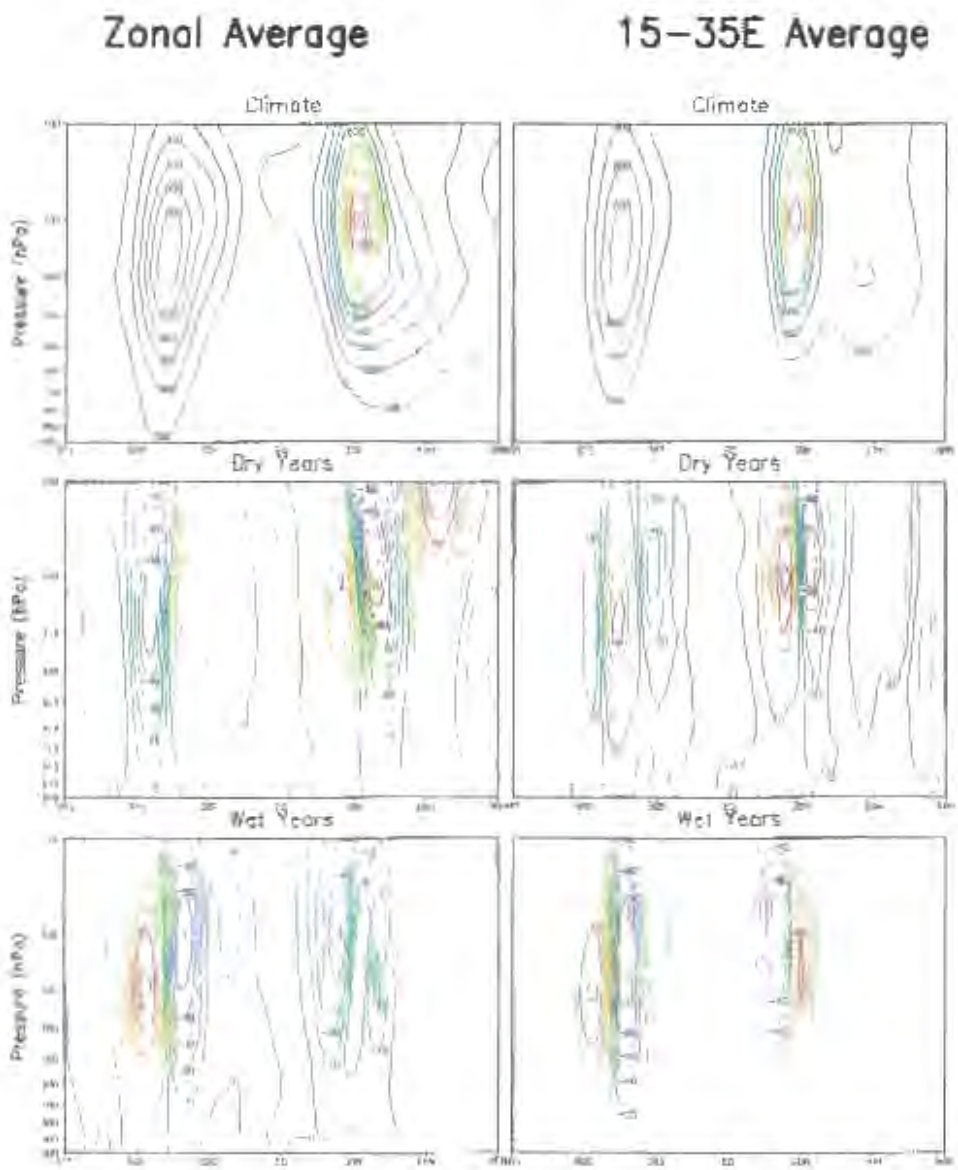

Figure 3.28: Vertical cross-section of the zonal wind component kinetic energy ($J.m^{-3}$) showing the position jet stream during all, dry and wet years, averaged zonally (left) and African longitudes (right).

A limitation of this chapter, where links between various modes of circulation and seasonal rainfall event characteristics are sought, is the constraint in quantifying the role of processes that are merely necessary but not sufficient for wet seasons. For example, moisture is necessary for rainfall to develop but additional processes are required to convert water-vapour into rainfall. This could offer an explanation why no clear distinction of moisture sources and transport between wet and dry years could be found using the methods described in this chapter. However, other processes such as changes in the kinetic energy of the mid-latitude westerlies and dry static energy clearly map to rainfall variability using the same methodology. In fact, several findings in this chapter merely confirm what has been known for over a decade, while others have provided new or improved insight. The strengthening and northward shift of the mid-latitude westerlies during dry years has been documented by, *inter alia*, Tyson (1986), Taljaard (1989) and Taljaard and Steyn (1991) and are consistent with the findings here.

Summary

The controls of rainfall in southern Africa are both complex and intermittent. Global-scale signals are weak in the region, doing little to raise the seasonal predictability of rainfall. This would certainly limit skill of prediction schemes relying totally on global signals. On a regional scale, vertical mean and shear kinetic energy in the Southern Ocean map clearly to inter-annual variability. Dry years are associated with a northward shift and strengthening of the subtropical jet. Also, an intensification of the southern Hadley Cell is coupled with dry seasons.

Moisture flux on a daily scale does not show a clear distinction between wet and dry years. This variable parameter needs to be examined in conjunction with the full energy cycle, as moisture is merely necessary but not sufficient on its own for rainfall. Moisture sources for rainfall in South Africa, according to the NCEP reanalysis data, are predominantly the Agulhas Current and Indian Ocean east of South Africa. This remains so for wet and dry seasons. Earlier work pointing to a moisture source northeast of Madagascar during wet years is not supported by the findings in this thesis.

The general pattern that has emerged from this chapter is that those aspects of the general circulation that control rainfall variability in southern Africa appear to be a combination of the global energy cycle and local conditions. The global energy cycle is manifest regionally in the Hadley Cells and energy exchange in the South Atlantic Ocean. Local conditions, particularly in terms of convection governed by vertical stability, modulate the position and intensity of the continent-based cloud band that is associated with a large part of the region's rainfall.

In light of the above, the static associations between rainfall and the general circulation forms a fundamental basis for the next chapter, where evolutionary aspects of the general circulation are investigated.

Chapter Four

Evolutionary Features of the General Circulation during Rainfall Events

Introduction

In the previous chapter static associations between rainfall and the general circulation were explored. These revealed how observed changes in rainfall can be related to changes in the strength of the Hadley cell and latitudinal shifts in the kinetic energy fields. In order to further our understanding of how and why these associations exist the evolution of energy fluxes through time-dependent equations of energy conversions are examined.

The atmospheric energy cycle and conversions among the potential and kinetic components are well-studied and documented (Lorenz, 1955; Oort, 1964; Holopainen, 1970). Briefly, the cycle is summarized as follows: It begins with the generation of potential energy through a net heating of the tropics and net cooling of the poles through differential radiative heat fluxes. The fraction of this energy that is available for conversion to Kinetic Energy (KE) accumulates as zonal Available Potential Energy (APE), most of which is converted into eddy APE by the eddies. Sinking motion in the colder parts of the eddies and rising motion in the warmer parts results in a conversion to eddy KE. Some dissipation of the eddy KE occurs and the

remainder is converted into zonal KE by the eddies. The zonal KE is then generally depleted by friction.

Numerous studies of the atmospheric general circulation have investigated and attempted estimates of energy conversions from one form to another. Oort (1964) formulated these conversions for three different methods of separating energy into the mean and eddy components. The first is the space domain, where the mean consists of the zonal average, and the eddies the departure from that mean. The Lorenz (1955) energy cycle is based on this approach. Other studies using this method include Pepler and Vincent (1983). Second, the time domain consists of a time average, of at least a season to a year in length, and departure from the mean. This method is useful in isolating transient systems. The final method is the mixed space-time domain where the mean is a time and zonal average. The eddy component is the residual consisting of the time-average departure from the zonal average plus the departure from the time average. This allows studies to include the role of stationary systems (e.g. Holopainen, 1970; Ulbrich and Speth, 1991).

The method of separating the wind fields into a vertical mean and shear, the deviation from the mean at each level, introduced by Wiin-Nielsen (1962) was used in the previous chapter to study atmospheric states. The energy conversions between these states, as proposed by Wiin-Nielsen, begins with APE being converted to KE of the shear flow and later to KE of the mean flow through barotropic decay. The terms barotropic and baroclinic have been used to describe the mean and shear components respectively by some authors (Chen and Yen, 1985; Ko and Vincent, 1995). Chen (1983) and Chen and Yen (1985) investigated the similarities between

the energetics of baroclinic and barotropic flows to that of transient and time-mean flows. They cautioned that although these appeared equivalent on the large-scale over long periods, locally there may be large differences. Notwithstanding the caveats of energy conversion calculations, Huang and Vincent (1985) argued that these do provide information which can be used to understand large-scale processes.

The objective of the chapter is to relate climatic variability over southern Africa to large-scale energy exchanges. These are then to be used to study the time-evolution of atmospheric processes during significant rainfall events. Special emphasis is placed on the start and breaks in the summer rainfall during December to February from 1979-1999.

Data and Methodologies

Unless otherwise stated all data used are daily, 2.5° x 2.5°, 00Z and 12Z fields for December to February from the NCEP reanalysis data for the period December 1979 to February 1999. Vertical levels used are lower boundary (sigma = 0.995) and pressure levels at 1000, 925, 850, 700, 600, 500, 400, 300, 200, 150 and 100 hPa. Vertical integrals are calculated in the pressure coordinate system, as in Chapter Three, using the trapezoidal method,

$$X_{INT} = \frac{1}{g} \int_{p_s}^{p_t} X \, dp \qquad (4.1)$$

where **X** is any scalar variable, **p** the pressure, $\mathbf{p_t}$ = 100hPa and $\mathbf{p_s}$ surface pressure.

In terms of mean and eddies, after Oort (1964), a scalar variable **X** may be written as the sum of four components:

$$X = [\overline{X}] + \overline{X}^{*} + [X]' + X'^{*} \qquad (4.2)$$

where the square brackets represent the zonal average, the asterisk the deviation from the zonal average, the over-bar a time mean and the single prime the deviation from the time mean.

Energy equations

Energy equations in the space domain provide information on the zonal-mean state and zonal eddies, and may be used to trace daily evolutions of each energy form over selected domains. The equations used here follow the definitions of Oort (1964) and are similar to that used by Huang and Vincent (1985).

There is notable concern about using energy equations to study atmospheric processes as these can be applied incorrectly. Also, boundary terms may be required for studies over limited domains. However, this study, as with Huang and Vincent (1985), attempts to demonstrate, at least qualitatively, how regional climate variability can be understood in terms of global energy. For correctness, spatial integrals are performed globally and their integrands analysed over two domains, *viz.*, the southern hemisphere from 0°S to 60°S and the southern Africa domain from 10°W to 70°E and 10°S to 60°S. Essentially the analysis considers local contributions to a global quantity.

In the vertical, integrals are done from the surface to 100 hPa. The zonal and eddy KE ($\mathbf{K_m}$ and $\mathbf{K_e}$) and zonal and eddy APE ($\mathbf{P_m}$ and $\mathbf{P_e}$) are defined in the space domain by the following equations:

$$K_m = \frac{1}{2}\int \overline{([u]^2 + [v]^2)}\, dm \tag{4.3}$$

$$K_e = \frac{1}{2}\int \overline{([u^*]^2 + [v^*]^2)}\, dm \tag{4.4}$$

$$P_m = \frac{1}{2}\, c_p \int \overline{\gamma [T]''^2)}\, dm \tag{4.5}$$

$$P_e = \frac{1}{2}\, c_p \int \overline{\gamma [T^*]^2}\, dm \tag{4.6}$$

In these equations (~) denotes an area average over a closed (global) pressure surface, ( )" the deviation from this average, $\mathbf{c_p}$ the specific heat at constant pressure, $\boldsymbol{\theta}$ the potential temperature, $\mathbf{R}$ the gas constant, $\mathbf{p_o}$ = 1000 hPa, and $\boldsymbol{\gamma}$ the stability parameter defined as:

$$\gamma = -\left(\frac{\theta}{T}\right)^2 \frac{R}{c_p p_0} \int_0^{p_0} \left(\frac{T}{\theta}\right) \frac{1}{p} \left(\frac{\partial \tilde{\theta}}{\partial p}\right)^{-1} dp \tag{4.7}$$

Energy equations in the mixed space-time domain allow one to study how the time-mean and zonal-mean state and the sum of transient and standing eddies are maintained (Oort, 1964). The time averaging used here is done independently over each DJF season. The zonal and eddy KE (K_m and K_e), zonal and eddy APE (P_m and P_e), conversions from zonal APE to zonal KE $C(P_m ; K_m)$, eddy APE to eddy KE $C(P_e ; K_e)$ and eddy KE to zonal KE $C(K_e ; K_m)$ are defined in the mixed space-time domain by the following equations (constants are as defined above):

$$K_m = \frac{1}{2}\int ([\bar{u}]^2 + [\bar{v}]^2)\, dm \tag{4.8}$$

$$K_e = \frac{1}{2}\int [\overline{u'^2} + \overline{v'^2} + \bar{u}^{*2} + \bar{v}^{*2}]\, dm \tag{4.9}$$

$$P_m = \frac{1}{2} c_p \int \gamma [\bar{T}]''^2 dm \tag{4.10}$$

$$P_e = \frac{1}{2} c_p \int \gamma [\overline{T'^2} + \bar{T}^{*2}]\, dm \tag{4.11}$$

$$C(P_m; K_m) = -\int [\bar{\omega}]''[\bar{\alpha}]'' dm \tag{4.12}$$

$$C(P_e; K_e) = -\int [\overline{\omega'\alpha'} + \bar{\omega}^*\bar{\alpha}^*] dm \tag{4.13}$$

$$C(K_e; K_m) = \int ([\overline{u'v'}] + [\bar{u}^*\bar{v}^*]) \cos\phi \frac{\partial}{a\partial\phi}([\bar{u}]\cos^{-1}\phi) dm$$

$$+ \int [\overline{u'\omega'}] + [\bar{u}^*\bar{\omega}^*]) \frac{\partial[\bar{u}]}{\partial p} dm + \int [\overline{v'^2}] + [\bar{v}^{*2}]) \frac{\partial[\bar{v}]}{a\partial\phi} dm$$

$$+ \int ([\overline{\omega'v'}] + [\bar{\omega}^*\bar{v}^*]) \frac{\partial[\bar{v}]}{\partial p} dm - \int [\bar{v}]([\overline{u'^2}] + [\bar{u}^{*2}]) \frac{\tan\phi}{a} dm \tag{4.14}$$

Many studies have used data solely on pressure levels. In the case of southern Africa, using data below the high-altitude plateau may lead to artificial energy fluxes and so contaminate the findings. Holopainen (1970) used a weighting function where the weight at a point in three-dimensions was related to the probability that the surface pressure would be higher than the pressure level. In this study, the equations applied are time-dependant and this method is not suitable. Masuda (1988) assigned zero transport to points below the ground in his study of heat transport. He conceded that although the results would be better they would not be entirely satisfactory. This study will use data from the surface upwards and ignore pressure level data below the ground. The stability parameter in the lowest layer from the surface to the first pressure level above the ground has been assigned the same value as the adjacent layer above. This is to avoid spurious values associated with surface temperature.

Identifying rainfall events

The chapter is aimed at investigating possible causes of significant changes to regional rainfall in time. This includes the onset of widespread and significant rainfall events and prolonged dry spells. In order to identify rainfall events, two parameters are considered. The first is a five-day running mean of regional rainfall, and the second the position of the node to which the 5-day running mean of relative humidity maps in the relative humidity SOM (Fig. 3.1). A 5-day running mean proved to be the best compromise between smoothing the data while maintaining the peaks of significant rainfall events. The evolution of SOM node position of instantaneous values of relative humidity was highly variable but when 5-day running mean values

of relative humidity were mapped to the SOM, clearer patterns emerged. One may argue that the time-averaged relative humidity values will exhibit a reduced variance when mapped to a SOM trained on instantaneous data. However, a comparison of the lateral node position for instantaneous and 5-day mean relative humidity fields (Fig. 4.1 - top panel) shows that the two fields follow each other reasonably well. The only differences occur where there are high frequency shifts in the instantaneous values, something which is undesirable in this analysis. Furthermore, this mapping is only used to help identify significant rainfall events that have both, a high amount of rainfall and a large spatial extent.

The significant peaks in rainfall are defined as those points exceeding one standard deviation, once the data is standardized. The SOM node position isolates those rainfall events that are associated with a well-defined cloud-band, which is an indicator of an organized synoptic event. In Chapter Three it was pointed out that the nodes on the right-hand-side of the SOM were associated with cloud-bands and those on the left with dry conditions. An abrupt regime shift from dry to wet may be easily identified by the trajectory of these nodes in time. An example of these fields is presented for the 1990/91 season (Fig. 4.1). The figure shows a rainfall event early in December followed by a break until the beginning of January. After this there is a temporary break followed by a period of good rainfall until late in February. In this season, the rainfall peak around the 5th of December, the break during the second half of December, and the onset of rain in January are of particular interest. In total there are 28 significant rainfall events in Region 2 and 34 in Region 3. This difference is consistent with the finding in Chapter Two that rainfall in Region 3 is more typical of organized weather systems than in Region 2.

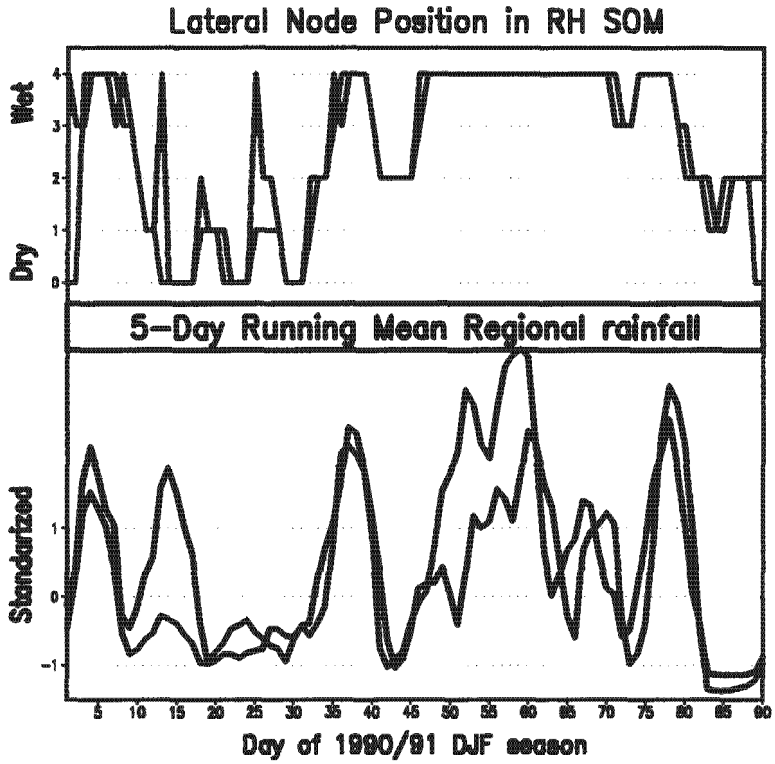

Figure 4.1: Time series of the lateral position of node mapping of 5-day running mean relative humidity (orange) and instantaneous values (blue) in the relative humidity SOM (top) (see Fig. 3.1) and 5-day running mean rainfall for Region 2 (black) and Region 3 (green) for the 1990/91 DJF season (bottom).

Time filtering

A sequence of twice-daily atmospheric data contains data on many scales of atmospheric motion. Some of the associated variance may not be relevant to the particular phenomenon being studied. An example is given in Lee (1981) where a slowly moving signal such as wind direction is corrupted by turbulence and

consequently the observation data needs to be filtered. Studies of synoptic-scale variability of 500 hPa heights require that low frequency variability and the annual cycle be removed from the data to extract the true characteristics of variability of the scale of interest (Blackmon, 1976; Trenberth, 1981). Lange (1979) used band-pass filtering to expand on Lorenz' work on the energy cycle to determine the relative roles of large-scale planetary waves and smaller scale motions on energy conversions.

This study concentrates on oscillations in the intra-seasonal time-scale. Vincent *et al.*(1998) suggest a band-pass filter of 6-25 days which would capture most of the variability associated with tropical-extratropical cloud-bands. The spectral analysis of daily regional rainfall, shown in figure 2.11, indicates a peak at about 23 days which falls into this range. Adjacent frequencies were also isolated to partition the different components of the energy cycle. The lower frequencies (longer than 25 days) were isolated using a low-pass filter and the 2-6 day band with a band-pass filter.

The filters were designed using a procedure outlined by Doblas-Reyes and Déqué (1998). The smoothing of the filter weights is done by using the Bloomfield (1976) convergence window. This has the advantage of reducing spurious oscillations near the stop-band. A span of 16 days was used for the 6-25 day band-pass filter.

Energy and Momentum Exchange at the Seasonal Time-scale

Evolution of energy exchange over time is contained in the space domain equations (4.3 to 4.6), but it is useful first to investigate energy conversions at the mixed space-time domain (eqns. 4.8 to 4.14). In this way areas may be identified where the inter-annual variability of energy conversions is highest. These areas are used in the formulation of the space domain equations later. Although the energy equations are only meaningful as integrals over the whole atmosphere, the mixed space-time domain equations do allow one to investigate the local contributions to the totals in a more appropriate way (Oort, 1964; Huang and Vincent, 1985).

A comparison of the atmospheric energetics for wet and dry seasons (defined in table 3.1 in Chapter Three) was done. Starting with the zonal available potential energy (Fig 4.2), all dry years have more available potential energy between 40°S and 50°S and in the tropics than during the wet seasons. At the opposite end of the energy cycle the peak of zonal kinetic energy is displaced 5° further north during dry years than during wet years (Fig 4.3). The conversion of energy from zonal available potential energy to zonal kinetic energy (Fig 4.4) does not reveal a distinct change between wet and dry seasons. However, the apparent latitudinal wave-like structure between 30°S and the equator, with a minimum at 25°S and a maximum at 10°S, is somewhat more amplified during dry seasons. Oort (1964) pointed out that this form of energy conversion is generally an order smaller than the conversions to the eddy components, suggesting that eddies play the dominant role in climate variability.

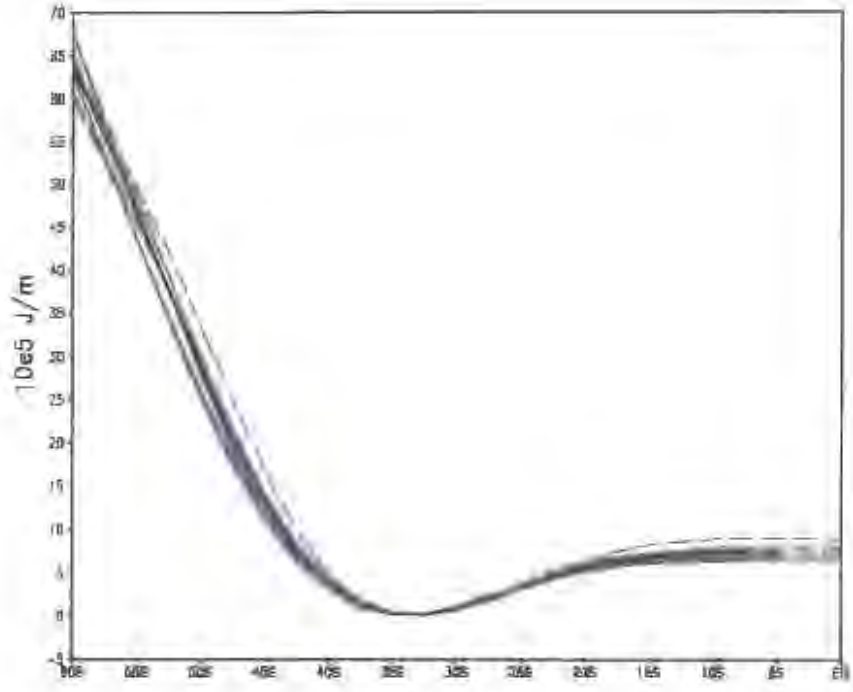

Figure 4.2: Mean zonal available potential energy for dry years (red), wet years (blue) and 1979-1999 DJF average (black).

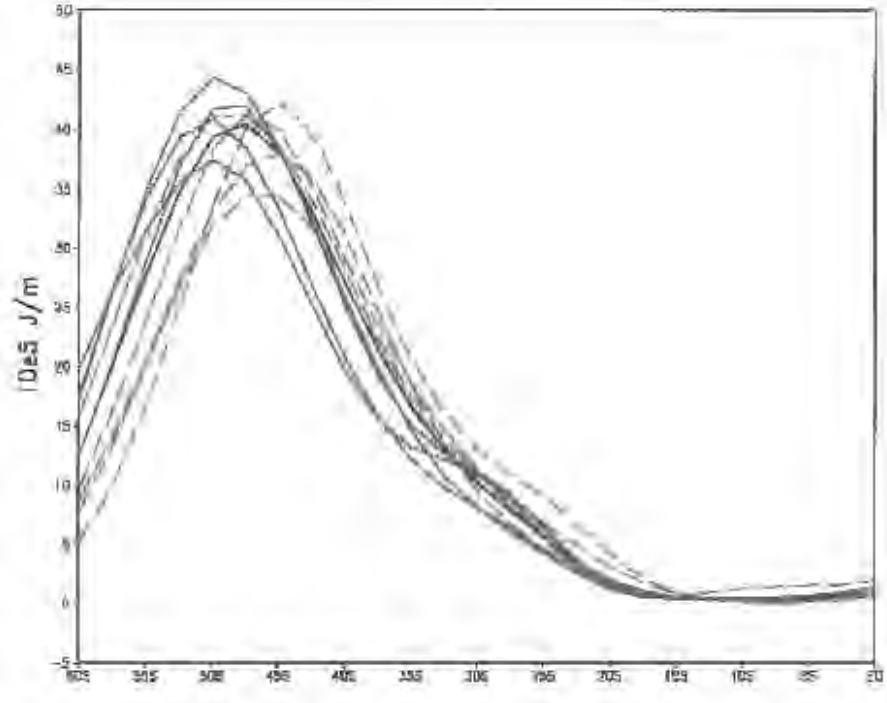

Figure 4.3: As for figure 4.2, but for mean zonal kinetic energy

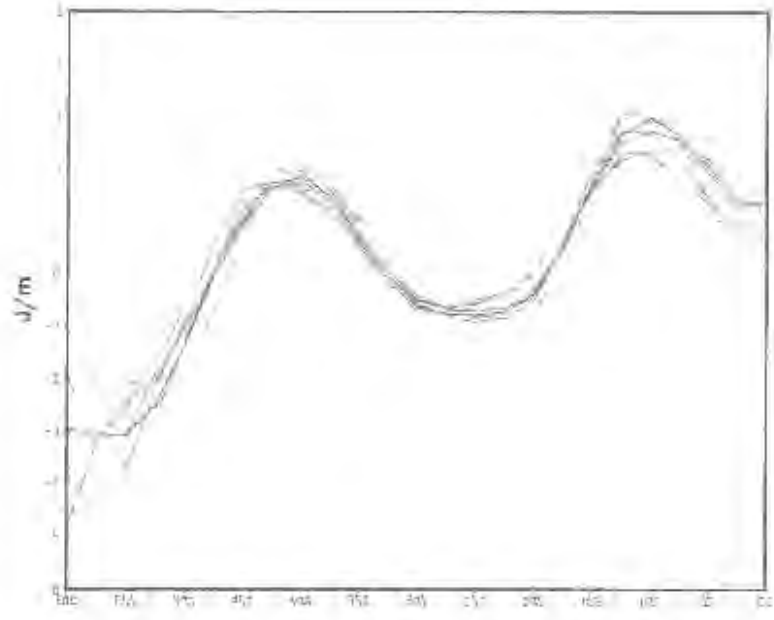

Figure 4.4: As for figure 4.2, but for conversion rate from mean available potential energy into mean kinetic energy by mean meridional circulations.

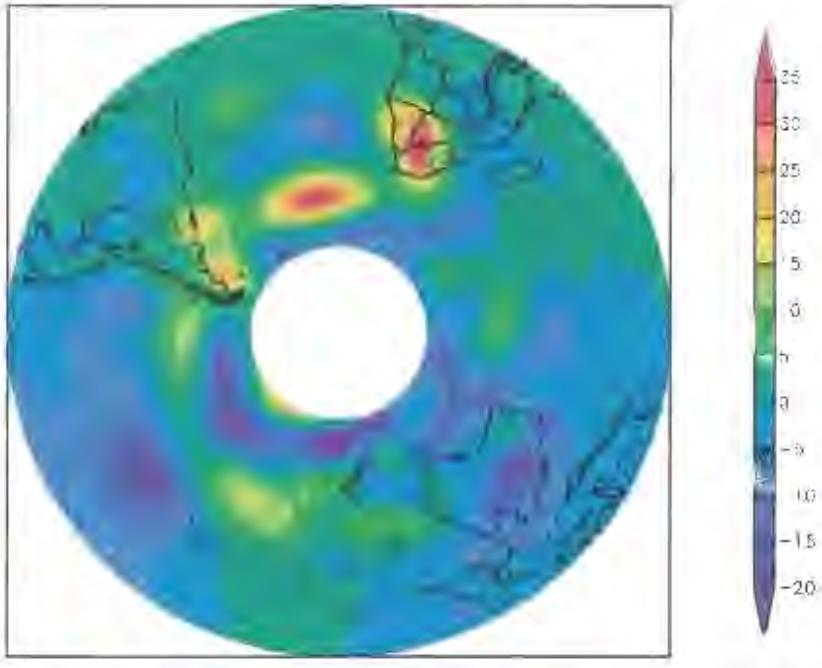

Figure 4.5: Difference between composites (dry-wet) of eddy available potential energy from the equator to 60°S (10^5 J.m^{-2}).

The eddy energy conversions have a longitudinal dependency enabling us to focus on the African longitudes. During dry years there is an anomalous build-up of eddy available potential energy in the South Atlantic Ocean centred at 45°S 10°W and over the southern Africa landmass (Fig 4.5). South of 50°S the sign reverses. In the central Pacific Ocean there is an anomalous reduction in eddy available potential energy at 45°S and a build-up further south. Eddy kinetic energy increases at 45°S almost throughout the southern hemisphere during dry years in South Africa, but most notably in a band south of Africa (Fig 4.6). The cause of the increase in eddy kinetic energy in this area appears to be related to an increase in the conversion from eddy available potential energy (Fig 4.7a). Isolating the transient component of this energy conversion (Fig 4.7b) reveals that the increase in the South Atlantic Ocean is almost entirely due to transient systems.

The band of decreased energy conversion during dry seasons, which roughly coincides with the tropical-extratropical cloud-band across South Africa (Fig. 4.7c) is also interesting. As this energy conversion is a result of large-scale overturning by eddies it is most likely linked to the processes associated with the cloud-band. The northern anchor of the cloud-band at the borders of Angola, Namibia and Botswana appears to be mainly stationary (Fig. 4.7b) while the southeastward extension is more transient in nature(Fig. 4.7a). This is consistent with the characteristics of the tropical-extratropical cloud band where is a land-based in the north (Cook, 2000) and linked to transient disturbances in the south.

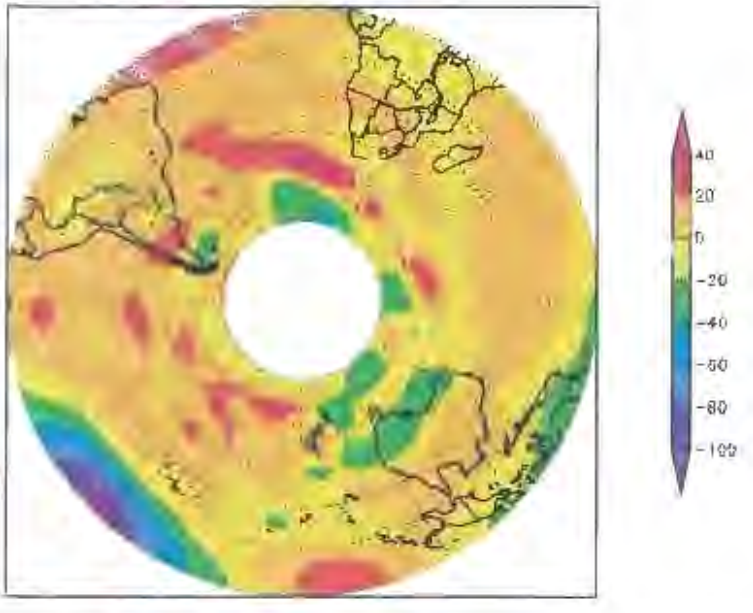

Figure 4.6: Difference between composites (dry-wet) of eddy kinetic energy from the equator to 60°S (10^5 J.m^{-2}).

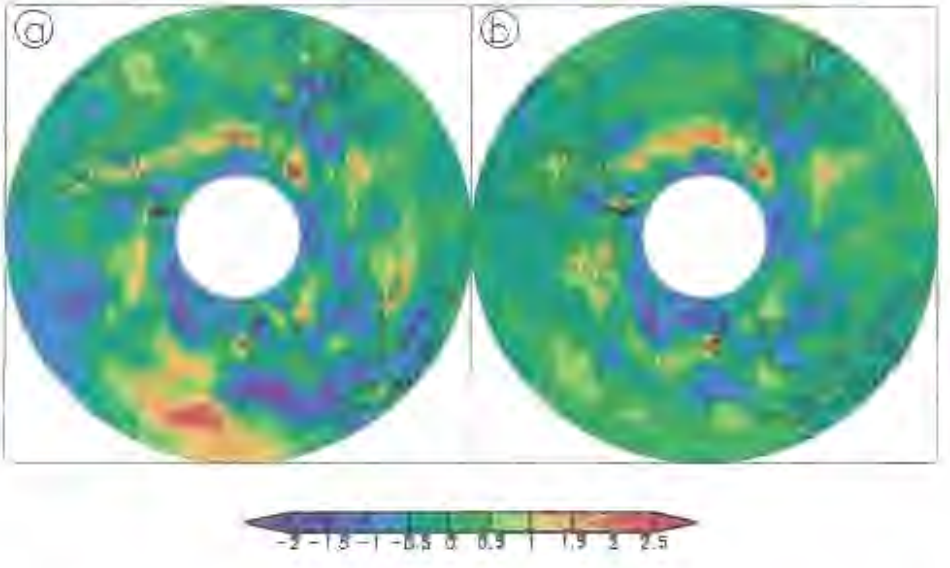

Figure 4.7: Difference between composites (dry-wet) of the conversion rate from eddy available potential energy into eddy kinetic energy by large-scale eddy convection. a) Stationary and transient eddies, b) transient eddies only (W.m^{-2}).

Another interesting feature is that the increased conversion of eddy APE to eddy KE is not complemented by increased conversion from zonal APE which would occur through the local tightening of temperature gradients by an increase in mid-latitude cyclone activity (Holton, 1992, p 267). Apart from horizontal transports of eddy APE, this suggests that there is an increase in the local generation of eddy APE during the dry seasons. Anomalous surface heating of the continents and SST anomalies in the South Atlantic Ocean (Mason, 1995) associated with dry periods over South Africa could account for the enhanced generation of eddy APE.

The final stage of the eddy conversions is from eddy KE to zonal KE (Fig 4.8). The increase in this energy conversion, associated with dry years, occurs in the same band as the increase in eddy KE. These changes are consistent with the notion that there is a northward shift in mid-latitude wave activity during dry seasons. This shift produces an overall increase in the magnitude of energy conversions in the South Atlantic Ocean.

The large-scale energy fluctuations are instructive but they do not explain the causes of wet and dry spells over South Africa. To answer this, processes that lead to widespread rainfall and dry spells over South Africa need to be investigated.

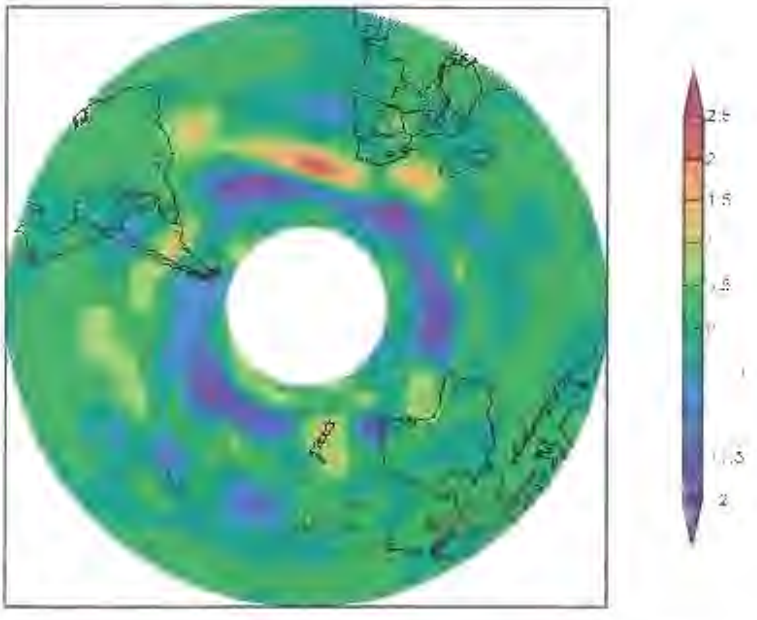

Figure 4.8: Difference between composites (dry-wet) of the conversion rate from eddy to mean kinetic energy ($W.m^{-2}$).

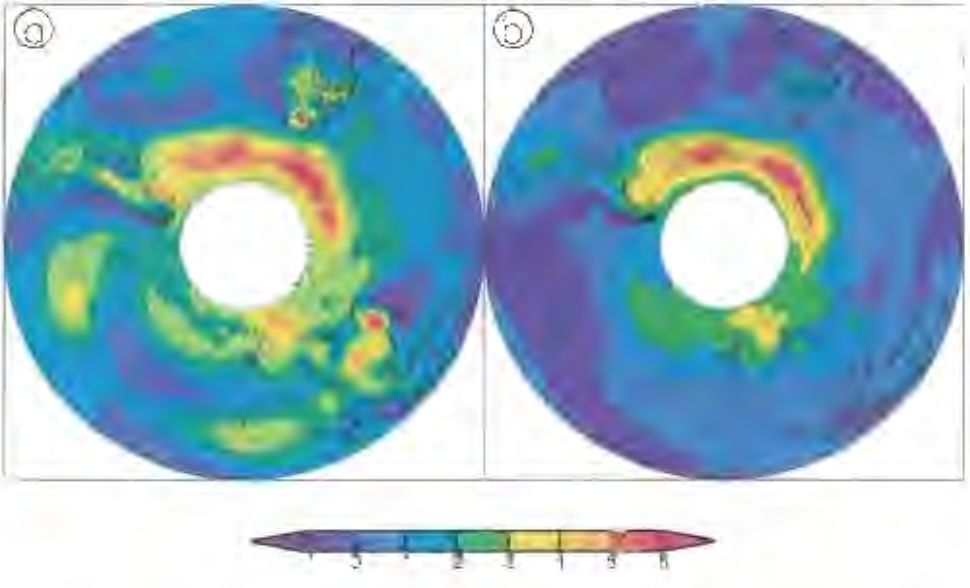

Figure 4.9: Climatological values (DJF 1979-1999) of the conversion rate from eddy available potential energy into eddy kinetic energy by large-scale eddy convection. a) Stationary and transient eddies, b) transient eddies only ($W.m^{-2}$).

Energy fluxes in the space domain

In the previous section it is evident that energy exchange in the Southern Ocean plays a key role in weather of southern Africa. In order to assess the role of this ocean in the global energy cycle a comparison is made with energy exchange in the Pacific Ocean. Climatologically, the southern hemisphere continents and the Southern Ocean south of Africa are the preferred areas of conversion from eddy APE to eddy KE (Fig 4.9). Over the continents and the South Pacific Convergence Zone (SPCZ) (Hurrell and Vincent, 1987) the energy exchange takes place mostly through convection. On the other hand, the conversions in the South Atlantic Ocean are chiefly through the action of transient mid-latitude waves (Fig. 4.9b). The space domain form of the equation of energy conversion from eddy APE to eddy KE shows that the average conversion rate in the South Atlantic Ocean is 2.46 $W.m^{-2}$ compared to 0.61$W.m^{-2}$ in the South Pacific Ocean. However, the variance of this conversion is higher in the South Pacific (1.78) than South Atlantic Ocean (1.58). This appears to be the result of a higher incidence of the conversion of eddy KE back into eddy APE in the Pacific Ocean. The net conversion of eddy APE to eddy KE is lower in the Pacific region, leaving the bulk of the energy conversion to take place in the South Atlantic Ocean.

Zooming in over the continent itself, the previous section made it clear that eddy APE over continental southern Africa is higher during dry years. This is a result of higher than normal surface temperatures, typical of dry years (Taljaard and Steyn,

1991, p 37). On a daily scale the conversion of eddy APE to eddy KE over the area 20°S to 35°S and 15°E to 30°E appears to be connected to rainfall events. This link is particularly strong during the 1993/94 season, consequently this season will be used for illustration purposes. As will be shown later, the results for this season are representative for most other seasons, although weakened in some instances.

During dry spells the conversion rate of eddy APE to eddy KE is weaker but increases rapidly during rainfall events (Fig. 4.10). Increases coinciding with rainfall peaks are evident at days 25 to 30, 37 to 40, 50 to 55 and 65 to 70 of the 1993/94 DJF season. The correlation between rainfall and the rate of eddy APE to eddy KE conversion for this season is 64%.

Eddy APE can be altered through four mechanisms: Increased convective cloud cover is generally associated with condensational heating in cooler air aloft and a reduction of sensible heating over the relatively warm land surface, and would reduce the local generation of eddy APE. The second is an increase in the transfer to eddy KE through the covariance of vertical velocity and temperature eddies (Fig. 4.10). Summer convective overturning associated with deep convection over continental areas, and mid-latitude cyclone activity are the main physical mechanisms behind this transfer. The third is a reduction in the transfer from zonal APE. However, over southern Africa the average transfer rate of zonal APE to eddy APE is nearly an order smaller during DJF (0.42 $W.m^{-2}$) than the conversion from eddy APE to eddy KE (5.61 $W.m^{-2}$). Finally, boundary fluxes alter the energy of a limited domain. Of these, the conversion of eddy APE to eddy KE is important locally, as found by Huang and Vincent (1985) for the South Pacific Convergence Zone.

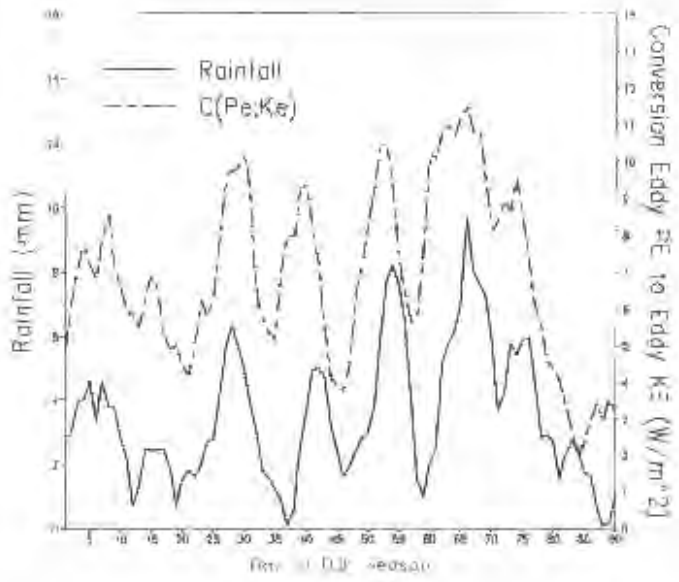

Figure 4.10: Time-series of 5-day running mean rainfall in Region 2 (solid) and the conversion rate of eddy available potential energy to eddy kinetic energy (dashed) for the 1993/94 season.

Figure 4.11: Seasonal correlation between 5-day running mean rainfall in Region 2 and the conversion of eddy available potential energy to eddy kinetic energy.

Expanding the analysis to all seasons, it becomes evident that the correlation, between regional rainfall and eddy APE conversion to eddy kinetic energy over the sub-continent, shows a large inter-annual variability (Fig. 4.11). Values range from as high as 79% for 5-day running-means of Region 3 rainfall to as low as 7%. The figure for the full period in Region 3 is 49%. The correlation between daily values is slightly lower at 11% to 58% with an average of 36%. Using the Student's *t*-distribution and 88 degrees of freedom the daily data correlations are significant at the 95% and 99% levels if they exceed 17% and 24.5% respectively. In Region 3, 16 out of 20 seasons have correlations significant at the 95% level, with 10 years significant at the 99% level. In Region 2 the correlations are lower, where 12 of the 20 seasons have correlations significant at the 95% level and 8 significant at the 99% level. This is most likely a consequence of the rainfall events in Region3 being more typical of mid-latitude synoptic systems, as suggested earlier. It is noteworthy that the correlation for all seasons from 1979-1999 is significant at the 99% level for both regions.

In a regional sense, it is clear that significant rainfall events over South Africa play a major role in the conversion of eddy available potential energy into eddy kinetic energy demonstrating that the region's rainfall and global energy exchange must be related in some way.

Time trajectories of moisture archetypes in SOM space

The evolution of the atmosphere may be studied by following temporal trajectories of archetypes created by a SOM. This is done by using sequential observations that have been mapped to particular SOM nodes. By selecting a node of interest, backward trajectories can be determined to map out typical sequences leading up to this mode. These include atmospheric states of relative humidity and circulation represented by moisture flux. In this way more light can be shed on the state of the atmosphere prior and leading up to a significant rainfall event.

Two major types of cloud-bands, *viz.* the truncated cloud-band and tropical-extratropical cloud-band, have a different evolution prior to the event. The SOM depicting these modes is presented in figure 3.1. The truncated cloud-band (Fig. 4.12a) is more persistent than the tropical-temperate-trough (Fig. 4.12b). Up to a week prior to any day when a truncated cloud-band is present, the majority of days map to within one node from the top right-hand corner where truncated cloud-bands are represented. Whereas the tropical-temperate-trough events are preceded by a more diverse array of modes. Among these is the node associated with dry conditions in the bottom-left of the SOM, that is prominent almost immediately one day before the event.

The evolution of moisture flux modes reveals another interesting factor. A SOM of moisture flux divergence is shown in figure 3.23. Nodes where there is a strong moisture flux across Region 2 (25°S; 27.5°E) from the Indian Ocean are found on the right-hand-side of the SOM with moisture flux returning to the Indian Ocean

on the left. The sequence of events leading up to the node in the top right-hand corner exhibit a strong variation. One day before this event there is a clear mapping to the node in the top left-hand corner. This part of the SOM contains the reverse circulation where there is a strong moisture flux towards a convergence zone extending southeastwards in the Indian Ocean (Fig. 4.13a). Three and seven days before this event the three opposite corners of the SOM are most frequently observed. In contrast, during periods of weak moisture flux, found towards the centre of the SOM, there is not such a large regime shift. Instead, there is a gradual spreading out across the SOM space (Fig. 4.13b).

The non-divergent nature of atmospheric circulation is clearly demonstrated in moisture transports (Rosen *et al.*, 1979b). Correlations across all DJF seasons from 1979 to 1999 between daily values of the total and non-divergent moisture flux over South Africa confirm this. Correlations of 0.88 for the zonal component and 81% for the meridional component are very high indeed. The correlation between the divergent and non-divergent part of moisture flux is quite different. The zonal component has a negative correlation of -29%, with the meridional component even more anti-correlated at -41%. This has ramifications for the transport of moisture across southern Africa, particularly during times of strong meridional transport as the divergence of moisture is likely to take place off axis, or even orthogonal, to the prevailing wind. This supports the findings in Chapter Three that the climatological moisture transport and divergent flux over South Africa take place at roughly right angles to each other. The significance of this is that divergent moisture flux is quite distinct from non-divergent transport and that non-divergent moisture flux could be mistaken for divergent flux.

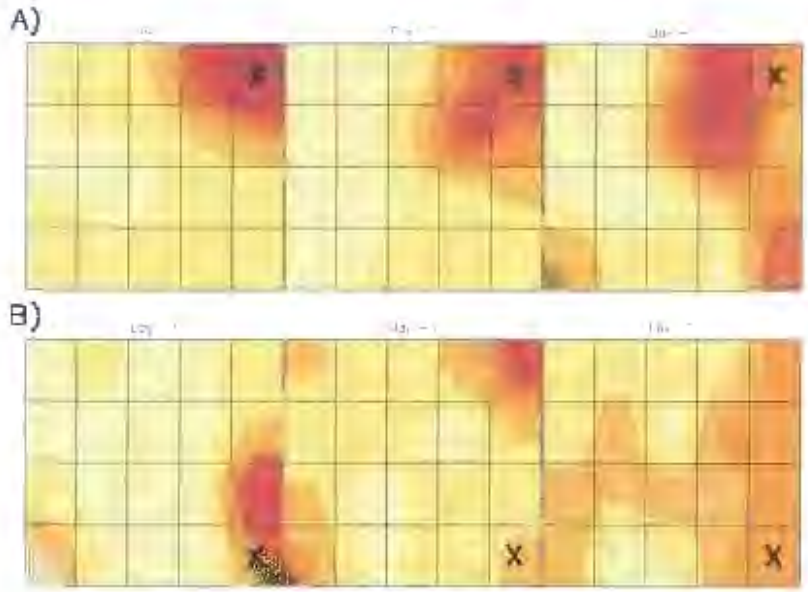

Figure 4.12: SOM node frequency plots at 1, 3 and 7 days prior to events mapping to the node marked **X** for vertically averaged relative humidity shown in figure 3.1.

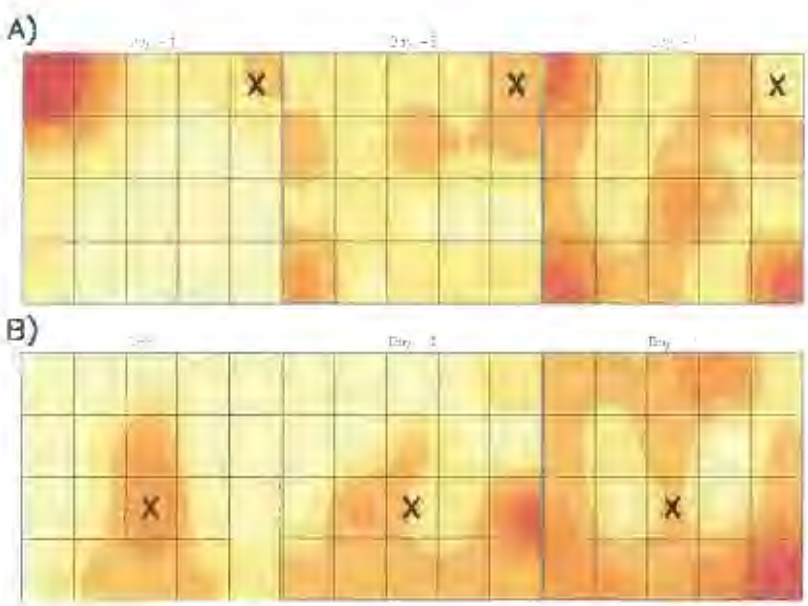

Figure 4.13: SOM node frequency plots at 1, 3 and 7 days prior to events mapping to the node marked **X** for low-level divergent moisture flux shown in figure 3.23.

Rainfall events

The final part of the analysis of events is to investigate characteristics and possible causes of each of the significant rainfall events, as defined earlier. This part of the study includes the use of Hovmöller plots of the kinetic energy of vertically-integrated mean and shear wind components, and SOMs of pressure-level streamfunction fields.

The kinetic energy fields are calculated from 6-25 day bandpass filtered wind data for two latitude bands, *viz.* 45°-30°S and 25°-15°S. The Hovmöller plots show the longitudinal progression of disturbances with time for the mid-latitudes and tropics respectively. From these it can be deduced whether a travelling disturbance most likely initiated a rainfall event or not. A subjective methodology was chosen here as it allows more user insight into the problem. Objective methods, apart from being difficult to implement, would introduce as many errors.

An example for the 1993/94 season in shown in figure 4.14. The rectangular boxes represent periods of significant rainfall over South Africa and the dashed lines approximate paths of tropical disturbances. The rainfall event between days 35 and 40 of the season appears to be initiated by both mid-latitude and tropical disturbances, while the event starting at day 75 only by a tropical disturbance. The former rainfall event is associated with a sharp enhancement of the shear kinetic energy east of South Africa. The analysis was applied in this way to all the years in the study and results summarized in tables 4.1 and 4.2.

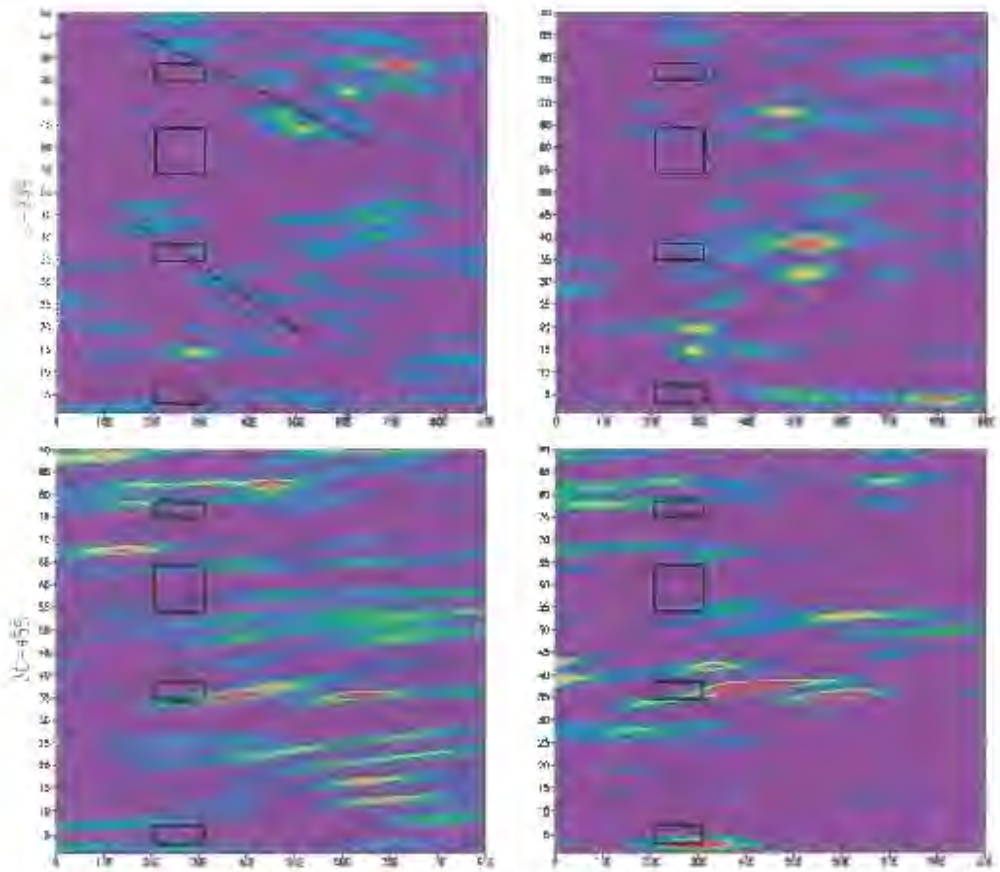

Figure 4.14: Hovmöller plots of kinetic energy of 6-25 day band-pass filtered vertical-mean (left) and shear (right) wind for the 1993/94 DJF season over the tropics (top) and mid-latitudes (bottom). Open boxes indicate rainfall events over South Africa and dashed lines a series of disturbances possibly manifest through a travelling signal.

Table 4.1: Number of cases of dominant circulation types during disturbances in the vertical-mean and shear wind associated with rainfall events in Region 2.

Region 2-28 Rainfall events													
Associated flow in the 6-25 day band	No. of Events out of 28	Dominant Circulation											
		850 hPa				500 hPa				200 hPa			
		TTT	TL	IA	HP	App	CE	C	A	App	CE	C	A
Mean Wind-Midlatitudes	9	6	0	1	3	6	1	2	1	5	1	1	3
Shear Wind-Midlatitudes	15	9	2	3	3	11	5	2	2	8	3	2	5
Downstream Shear	11	5	2	1	4	7	2	4	1	7	2	3	4
Mean Wind-Tropics	15	7	4	3	3	11	3	4	1	8	1	5	4
Shear Wind-Tropics	10	6	3	4	1	9	2	3	0	6	0	4	4

Table 4.2: As for table 4.1, but for Region 3.

Region 3-34 Rainfall events													
Associated flow in the 6-25 day band	No. of Events out of 34	Dominant Circulation											
		850 hPa				500 hPa				200 hPa			
		TTT	TL	IA	HP	App	CE	C	A	App	CE	C	A
Mean Wind-Midlatitudes	8	5	0	1	3	6	1	1	2	4	2	2	2
Shear Wind-Midlatitudes	17	8	2	6	3	13	7	1	3	10	3	2	8
Downstream Shear	11	6	2	3	4	8	3	4	2	7	2	3	6
Mean Wind-Tropics	20	6	5	8	4	16	5	3	3	12	1	6	6
Shear Wind-Tropics	8	3	2	3	2	6	2	2	0	5	0	4	2

Streamfunction fields are used to categorize the circulation into various patterns of cyclones and anticyclones at three levels in the troposphere, *viz.* 850-, 500-, and 200 hPa. The 850 hPa SOM is grouped into four main types: Tropical-Temperate-Trough (TTT), Indian Ocean Anticyclone (IA), Tropical Low (TL) and Continental Anticyclone (HP). The 500 hPa SOM is split into Approaching Trough (App), Continental Anticyclone (HP), Cyclonic Flow (LP) and Trough East of South Africa (CE). The 200 hPa circulation consists of the same groups as the 500 hPa level.

Overall the dominant circulation during rainfall events is a tropical-temperate-trough at 850 hPa overlain by an approaching trough at 500 hPa and, to a lesser degree, at 200 hPa. An anticyclone is also quite dominant at 200 hPa, indicating the tropical nature of the circulation over southern Africa during DJF. This system is also known to transport moisture southward around its western periphery (Taljaard, 1996, p51-52).

Using the Hovmöller plots, disturbances in the shear-component of the wind account for about half of the forcing of rainfall events. The number of events attributed to mean-wind disturbances, amount to half of that, although some of these consist of both mean- and shear-disturbances simultaneously. Certainly there is a clear link between vertical wind shear in the mid-latitudes and the initiation of rainfall events.

Shifting the focus to the tropics it is again clear that more than half of the rainfall events are associated with tropical disturbances, especially in Region 3. In the

tropical latitudes the major component of the wind is the mean or barotropic part, whereas in the mid-latitudes, it is the shear-component. Vertical wind shear is much weaker in the tropics, possibly accounting for this difference.

Another aspect of the rainfall events is whether they originate spontaneously over the continent and then initiate a shear-disturbance that moves downstream into the westerlies. Approximately a third of the events fall into this category. This figure, combined with that of events initiated by mid-latitude disturbances, shows that rainfall events over South Africa are strongly linked through vertical wind shear to the mid-latitudes, even during the high summer months.

The dominant circulation types during each event, partitioned according to the type of forcing, reveals more characteristics about the forcing mechanism. In Region 3 the Indian Ocean anticyclone is very much part of the forcing by mid-latitude shear and tropical disturbances. This reinforces the notion that rainfall in this region depends on moisture supply from the Agulhas region, in contrast to the literature of D'Abreton and Tyson (1995).

In the mid- and upper-troposphere approaching troughs are clearly dominant as they assist in transporting tropical air-masses southward and provide large-scale dynamical uplift. Some of these throughs form into cut-off low pressure systems. These account for many of the significant rainfall events in the region (Harrison, 1984b; Taljaard, 1996, pp 64-69; Tyson and Preston-Whyte, 2000, pp 196+197). Here the vertical mean and shear components of the wind become important. Sutcliffe (1966, pp 108-109) describes the development of cut-off low systems as

part of the life-cycle of a baroclinic depression. The process of low-level convergence and upper-level divergence which allows the vortex to develop produces wide-spread uplift and precipitation. This vertical structure contributes to the shear-component of the wind field. The process of cut-off low development is termed *anticyclonic disruption* because a high pressure builds across the neck of a large-amplitude trough cutting off the low-latitude upper low (Sutcliff, 1953). This pattern of systems corresponds to an increase in the kinetic energy of the shear-component over the continent and a simultaneous decrease in the vertical-mean component south of the continent. Often substantial rainfall occurs with a medium-amplitude mid-tropospheric trough, without it becoming a cut-off low. Results show that approaching mid-tropospheric waves are associated with more than half of the rainfall events.

Discussion

The question of what causes rainfall variability in South Africa is not an easy one to answer. Evidence in this analysis shows that the hemispheric energy cycle is clearly linked to rainfall at a seasonal scale, despite the relatively small apparent global forcing through teleconnections. The problem becomes more nebulous when studying daily rainfall. On the one hand, increased baroclinic activity south of Africa is associated with drier conditions but at the same time baroclinic systems are an essential component or initiator of the tropical-extratropical cloud-band. Studies of tropical mid-latitude interactions have shown that the mid-latitudes first force the tropical convection via pressure surges and upper-level wave energy, with feedbacks afterwards towards the southeast (Meehl *et al.*, 1996). Watanabe and Kimoto (1999) emphasize that height anomalies, which are a proxy for mid-latitude waves, are mainly generated by transient eddy forcing in the mid-latitudes rather than by diabatic heating in the tropics associated with SST anomalies. Sheng *et al.* (1998) also showed that transient systems are central to the dynamics of the PNA pattern, reinforcing the evidence of the importance of the transient systems. These findings are consistent with patterns found in southern Africa and assist in explaining how mid-latitude dynamics cause rainfall variability in the region.

The importance of dynamical forcing is further highlighted by the fact that moisture transports do not exhibit any clear link to rainfall either at a daily scale or seasonal scale. Obviously moisture needs to be present for rainfall, but it is the dynamics that produce uplift and cooling that are of primary importance. A box-and-whisker plot of precipitable water for each season at 25°S 27.5°E (Region 2) and at

27.5°S 25°E (Region 3), shows the averages, standard deviation and extremes for each season (Fig. 4.15). In Region 2 the average of the precipitable water in summer with one standard deviation above and below remains above the average for any other season. In fact, assuming a normal distribution based on a histogram (not shown), only about 16% of summer values are lower than the autumn average. In Region 3 there is a slight overlap with autumn, but summer days are clearly far more humid than days in other seasons. This is because precipitable water is in part a function of temperature. From a climatological point of view, moisture and rainfall are inextricably linked, but intra-seasonal rainfall variability is dependent on more than moisture alone.

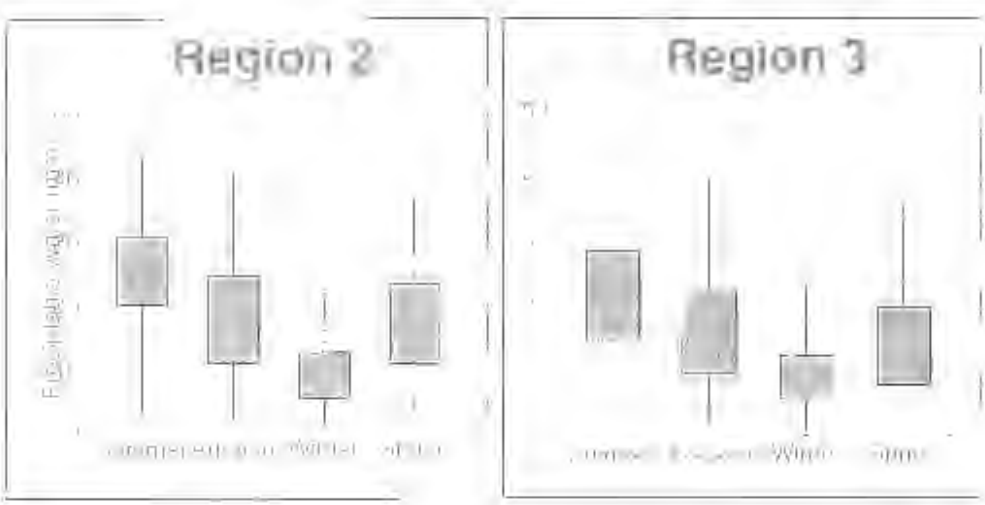

Figure 4.15: Box-and-Whisker plot of climatological (1979-1999) precipitable water for each season indicating the standard deviation (box) and extremes of daily values (whiskers).

This study has shown that rainfall variability in South Africa is closely tied to baroclinic activity in the South Atlantic both at a seasonal and daily scale. Various papers in the literature offer some insight into the circulation in this area. Kalnay *et al.* (1986) suggest that an eastward displaced SPCZ and altered convective activity over South America impact the South Atlantic Convergence Zone (SACZ). They also eliminated the Andes Mountains as an initiator of Rossby waves. The cause of variability in the baroclinic activity in the South Atlantic may be linked to changes in isentropic slopes which alter baroclinic instability (Staley, 1991) and interactions with the Antarctic Circumpolar Wave (Peterson and White, 1998). However, this topic requires further research before conclusive answers may be found as to the actual cause of baroclinic activity fluctuations in this region.

Notwithstanding, findings in this thesis offer a framework to possibly explain the observed changes in baroclinic activity south of Africa between wet and dry years. When the zonal available potential energy increases, perhaps through ENSO events and/or fluctuations in solar activity (Ruzmaikin, 1999), that areas of preferred energy conversion become more active through increased transient wave activity. This mechanism, similar to that described by Hou (1998) for a winter hemisphere, is that a stronger Hadley Cell increases baroclinicity in the subtropics through an increased poleward flux of angular momentum. Lorenz (1967, p 81, p 95) first explained how the westerly jet is maintained through angular momentum flux from the tropics. The analyses in Chapter Three clearly associated a stronger southern Hadley Cell with dry conditions in South Africa. The southern hemisphere has four zones of preferred conversion of eddy potential energy to eddy kinetic energy (baroclinic zones), as found in this thesis and supported by the literature (Hurrel and

Vincent; 1987; Todd and Washington, 1999; Cook, 2000). One such area is the south Atlantic convergence zone (Jones and Simmonds, 1993). Despite being more predominant during winter, activity in this zone is certainly evident during summer. Furthermore, in terms of transient systems, the speed of cyclone vortices is fastest in this area, again emphasizing the importance of transient systems in this area. The influence of transient systems on rainfall in South Africa, and on the weather patterns elsewhere (Sheng *et al,*, 1998; Watanabe and Kimoto, 1999), has been ascertained. Watanabe and Kimoto (1999) state that the details of how the tropics influence the mid-latitudes (North Atlantic area in their study) are yet to be determined. Findings in this thesis suggest that this takes place as part of the normal energy cycle with the transfer of zonal available potential energy through eddies to zonal kinetic energy. In this way tropical anomalies are transferred to the sub-tropics through the Hadley Cell, which increases the baroclinicity in the mid-latitudes resulting in more intense and northward displaced transient activity.

The findings here point to a situation where this increased hemispheric energy transfer becomes disruptive to summer rains in southern Africa. Increased energy conversions ultimately increase the zonal kinetic energy, or barotropic component. Although disturbances of this component of the circulation were shown to be an initiator of rainfall events, the number of cases where less than half of those associated with the shear component. Sutcliff's anticyclonic disruption (Sutcliff, 1953) which favours the development of cut-off lows in the mid-troposphere, was shown to occur when there is an increase in the shear component of the wind and a decrease in the vertical mean component. These systems, which are clearly associated with significant rainfall events, will be less favoured during periods of higher zonal

kinetic energy. Furthermore, the wettest months correspond to the warmest austral months, when energy transfer from the tropics to pole is at a minimum, giving further support to the theory that increased energy exchange disrupts summer rainfall. Therefore, it would appear that although transient systems are important for the initiation of rainfall events, the maintenance of summer rainfall, especially during normal years, is governed to a large degree by local forcing. This occurs typically through positive feedback mechanisms with soil moisture (e.g. Douville *et al.*, 2001) and vegetation (e.g. Zheng and Eltahir, 1998). In this case, local forcing possibly plays a much greater role in rainfall variability over South Africa than was previously believed.

Summary

The chapter paints a compound picture of large-scale energy exchange and how it appears to be linked to rainfall in South Africa through interactions of mid-latitude and tropical disturbances. During rainfall events the dominant circulation near the surface is a tropical-temperate-trough with an approaching trough in the mid-troposphere. The conversion of eddy available potential energy to eddy kinetic energy over the land at this time clearly demonstrates the importance of the cloud-band in the energy cycle

The South Atlantic Ocean is one of four preferred areas of energy conversion in the southern hemisphere, the reason for which is yet to be determined. The energy conversion takes place mostly through transient system activity. Generally this activity intensifies and shifts northward during dry summer seasons in South Africa. Results suggest that a stronger global energy exchange generally disrupts summer rainfall in South Africa. Also, local forcing probably plays an important role in rainfall variability.

Chapter Five

Operational Possibilities using GCMs

Introduction

This study has examined various key elements regarding the question of rainfall variability in South Africa. Foremost among these is the energy cycle. For example, a stronger southern Hadley Cell in the tropics and increased baroclinic mid-latitude wave activity south of Africa are associated with drier conditions. This chapter now undertakes a preliminary evaluation of one area of relevance for these conclusions reached so far, namely the application of General Circulation Models (GCMs) for seasonal forecasting. In the quest to provide seasonal forecasts using GCMs it is fundamental that the models accurately reflect the atmospheric dynamics. Failing to do so would indicate a serious deficiency in the GCMs and cast doubt on their usability in seasonal forecasting.

The objectives of this chapter are to perform a general evaluation of inter-annual and intra-seasonal variability in two GCMs in a qualitative and quantitative sense, and to assess the potential for these models to produce skilful seasonal forecasts of various rainfall characteristics.

General Circulation Model Simulations

Daily output from two atmospheric GCM hindcasts is available for a fifteen-year period from 1985 to 1999. The runs were performed as part of a project funded by the Innovation Fund sponsored by the South African government Department of Arts, Culture, Science and Technology[4]. The purpose of the hindcast simulation is to assess each model's ability to capture the general circulation from the daily to inter-annual scale when forced with observed global sea surface temperatures (as decribed later). Very often GCMs simulate the time-averaged circulation adequately but fail to reproduce synoptic-scale systems at the correct frequency and intensity. This can be particularly evident in long simulations after the effect of initial conditions has elapsed. For this reason the 15-year simulations provide an ideal opportunity for GCM evaluation in terms of the above considerations.

The first GCM evaluated here is a coarse resolution (T30) spectral model, developed at the Center for Ocean-Land-Atmosphere Studies (COLA). The model has been used operationally since 1995 at the South African Weather Service to produce monthly and seasonal forecast guidance. The model is described by Kirtman *et al.* (1997) and its application at the SA Weather Service by Tennant (1999). The model has 18 unevenly spaced sigma layers in the vertical. Prognostic variables include surface pressure, divergence, vorticity, virtual temperature and specific humidity on all 18 levels. The physics include a Simple Biosphere model (SiB) (Sellers *et al.*, 1986).

---

[4] http://www.dacst.gov.za/science_technology/innovation/innov_home.htm

The second model is the Third Hadley Centre Atmospheric Model (HADAM3). This hydrostatic grid-point model has a resolution of 3.75° longitude by 2.5° latitude. The vertical scheme uses hybrid *eta* coordinates on 19 levels and the prognostic variables include zonal and meridional wind components, geopotential height, specific humidity and liquid-water potential temperature. A comprehensive description of this model and an evaluation in terms of mean climate and the impacts of the physical parameterizations can be found in Pope *et al.* (2000).

Observed sea surface temperature (SST) data used for these model simulations were derived from the Reynolds monthly mean dataset on a 1° x 1° grid (Reynolds and Smith, 1994). An ensemble of five simulations were generated by initializing the models one month apart, at the start of July to November of 1985. Simulations were continued until the end of 1999.

The December-January-February (DJF) daily data were extracted and a number of energy and flux fields calculated, as done using the NCEP reanalysis data in the previous chapters. Four standard pressure levels in the vertical were available from both GCMs, *viz.* 850-, 700-, 500- and 200-hPa, and were used for the comparative analysis. It is felt that the four standard pressure levels are sufficient for the purpose of evaluation in this instance. Owing to the difference in the horizontal resolution of the two GCMs and the reanalysis data a direct comparison of the data requires horizontal interpolation. However, a qualitative assessment of the inter-annual and intra-seasonal variability is sufficient to determine whether these GCMs have the potential to be used as guidance for predicting event characteristics on a seasonal scale. Seasonal values of zonal-mean kinetic and available potential energy,

the conversion of eddy available potential energy into eddy kinetic energy and daily values of moisture flux in the 850-700 hPa layer were calculated on the respective model output grids.

Quantitative comparisons between the GCMs require data on a common grid. An interpolation function using the model output grid-box average was used to convert the 850 hPa streamfunction to a 2.5° x 2.5° grid. The grid-box average was chosen because gridded GCM output is representative of the entire grid box. When interpolating the model output to a finer grid (*viz.* NCEP reanalysis grid) the NCEP data will, by comparison, have a higher variance. However, the decrease in model grid-point distance is not more than two-thirds of the original size. The comparison between models and NCEP data was done through the use of a SOM frequency map, to ascertain whether the GCMs simulated the observed daily circulation at the correct frequency. Reduced variance in GCM output may impact the actual frequency values but the pattern of frequencies across the SOM should still be similar to the observed, provided the GCM is doing a reasonable job. Biases attributable to coarse resolution may then be easily identified. It is shown later that this interpolation does not treat the coarser model unfairly.

Vertical mean- and shear-components of the wind were calculated for the GCMs using equations 3.8-3.11, except that only four pressure levels (*viz.* 850, 700 500 and 200 hPa) were used. These were submitted to a SOM analysis and the interannual changes in the node frequencies studied.

Qualitative General Circulation Model Evaluation

One of the most striking findings in the earlier stages of this thesis was the clear relationship between seasonal rainfall total and the latitudinal fluctuation of the kinetic energy of the mid-latitude westerlies. Consequently, as a starting point the wet season 1988/89 (La Niña) is now compared with the dry season 1991/92 (El Niño), firstly by considering the results from the NCEP reanalysis data, then comparing this with the GCM results. The NCEP reanalysis data shows that the mid-latitude jet in both hemispheres shifts closer to the equator during the dry season (Fig 5.1). In the southern hemisphere it has a lower energy peak but in the northern hemisphere it is higher. Both the COLA and HADAM3 GCMs capture the latitudinal shift of the jet, which is consistent through all the ensemble-members. The HADAM3 exhibits a larger spread among the ensemble-members, especially during the La Niña season (1988/89) suggesting that this model has higher internal variability. The COLA model has a particularly small spread across the ensembles in the southern hemisphere for both seasons. This would indicate a stable atmospheric response to a prescribed SST field but perhaps too restricted in terms of daily synoptic-scale disturbances generated by the model. The GCM kinetic energy peaks are higher than observed, particularly in the COLA GCM, but the HADAM3 captures the intensity changes reasonably accurately.

While the kinetic energy fields highlight the GCM's circulation properties, zonal mean available potential energy, which is based on temperature distribution, should reveal more about the GCMs ability to simulate the radiative processes in the atmosphere. During the El Niño event, an increase in available potential energy is

observed in the tropics (Fig. 5.2). This direct response to warmer tropical SSTs in the Pacific Ocean was well captured by both models. In the southern hemisphere mid-latitudes the potential energy minimum shifts towards the equator during El Niño events. The HADAM3 reproduces this shift more clearly than the COLA model, which over-estimates the available potential energy in the high latitudes.

These findings demonstrate that GCMs capture the inter-annual variability of seasonal-mean kinetic and potential energy fields reasonable accurately. It is also instructive to assess the spatial patterns of the eddies generated by the GCMs. For this, the time-averaged conversion of eddy available potential energy transfer to eddy kinetic energy for the simulation period is shown (Fig. 5.3). The NCEP data shows a band of transient wave activity in the Southern Ocean and in the vicinity of the Angola heat low, at 20°S over the African continent. The GCMs show the band of westerly systems in the Southern Ocean. However, the COLA model overestimates the intensity of the conversion and places the band somewhat to the north of the observed position. The HADAM3 model shows a weaker band than NCEP but seems to present the pattern more realistically than COLA. Over the continent the transient activity of the Angola heat low is not present in the COLA or HADAM3 models. Apart from this feature, the HADAM3 does a reasonable simulation of the transient subtropical energy conversions, while the COLA model produces a broad area of energy conversion over southern Africa.

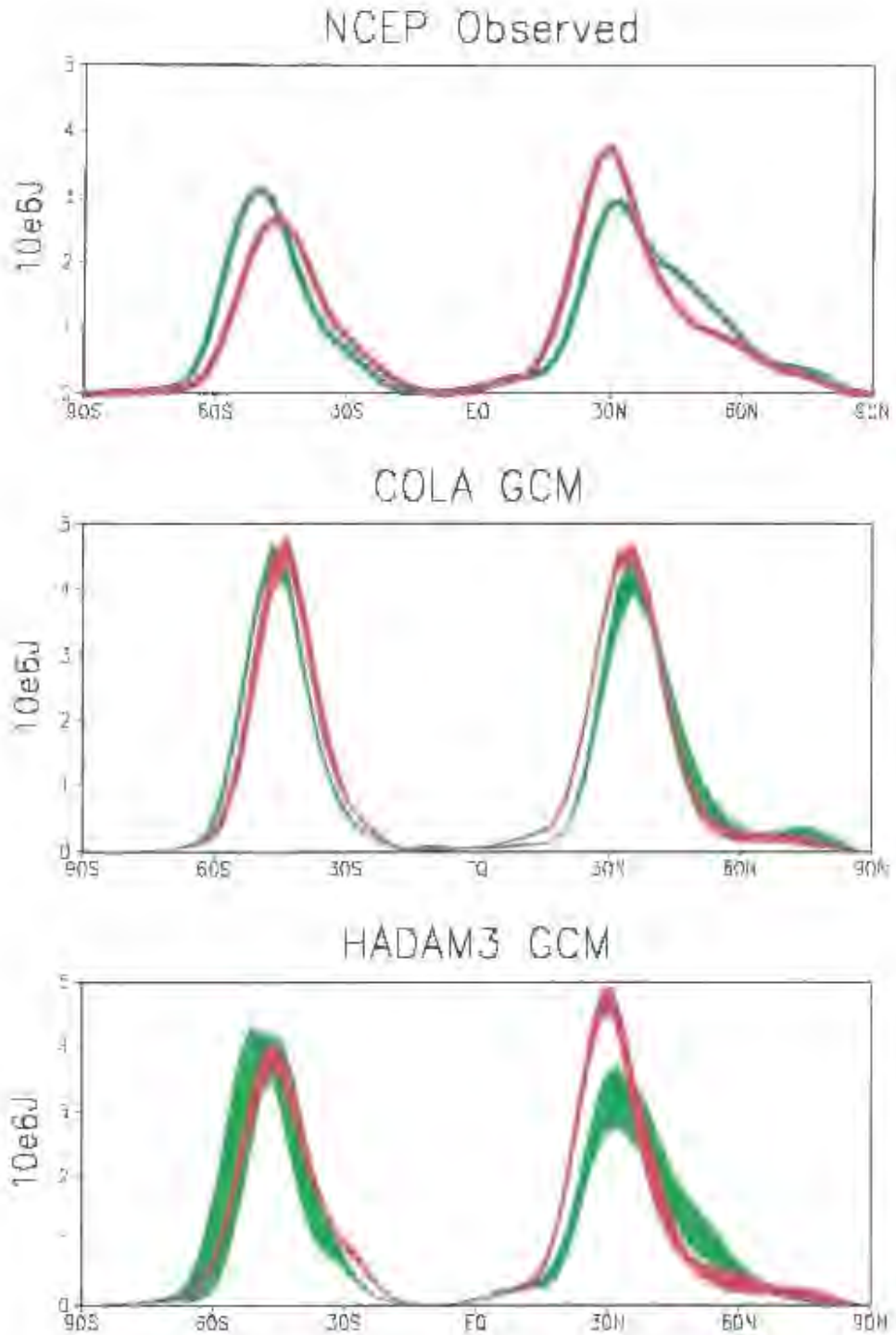

Figure 5.1: Composite of mean zonal kinetic energy for dry years (red) and wet years (green) for NCEP reanalysis, COLA and HADAM3 GCMs. Thickness of lines for GCMs represent 5-member ensemble spread.

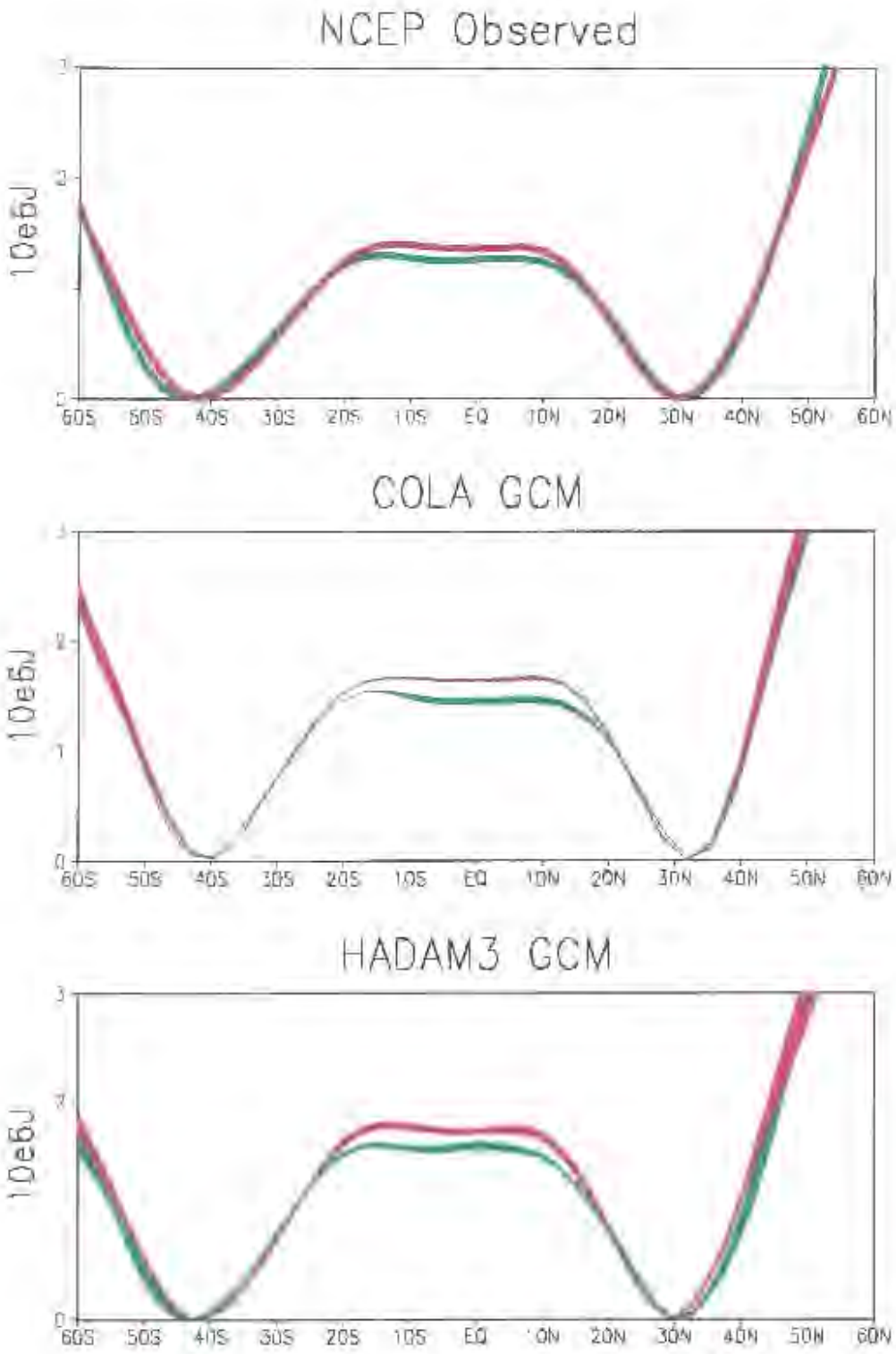

Figure 5.2: As for figure 5.1 but for mean zonal available potential energy.

The stationary component of energy conversion is shown by NCEP to consist of a northwest-southeast aligned trough axis across the central parts of South Africa and Namibia. Again the HADAM3 model makes a good spatial representation of the feature but underestimates its intensity. COLA spreads this feature to the northeast but anchors it to the Angola heat low. All models accurately capture the subsidence of warm air over the cold Benguela Current west of South Africa and Namibia, shown by the green shading in figure 5.3.

Another vital component of the atmosphere system is the transport of moisture, that takes place particularly in the lower layers. The zonal average of moisture transport, derived using equation 3.5, by the GCMs and NCEP in the 850-700 hPa layer is shown in figure 5.4. The GCMs capture the overall pattern quite well but overestimate the low-level inflow of the northern Hadley Cell during the austral summer. However, over the African longitudes (15°-37.5°E) the HADAM3 model's moisture transport is much closer to the NCEP pattern. There is a slight underestimation of southward transport in the mid-latitudes (possibly linked to the lower energy conversion shown for this region in figure 5.3) and a northward shift of the pattern in the tropics. The COLA model's overestimation of the northern Hadley Cell inflow is also evident over Africa but the peak of the southward flow is correctly placed between 10°-15°S. The model simulates the poleward transport of moisture in the mid-latitudes poorly in both hemispheres. The ensemble spread of the HADAM3 model is again quite high in the southern hemisphere, indicating high levels of internal variability in this model for that area.

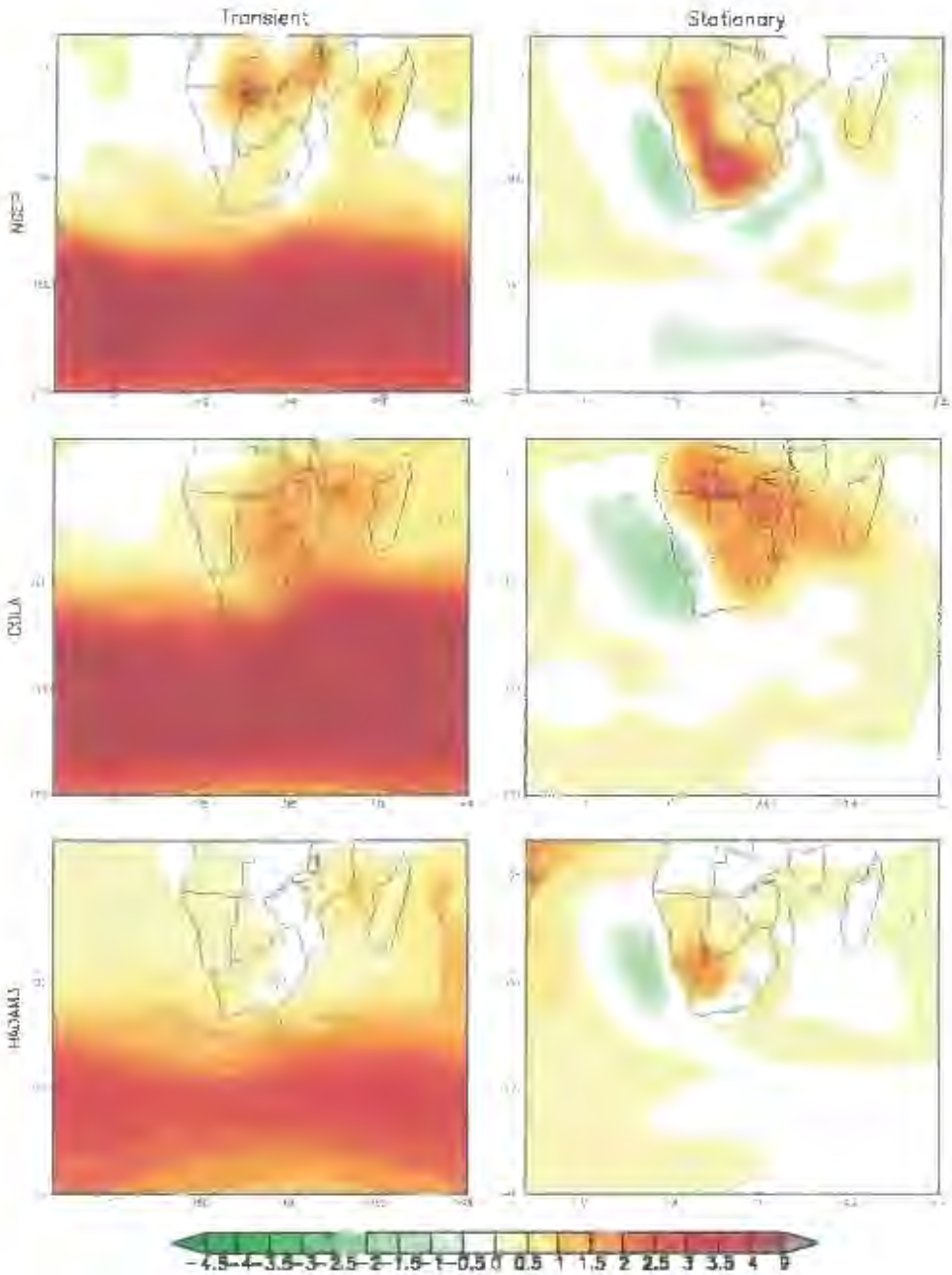

Figure 5.3: Climatological mean (1985-1999) conversion rate ($W.m^{-2}$) from eddy available potential energy into eddy kinetic energy by large-scale eddy convection by transient eddies (left) and stationary eddies (right) for NCEP reanalysis (top), COLA GCM (middle) and HADAM3 GCM (bottom). GCMs consist of 5-member ensemble average.

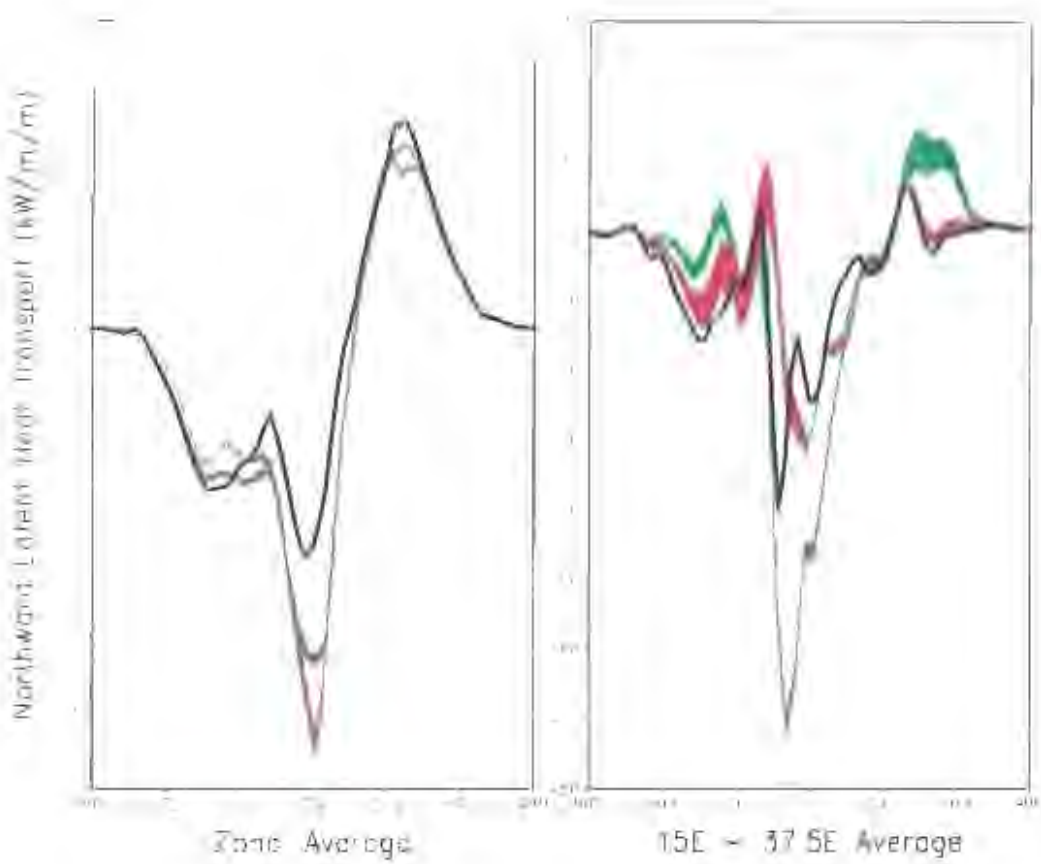

Figure 5.4: DJF climatological (1985-1999) 850-700 hPa layer-mean northward latent heat flux for NCEP reanalysis (black), COLA GCM (green) and HADAM3 GCM (red), zonally averaged (left) and African sector (right). Thickness of lines for GCMs represent 5-member ensemble spread.

Quantitative General Circulation Model Evaluation

The previous sections have hinted at possible deficiencies in the GCMs regarding the generation of specific circulation systems at the correct frequency. One way of quantifying this problem is to compare the daily frequency of particular circulation types as generated by the GCMs with the reanalysis data. The circulation types are defined by the nodes in a SOM trained on the reanalysis data (Fig. 5.5). The daily GCM output is then mapped to the SOM nodes and frequencies calculated (Fig. 5.6). The COLA model has a frequency pattern quite different from the observed, while the HADAM3 model does a better job but still has some problems.

Specifically, the COLA model overdoes the frequency of transient west-wind troughs south of South Africa (upper left of SOM) and the anticyclone centred at 30°S 30°E (right-hand-side of top row) (Figs. 5.5 & 5.6). It underestimates the scenario of zonal westerlies south of the country and elongated Indian Ocean anticyclone separated from the South Atlantic anticyclone by an inverted v-shaped trough over the western parts of South Africa and Namibia (centre of SOM). It also fails to simulate strong tropical cyclonic circulations in the Mozambique channel that are blocked by a southward displaced Indian Ocean anticyclone (bottom right corner). This is probably a symptom of the model's coarse resolution, and not a result of the interpolation to a finer grid, because the HADAM3 model, which was also interpolated and has a nominally equivalent resolution, does capture these features satisfactorily. Also, the COLA model overestimates variance of other cyclones in the mid-latitudes, as seen in the analysis.

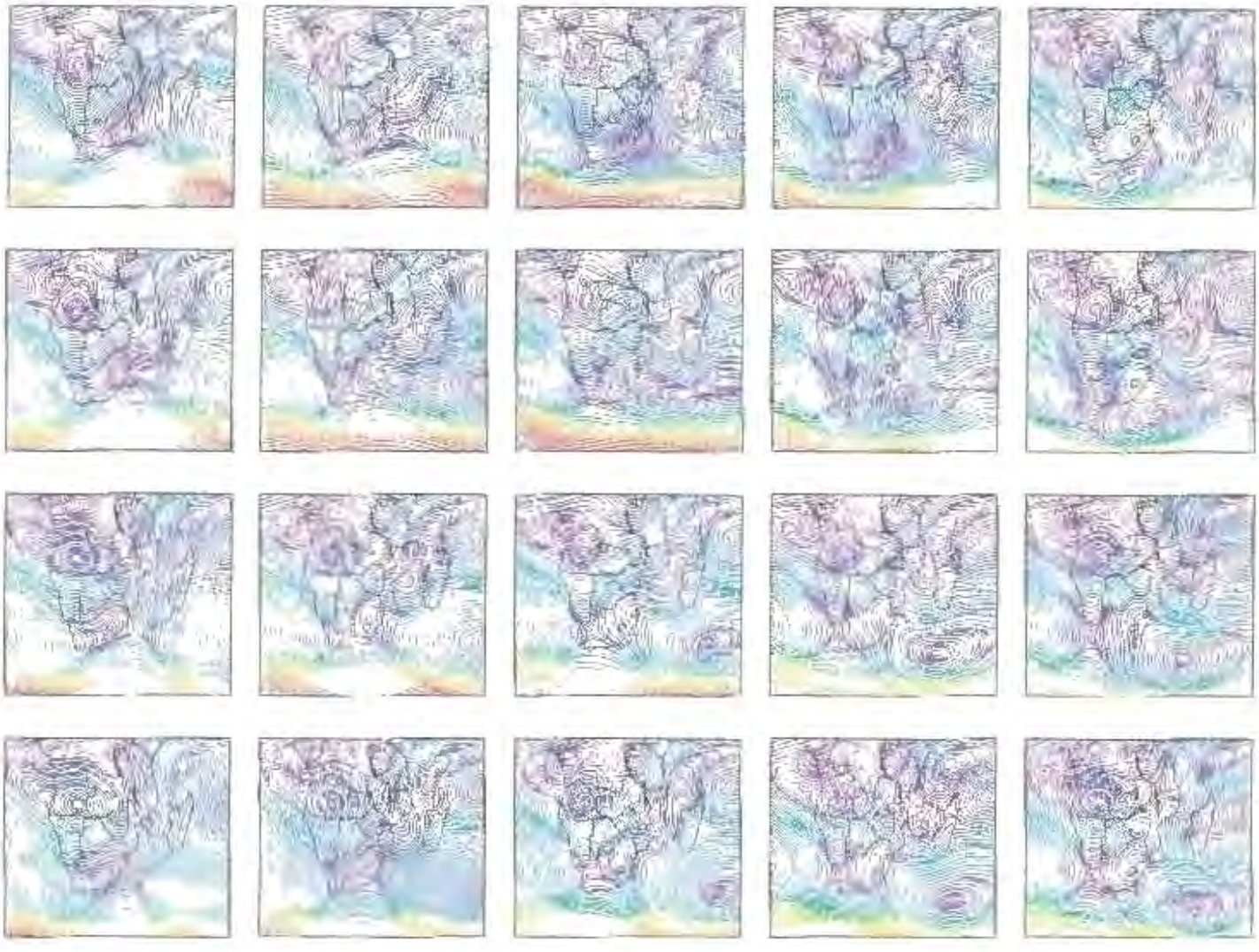

Figure 5.5: SOM of daily 850-hPa streamlines (non-divergent wind) of NCEP reanalysis data for DJF from 1985 to 1999. Shading indicates wind magnitude ($m.s^{-1}$).

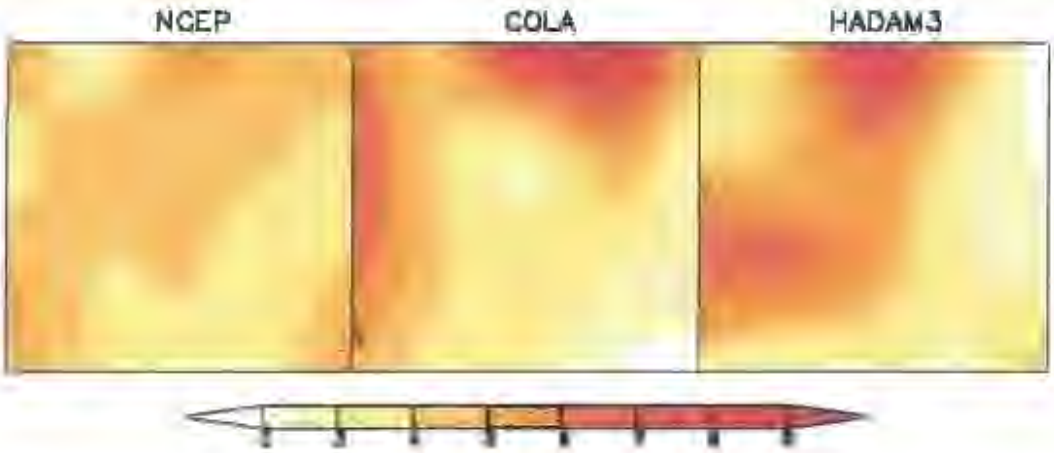

Figure 5.6: SOM-node frequency maps (%) for the 850 hPa streamlines (see figure 5.5) for the NCEP reanalysis, COLA GCM and HADAM3 GCM simulations. The GCM frequency maps include daily data from all five ensemble members.

The HADAM3 model seems to lack adequate frequency of occurrence of ridging South Atlantic anticyclones south of the country (top-right corner), and differs from NCEP in the frequency of northward protruding west-wind troughs (top-left corner). It does a satisfactory job with the simulation of cyclones around Madagascar. In this case the interpolation may play a role in the increased frequencies of the more prevalent nodes of the SOM (Fig. 5.6) but the overall pattern of frequencies is still a better representation of reality than that of COLA.

Thus it would appear that the GCMs have unique strengths and weaknesses. The COLA model's simulation of the large-scale energy processes is somewhat different to that observed with stronger energy exchange indicated by increased transient activity in the mid-latitudes, consistent with the high kinetic energy values shown in figure 5.1. The HADAM3 model represents the observed circulation much better but has errors in simulating eastward propagating systems near the continent.

Following this, a final step in this GCM evaluation is to determine whether the GCMs could be used successfully to provide skilful seasonal forecasts. Bearing in mind that the predictions are aimed at giving a probability that the seasonal rainfall will fall into either of the outer or middle three quintiles and what the event characteristics are likely to be. One of the strongest associations between rainfall and the general circulation was found (in Chapter Three) with the vertical mean- and shear-components of the wind. A composite of the SOM-node frequency changes between three dry (1991/92; 1992/93 & 1994/95) and three wet (1988/89; 1993/94 & 1995/96) seasons for both the vertical-mean wind (Fig. 5.7) and shear-wind (Fig. 5.8) show that the models capture this distinction in the daily circulation remarkably well. The COLA model is less clear with the shear-component which is possibly related to the problems the model has in simulating certain finer aspects of the circulation. The pattern distinctions between the wet and dry seasons as simulated by the GCMs (not shown) closely resemble those found in figures 3.16 and 3.17. It is interesting to note that not all of the years in these composites are associated with strong SST anomalies in the tropical Pacific Ocean. This means that the GCM predictability of the vertical mean and shear components of the atmospheric circulation can be skilful even when strong SST anomaly forcing is not present.

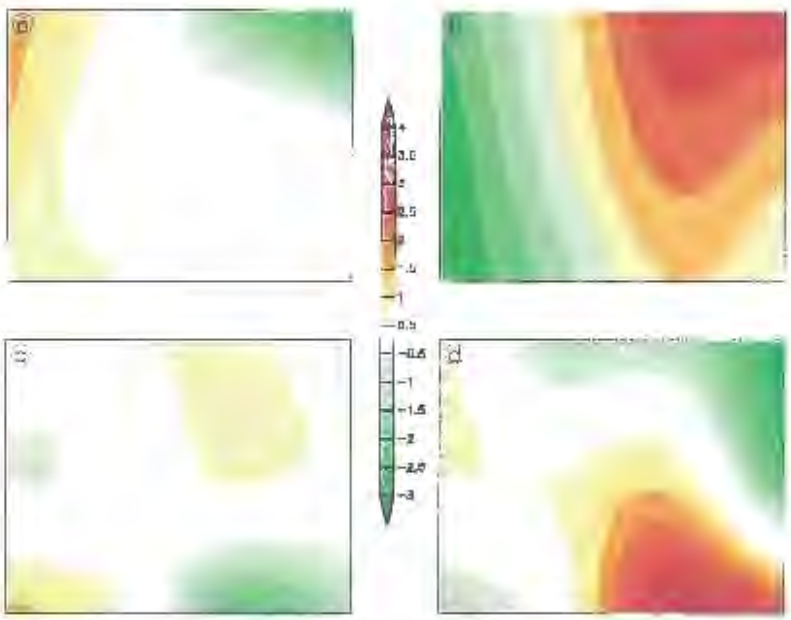

Figure 5.7: SOM-node frequency anomaly maps (%) for the vertical-mean wind from the COLA GCM simulation during a) dry and b) wet seasons, and HADAM3 GCM c) and d) respectively.

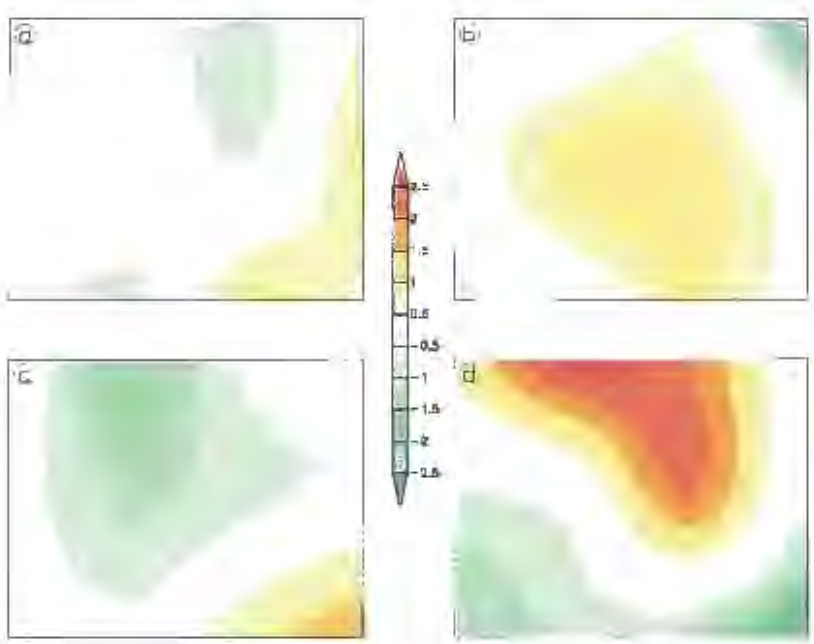

Figure 5.8: As for figure 5.7, but for the shear wind component.

In a study on the seasonal predictability of the Asian summer monsoon (Sperber *et al.*, 2001), the COLA and an earlier version of the HADAM3 model (*viz.* HADAM2b) were assessed. The authors concluded that errors in the sub-seasonal processes related to 850 hPa circulation are not correctly simulated by any of the seven GCMs tested and this affects the interannual variability and subsequent forecast skill. In contrast, this thesis has shown a link between South African summer rainfall and large-scale circulation aspects, which may not be so badly affected by the poor simulation of sub-seasonal processes by GCMs. This raises hope of more skilful seasonal predictions for this region at a large scale. Rainfall characteristics found in Chapter Two can assist in temporal downscaling of predictions leading to a greater range of forecast products without having to rely on GCM guidance. However, spatial downscaling would require far greater input from local forcing than is currently handled by GCMs. This is probably a task for fine-resolution limited area models.

Summary

A qualitative and quantitative evaluation is presented for a 15-year hindcast of two GCMs forced by observed SST data. GCMs accurately capture the inter-annual variability of zonal kinetic energy and zonal available potential energy between El Niño (dry) and La Niña (wet) years. The model climatology of the conversion of eddy available potential energy to eddy kinetic energy shows a good spatial representation of that observed. A comparison of the two GCMs shows that the HADAM3 model has a higher variability among ensemble members and is more realistic than the COLA model in most cases.

A SOM depicting the frequency of occurrence of different nodes (archetypes of 850 hPa streamfunction) shows that the HADAM3 model captures most of these nodes at a frequency similar to the NCEP data, but the COLA model has a somewhat different pattern. Nevertheless, both models are able to capture alterations to the frequency of SOM nodes trained on vertical-mean and shear components of the wind such that skilful forecasts of rainfall characteristics, which have been linked to these different nodes in Chapter Three, can be made.

Chapter Six

Conclusion and Recommendations

This thesis is a renewed examination into the underlying causes of rainfall variability in southern Africa. However, the approach is novel in the sense that recently available reanalysis data has been used to return to the basics of atmospheric motion in terms of the energy cycle. Furthermore, highly sophisticated multi-variate analysis techniques have provided new insight into circulation at the daily scale and also how this is linked to rainfall variability.

It has been clearly demonstrated that an analysis of a number of rainfall characteristics is a vital component in understanding rainfall variability and how this is linked to the general circulation. Many studies in the literature regarding seasonal forecasting or rainfall variability investigation restrict their analysis to seasonal rainfall totals. This study has addressed this issue by including nine different rainfall characteristics in the analysis, from which many interesting facts have emerged.

Foremost among these, is that categorizing rank ordered rainfall should be done in accordance with discontinuities in the data. The traditional tercile (three equiprobable categories) approach is not suited to the summer rainfall areas of South Africa. Rather, three categories consisting of the lowest quintile (five equiprobable categories), middle three quintiles combined and the highest quintile should represent below normal, normal and above normal rainfall respectively.

A second aspect is that significant rainfall events, in terms of wide-scale spread and high amounts, make up a large part of the seasonal rainfall total. This is confirmed when relating SOM nodes of vertically averaged relative humidity to rainfall characteristics and is consistent with the literature, providing the basis for an investigation into the causes of these significant rainfall events and their possible relation to large-scale atmospheric processes.

As has been found in the past, South African rainfall variability does relate clearly to the general circulation in the region. This is most evident in the frequency of daily archetypes of kinetic energy of the vertical mean and shear component of the wind in the mid-latitudes. Typically drier conditions are associated with a northward shift of the belt of mid-latitude westerlies. During wet years the kinetic energy of the vertical shear component of the wind increases over South Africa while the westerly belt shifts southward. This pattern is confirmed with analyses of zonal kinetic and available potential energy, the conversion of eddy available potential energy into eddy kinetic energy through large-scale overturning by the eddies and dry static energy fields.

Large-scale transport of moisture, heat and momentum, particularly over the African sector, show an inter-annual variability related to variability in rainfall characteristics. Dry conditions in South Africa and a stronger Hadley Cell are linked such that the stronger outflow from the Hadley Cell increases the subtropical jet and hence a northward displacement of the westerlies.

The majority of significant rainfall events in South Africa seem to be forced or associated with disturbances travelling in the 6-25 day band of the shear, and to a lesser extent the vertical-mean, component of the wind in the mid-latitudes. These were found to be mainly in the form of approaching mid-tropospheric troughs or cut-off low pressure systems accompanied by an Indian Ocean anti-cyclone at the surface. A series of equivalent barotropic (vertical mean) systems passing close to the country tended to result in drier periods.

Rainfall events play an important role in the energy exchange of the region, with a high correlation between rainfall and the conversion of eddy available potential energy to eddy kinetic energy. Similar energy exchange forms a fundamental part of the other cloud bands in the southern hemisphere, including the South Pacific Convergence Zone and the South Atlantic Convergence Zone. Activity around the southern hemisphere does appear to be linked. However, the mechanisms of these linkages are still somewhat in debate.

Direct coupling of South African rainfall to events such as ENSO does not appear to be robust. There does not seem to be any stationarity in such a link and global velocity potential fields show that strong anomalies in the Pacific Ocean do not extend all the way to Africa. Also, the Walker Cells along the equator do not show a clear sign reversal over Africa on an inter-annual scale.

The theory this thesis proposes is that these events in the southern hemisphere are linked but that the mechanism is somewhat different than a simple shift in the Walker Cells. It all comes back to the global energy cycle. When there are

fluctuations in the zonal available potential energy (a measure of the pole to equator temperature gradient) these affect the Hadley Cells. The result of this is that the mid-latitude westerlies are changed in sync with the poleward momentum flux. The resultant perturbations in the form of eddies in the westerlies are governed by baroclinicity in the region. Owing to a longitudinal variation of land and sea surface heat fluxes in the southern hemisphere (which in themselves are tied to atmospheric processes) the baroclinic activity tends to focus in preferred areas. The South Atlantic Ocean is one such area, and its proximity to South Africa results in the mid-latitude activity in this area having a great impact on South African rainfall, as seen in the forcing of rainfall events.

The cycle continues by mid-latitude disturbances forcing tropical disturbances which later feed back to the mid-latitudes through tropical-temperate-troughs, a well-known feature in the South African climate. This cycle, as described, is supported in the literature applied to tropical-extratropical interactions in the southern hemisphere, Pacific North America and North Atlantic regions.

The inherent variability and non-linear interaction in the mid-latitude processes is consistent with observed low predictability of the seasonal climate in the mid-latitudes and sub-tropics. However, having established robust links between rainfall and the global energy cycle, which is a stable component of the atmosphere system, prospects of skilful predictions of seasonal rainfall characteristics are greatly improved. One of the most encouraging findings in this thesis is that a preliminary evaluation of an ensemble of 15-year hindcasts from two GCMs reveals that these models are able to capture fluctuations in the global energy cycle reasonably

accurately. This makes it possible that the techniques developed in this study to link archetypes of the atmospheric circulation to rainfall characteristics may be used to provide skilful predictions of these rainfall characteristics. This is possible without the GCMs capturing the smaller-scale processes accurately, however, it is also clear from this thesis that local conditions play an important role in rainfall. One such condition is the vertical stability of the atmosphere which appears to be closely related to rainfall in South Africa, in that stable conditions possibly imposed by larger-scale forcing reduce locally forced convection. This is in turn affected by local features, such as topography and soil moisture.

The lack of a clear link between moisture flux and rainfall could be the result of two issues. The first is that moisture is a necessary but not sufficient requirement for rainfall. This is where the dynamical forcing from the mid-latitudes plays an important role. The second, and equally important, is that moisture supply over continental areas, although ultimately sourced from the oceans, is also sourced from the soil and vegetation. Fluctuations in soil moisture and vegetation are known to have large effects on rainfall and in order to really model the atmosphere well these local forcings must be simulated as realistically as possible. One such way is through high resolution regional limited area models, nested in a global model.

Findings here have opened up a new view on the variability of the southern Africa climate system, and consequently raised a number of intriguing questions about the general circulation and rainfall variability, providing avenues for further research in this field. Foremost among these are:

a) Quantifying how much of South Africa's rainfall variability is determined by local forcing in terms of antecedent conditions which affect soil moisture and vegetation cover.

b) Why is baroclinic activity in the South Atlantic Ocean stronger than elsewhere in the southern hemisphere and is this an evolving feature which so happened to occur during the period of this study or is it a stable climatological feature related to southern hemisphere topography?

c) What causes fluctuations in the zonal available potential energy field at the seasonal to inter-annual timescale. Is it related to extra-terrestrial forcing by the sun or lunar tides, or is it simply part of the natural internal variability of the ocean-atmosphere climate system?

Finally, the five hypotheses introduced in Chapter One have been positively satisfied. Rainfall characteristics do reveal a number of aspects that enhance the understanding of processes related to rainfall, and in Chapter Two, it was shown how the rainfall total alone cannot adequately describe the nature of a season's rainfall. Normal rainfall is often loosely regarded as the middle tercile but findings in Chapter Two indicate that, for summer rainfall regions of South Africa, the middle three quintiles combined best represent normal rainfall. Seasons where the rainfall coincided with the highest and lowest quintiles are clearly associated with changes in the frequencies of daily circulation types, as demonstrated in Chapter Three. This

is particularly true with the kinetic energy of the vertical-mean and shear-components of the wind and other aspects related to the global energy cycle. Significant rainfall events, defined in Chapter Four, were predominantly associated with mid-latitude and/or tropical disturbances indicating the importance of these disturbances in initiating rainfall events over South Africa. GCMs, evaluated in Chapter Five, are reasonably capable of capturing inter-annual variability but not all are able to simulate the daily circulation satisfactorily. Notwithstanding, SOM-node frequency maps of GCM simulations showed that the GCMs certainly do posses predictive skill, particularly in terms of the energy cycle. Consequently, seasonal forecasts may be improved if GCM forecast output, including ensemble products, were used more productively. This would require a re-visit to establish the links between regional rainfall and the large-scale circulation.

Appendix A

LIST OF ABBREVIATIONS

ACW	Antarctic Circumpolar Wave
APE	Available Potential Energy
App	Approaching Trough
CE	Trough East of South Africa
COLA	Center for Ocean-Land-Atmosphere Studies
DACST	Department of Arts, Culture, Science and Technology
DJF	December - January - February
ENSO	El Niño Southern Oscillation
EOF	Empirical Orthogonal Function
GARP	Global Atmospheric Research Project
GCM	General Circulation Model of the atmosphere
GDAS	Global Data Assimilation System
HADAM3	Third Hadley Centre Atmospheric Model
HP	Continental Anticyclone
IA	Indian Ocean Anticyclone
ITCZ	Inter-Tropical Convergence Zone
LP	Cyclonic Flow
MSE	Moist Static Energy
NCEP	National Centers for Environmental Prediction

NMS	National Meteorological Service
PAOB	Australian Bureau of Meteorology Paid Observations
PNA	Pacific North America
SACZ	South Atlantic Convergence Zone
SARCOF	Southern African Regional Climate Outlook Forum
SASAS	South African Society for Atmospheric Sciences
SiB	Simple Biosphere
SOM	Self Organizing Map
SPCZ	South Pacific Convergence Zone
SST	Sea Surface Temperature
T30	Spectral GCM with triangular truncation at wave number 30 (Resolution of the COLA GCM discussed in this thesis)
TL	Tropical Low
TTT	Tropical Temperate Trough
UCT	University of Cape Town

References

Barnett, T.P. and R. Preisendorfer, 1987. Origins and Levels of Monthly and Seasonal Forecast Skill for United States Surface Air Temperatures Determined by Canonical Correlation Analysis. *Mon. Wea. Rev.*, **115**, 1825-1850.

Barnston, A.G. and C.F. Ropelewski, 1992. Prediction of ENSO episodes using canonical correlation analysis. *J. Climate*, **5**, 1316-1345.

Blackmon, M.L., 1976. A Climatological Spectral Study of the 500 mb Geopotential Height of the Northern Hemisphere, *J. Atmos. Sci.*, **33**, 1607-1623.

Bloomfield, P., 1976. *Fourier Analysis of Time Series: An Introduction.* Wiley, New York, 258 pp.

Chen, T-C., 1983. The Energy Exchange between the Baroclinic and Barotropic Components of Atmospheric Flow in the Tropics during the FGGE Summer. *Mon. Wea. Rev.*, **111**, 1389-1396.

Chen, T-C. and M-C. Yen, 1985. Note on the kinetic energy budget analysis of the atmospheric baroclinic and barotropic flows. *J. Meteorol. Soc. Japan*, **63**, 685-693.

Cook, K.H., 2000. The South Indian Convergence Zone and Interannual Rainfall Variability over Southern Africa. *J. Climate*, **13**, 3789-3804.

D'Abreton, P.C. and J.A. Lindesay, 1993. Water vapour transport over southern Africa during wet and dry early and late summer months. *Int. J. Climatol.*, **13**, 151-170.

D'Abreton, P.C. and P.D. Tyson, 1995. Divergent and Non-Divergent Water Vapour Transport over Southern Africa During Wet and Dry Conditions. *Meteorol. Atmos. Phys.*, **55**, 47-59.

Doblas-Reyes, F.J. and M. Déqué, 1998. A Flexible Bandpass Filter Design Procedure Applied to Midlatitude Intraseasonal Variability. *Mon. Wea. Rev.*, **126**, 3326-3335.

Douville, H., F. Chauvin and H. Broqua, 2001. Influence of Soil Moisture on the Asian and African Monsoons. Part I: Mean Monsoon and Daily Precipitation. *J. Climate*, **14**, 2381-2403.

Doviak, R.J., 1983. A Survey of Radar Rain Measurement Techniques, *J. Appl. Meteorol.*, **22**, 832 - 849.

Eastin, M.D. and D.G. Vincent, 1998. A 6-Yr Climatology of Vertical Mean and Shear Components of Kinetic Energy for the Australian-South Pacific Jet Stream. *J. Climate*, **11**, 283-291.

Eckert, P., D. Cattani and J. Ambühl, 1996. Classification of ensemble forecasts by means of an artificial neural network. *Meteorol. Appl.*, **3**, 169-178.

Ellis, R. and D. Gulick, 1986. *Calculus with Analytical Geometry 3rd Edition*, Harcourt Brace Jovanovich Publishers, San Diego, p 407-410.

Gong, X. and M.B. Richman, 1995. On the Application of Cluster Analysis to Growing Season Precipitation Data in North America East of the Rockies. *J. Climate*, **8**, 897-931.

Haltiner, G.J. and R.T. Williams, 1975. Some Recent Advances in Numerical Weather Prediction. *Mon. Wea. Rev.*, **103**, 571-590.

Harrison, M.S.J., 1983. Rain day Frequency and Mean Daily Rainfall Intensity as Determinants of Total Rainfall over the Eastern Orange Free State, *J. Climatol.* **3**, 35-45.

Harrison, M.S.J., 1984a. The annual rainfall cycle over the central interior of South Africa. *S. Afr. Geogr. J.*, **66**, 47-64.

Harrison, M.S.J., 1984b. A generalized classification of South African summer rain-bearing synoptic systems. *J. Climatol.*, **4**, 547-560.

Hewitson, B.C and R.G. Crane, 1996. Climate downscaling: techniques and application. *Climate Res.*, **7**, 85-95.

Hewitson, B.C and R.G. Crane, 2002. Self Organizing Maps: Applications to Synoptic Climatology. *Accepted for publication in Climate Res.*

Holopainen, E.O., 1970. An observational study of the energy balance of the stationary disturbances in the atmosphere. *Quart. J. R. Meteorol. Soc.*, **96**, 626-644.

Holton, J.R., 1992. *An Introduction to Dynamic Meteorology, Third Ed.*. Academic Press, San Diego, 511 pp.

Hou, A.Y., 1998. Hadley Circulation as a Modulator of the Extratropical Climate. *J. Atmos. Sci.*, **55**, 2437-2457.

Huang, H-J. and D.G. Vincent, 1985. Significance of the South Pacific Convergence Zone in Energy Conversions of the Southern Hemisphere during FGGE, 10-27 January 1979. *Mon. Wea. Rev.*, **113**, 1359-1371.

Huffman, G.J., R.F. Adler, P. Arkin, A. Chang, R. Ferraro, A. Gruber, J. Janowiak, A. McNab, B. Rudolf and U. Schneider, 1997. The Global Precipitation Climatology Project (GPCP) Combined Precipitation Dataset, *Bull. Amer. Meteor. Soc.*, **78**, 5-20.

Hurrell, J.W. and D.G. Vincent, 1987. Significance of the South Pacific Convergence Zone (SPCZ) in the Energy Budget of the Southern Hemisphere Tropics. *Mon. Wea. Rev.*, **115**, 1797-1801.

Huth, R., 2001. Disaggregating Climatic Trends by Classification of Circulation Patterns, *Int. J. Climatol.*, **21**, 135-153.

Jones, D.A. and I. Simmonds, 1993. A climatology of Southern Hemisphere extratropical cyclones. *Clim. Dynamics*, **9**, 131-145.

Jury, M.R., H.R. Valentine and J.R.E. Lutjeharms, 1993. Influence of the Aghulas Current on Summer Rainfall along the Southeast Coast of South Africa. *J. Appl. Meteorol.*, **32**, 1282-1287.

Jury, M.R., C.A. McQueen and K.M. Levey, 1994. SOI and QBO signals in the African region. *Theor. Appl. Climatol.*, **8**, 17-30.

Jury, M.R., B. Pathack, C.J. de W Rautenbach and J. van Heerden, 1996. Drought over South Africa and Indian Ocean SST: Statistical and GCM Results. *The Global Atmosphere and Ocean System*, **4**, 47-63.

Jury, M.R., 1999. Intra-seasonal Convective Variability over Southern Africa: Principal Component Analysis of Pentad Outgoing-longwave Radiation Departures 1976-1994. *Theor. Appl. Climatol.*, **62**, 133-146.

Jury, M.R., H.M. Mulenga and S.J. Mason, 1999. Exploratory Long-Range Models to Estimate Summer Climate Variability over Southern Africa. *J. Climate*, **12**, 1892-1899.

Kalnay, E., K.C. Mo and J. Paegle, 1986. Large-Amplitude, Short-Scale Stationary Rossby Waves in the Southern Hemisphere: Observations and Mechanistic Experiments to Determine their Origin. *J. Atmos. Sci.*, **43**, 252-275.

Kalnay, E., M. Kanamitsu, R. Kistler, W. Collins, D. Deaven, L. Gandin, M. Iredell, S. Saha, G. White, J. Woollen, Y. Zhu, M. Chelliah, W. Ebisuzaki, W. Higgins, J. Janowiak, K.C. Mo, C. Ropelewski, J. Wang, A. Leetma, R. Reynolds, R. Jenne and J. Dennis, 1996: The NCEP/NCAR 40-year reanalysis project. *Bull. Amer. Meteorol. Soc.*, **77**, 437-471.

Kalnay, E., S.J. Lord and R.D. McPherson, 1998. Maturity of Operational Numerical Weather Prediction: Medium Range. *Bull. Amer. Meteorol. Soc.*, **79**, 2753-2892.

Kanamitsu, M., J.C. Alpert, K.A. Campana, P.M. Caplan, D.G. Deaven, M. Iredell, B. Katz, H.-L. Pan, J. Sela, and G.H. White, 1991. Recent Changes Implemented into the Global Forecast System at NMC. *Wea. Forecasting*, **6**, 425-435.

Kann, D.M., S-K. Yang and A.J. Miller, 1994. Mean meridional transport of energy in the earth-atmosphere system using NMC global analyses and ERBE radiation data. *Tellus*, **46A**, 553-565.

Kelbe, B.E., M. Garstang and G. Brier, 1983. Analysis of Rainfall Variability in the Northeastern Region of South Africa. *Arch. Met. Geoph. Biocl.*, Ser B, **32**, 231-252.

Kidson, J.W., 1999. Principal Modes of Southern Hemisphere Low-Frequency Variability Obtained from NCEP-NCAR Reanalyses. *J. Climate*, **12**, 2808-2830.

Kirtman, B.P., J. Shukla, B. Huang, Z. Zhu and E.K. Schneider, 1997. Multiseasonal Predictions with a Coupled Tropical Ocean-Global Atmosphere System. *Mon. Wea. Rev.*, **125**, 789-808.

Kistler, R., E. Kalnay, W. Collins, S. Saha, G. White, J. Woollen, M. Chelliah, W. Ebisuzaki, M. Kanamitsu, V. Kousky, H. van den Dool, R. Jenne, and M. Fiorino, 2001. The NCEP-NCAR 50-Year Reanalysis: Monthly Means CD-ROM and Documentation. *Bull. Amer. Meteorol. Soc.*, **82**, 247 - 268.

Klopper, E., 1999. The use of seasonal forecasts in South Africa during the 1997/98 rainfall season. *Water SA*, **25**, 311-316.

Ko, K-C. and D.G. Vincent, 1995. A Composite Study of the Quasi-Periodic Subtropical Wind Maxima over the South Pacific during November 1984-April 1985. *J. Climate*, **8**, 579-588.

Kohonen, T., 1995. *Self-organizing maps*. Springer, Berlin, 362 pp.

Kuhnel, I. 1990. Tropical-extratropical cloudbands in the Australian region. *Int. J. Climatol.*, **10**, 341-364

Kutzbach, J.E., 1967. Empirical Eigenvectors of Sea-Level Pressure, Surface Termperature and Precipitation Complexes over North America. *J. Appl. Meteorol.*, **6**, 791-802.

Lamb, H.H., 1950. Types and spells of weather around the year in the British Isles : Annual trends, seasonal structure of the year, singularities. *Q. J. Roy. Meteorol. Soc.*, **76**,393-438.

Lamb, H.H., 1988. *Weather, Climate and Human Affairs*. Routledge, London, 364 pp.

Landman, W.A. and S.J. Mason, 1999a. Operational Long-Lead Prediction of South African Rainfall using Canonical Correlation Analysis. *Int. J. Climatol.*, **19**, 1073-1090.

Landman, W.A. and S.J. Mason, 1999b. Change in the association between Indian Ocean sea-surface temperatures and summer rainfall over South Africa and Namibia. *Int. J. Climatol.*, **19**, 1477-1492.

Landman, W.A., S.J. Mason, P.D. Tyson and W.J. Tennant, 2001. Retro-active Skill of Multi-tiered Forecasts of Summer Rainfall over Southern Africa. *Int. J. Climatol.*, **21**, 1-19.

Lange, H.J., 1979. Spectral Energetics by Numerical Analysis, *Contrib. Atmos. Phys.*, **52**, 106-125.

Lee, A.C.L., 1981. Smoothing and filtering of meteorological data, *Meteorol. Mag.*, **110**, 115-132.

Levey, K.M. and M.R. Jury, 1996. Composite Intraseasonal Oscillations of Convection over Southern Africa, *J. Climate*, **9**, 1910-1920.

Lindesay, J., M.S.J. Harrison and M.P. Haffner, 1986. The Southern Oscillation and South African rainfall. *S. Afr. J. Sci.*, **82**, 196-198.

Lindesay, J.A. and M.R. Jury, 1991. Atmospheric Circulation Controls and Characteristics of a Flood Event in Central South Africa. *Int. J. Climatol.*, **11**, 609-627.

Lorenz, E.N., 1955. Available Potential Energy and the Maintenance of the General Circulation. *Tellus*, **7**, 157-167.

Lorenz, E.N., 1956. Empirical orthogonal functions and statistical weather prediction. M.I.T. Dept. of Meteorology, Sci. Rept. No. 1, Contract AF19(604)-1566, 49 pp.

Lorenz, E.N., 1963. Deterministic nonperiodic flow. *J. Atmos. Sci.*, **20**, 130-141.

Lorenz, E.N., 1967. *The Nature and Theory of the General Circulation of the Atmosphere.* World Meteorological Organization, Geneva, 161 pp. (WMO No. 218-TP. 115)

Marshall, G.J. and S.A. Harangozo, 2000. An appraisal of NCEP/NCAR reanalysis MSLP data viability for climate studies in the South Pacific. *Geophys. Res. Lett.*, **27**, 3057-3060.

Mason, S.J. and P.D. Tyson, 1992. The Modulation of Sea Surface Temperature and Rainfall Associations over Southern Africa with Solar Activity and the Quasi-Biennial Oscillation. *J. Geophys. Res.*, **97**, 5847-5856.

Mason, S.J., 1995. Sea-surface Temperature-South African Rainfall Associations, 1910-1989. *Int. J. Climatol.*, **15**, 119-135.

Mason, S.J. and M.R. Jury, 1997. Climate variability and change over southern Africa: a reflection on underlying processes. *Prog. Phys. Geogr.*, **21**, 23-50.

Mason, S.J., 1998. Seasonal forecasting of South African rainfall using a non-linear discriminant analysis model. *Int. J. Climatol.*, **18**, 147-164.

Masuda, K., 1988. Meridional heat transport by the atmosphere and the ocean: analysis of FGGE data. *Tellus*, **40A**, 285-302.

Meehl, G.A., G.N. Kiladis, K.M. Weickmann, M. Wheeler, D.S. Gutzler and G.P. Compo, 1996. Modulation of equatorial subseasonal convective episodes by tropical-extratropical interaction in the Indian and Pacific Ocean regions. *J. Geophys. Res.*, **101**, 15033-15049.

Michaud, R. and J. Derome, 1991. On the mean meridional transport of energy in the atmosphere and oceans as derived from six years of ECMWF analyses. *Tellus*, **43A**, 1-14.

Newell, R.E., J.W. Kidson, D.G. Vincent and G.J. Boer, 1972. *The General Circulation of the Tropical Atmosphere and Interactions with Extratropical Latitudes, Volume I.* The MIT Press, Cambridge, 258 pp.

Nicholls, N., 1977. Tropical-extratropical interactions in the Australian region. *Mon. Wea. Rev.*, **105**, 826-832.

North, G.R., 1984. Empirical Orthogonal Functions and Normal Modes. *J. Atmos. Sci.*, **41**, 879-887.

Oort, A.H., 1964. On Estimates of the Atmospheric Energy Cycle. *Mon. Wea. Rev.*, **92**, 483-493.

Oort, A.H., 1971. The Observed Annual Cycle in the Meridional Transport of Atmospheric Energy. *J. Atmos. Sci.*, **28**, 325-339.

Palmer, T.N., 1993. Extended-Range Atmospheric Prediction and the Lorenz Model. *Bull. Amer. Meteorol. Soc.*, **74**, 49-66.

Peppler, R.A., D.G. Vincent, 1983. Basic State Energy Budget Analysis for Phases 1, 2 and 3 of GATE. *Mon. Wea. Rev.*, **111**, 359-369.

Peterson, R.G. and W.B. White, 1998. Slow oceanic teleconnections linking the Antarctic Circumpolar Wave with the tropical El Niño-Southern Oscillation. *J. Geophys. Res.*, **103**, 24 573-24 583.

Pfeffer, R.L., 1960. *Dynamics of Climate*. Pergamon Press, Oxford, 137 pp.

Pope, V.D., M.L. Gallani, P.R. Rowntree and R.A. Stratton, 2000. The impact of new physical parametrizations in the Hadley Centre climate model: HadAM3. *Climate Dynamics*, **16**, 123-146.

Reason, C.J.C., R.J. Allan, J.A. Lindesay and T.J. Ansell, 2000. ENSO and Climatic Signals across the Indian Ocean Basin in the Global Context: Part I, Interannual Composite Patterns. *Int. J. Climatol.*, **20**, 1285-1327.

Reason, C.J.C., 2001a. Evidence for the Influence of the Agulhas Current on Regional Atmospheric Circulation Patterns. *J. Climate*, **14**, 2769-2778.

Reason, C.J.C., 2001b. Subtropical Indian Ocean SST dipole events and southern African rainfall. *Geophys. Res. Lett.*, **28**, 2225-2227.

Reynolds, R.W. and T.M. Smith, 1994. Improved global sea surface temperature analyses using optimum interpolation. *J. Climate*, **7**, 929-948.

Rhea, J.O., 1966. A Study of Thunderstorm Formation Along Dry Lines. *J. Appl. Meteorol.*, **5**, 58-63.

Richman, M.B., 1986. Rotation of Principal Components. *J. Climatology*, **6**, 375-378.

Rinne, J. and V. Karhila, 1979. Empirical orthogonal functions of 500mb height in the northern hemisphere determined from a large data sample. *Quart. J. R. Met. Soc.*, **105**, 873-884.

Rosen, R.D. D.A. Salstein and J.P. Peixoto, 1979a. Variability in the Annual Fields of Large-Scale Atmospheric Water Vapor Transport. *Mon. Wea. Rev.*, **107**, 26-37.

Rosen, R.D. D.A. Salstein and J.P. Peixoto, 1979b. Streamfunction Analysis of Interannual Variability in Large-Scale Water Vapor Flux. *Mon. Wea. Rev.*, **107**, 1682-1684.

Ruzmaikin, A, 1999. Can El Niño amplify the solar forcing of climate? *Geophys. Res. Lett.*, **26**, 2255-2258.

Salstein, D.A., R.D. Rosen, and J.P. Peixoto, 1980. Hemispheric Water Vapor Flux Variability-Streamfunction and Potential Fields. In: Deepak, A., T.D. Wilkerson and L.H. Ruhnke (eds.). *Atmospheric Water Vapor*, pp 557-574. Academic Press, New York.

Sammon, J.W. Jr., 1969. A non-linear mapping for data structure analysis, *IEEE Transactions on Computers*, **C-18(5)**, 401-409, May 1969.

Schulze, B.R., 1965. *Climate of South Africa: Part 8: General Survey, WB28.* South African Weather Bureau, Pretoria, 330 pp.

Schulze R.E., 1997. *South African Atlas of Agrohydrology and -Climatology.* Water Research Commission, Pretoria, Report TT82/96, p265.

Sela, J.G., 1980. Spectral Modeling at the National Meteorological Center. *Mon. Wea. Rev.*, **108**, 1279 - 1292

Sellers, P.J., Y. Mintz, Y.C. Sud and A. Dalcher, 1986. A Simple Biosphere Model (SIB) for Use within General Circulation Models. *J. Atmos. Sci.*, **43**, 505-531.

Sheng, J., J. Derome and M. Klasa, 1998. The Role of Transient Disturbances in the Dynamics of the Pacific-North American Pattern. *J. Climate*, **11**, 523-536.

Shukla, J. and K.R. Saha, 1974. Computation of Non-Divergent Streamfunction and Irrotational Velocity Potential from the Observed Winds. *Mon. Wea. Rev.*, **102**, 419-425.

Shukla, J., 1981. Dynamical prediction of monthly means. *J. Atmos. Sci.*, **38**, 2547-2572.

Shukla, J., L. Marx, D. Paolino, D. Straus, J. Anderson, J. Ploshay, D. Baumhefner, J. Tribbia, C. Brankovic, T. Palmer, Y. Chang, S. Schubert, M. Suarez and E. Kalnay, 2000. Dynamical Seasonal Prediction. *Bull. Amer. Meteorol. Soc.*, **81**, 2593-2606.

Sonka, S.T., S.L. Hofing and S.A. Changnon Jr., 1992. How Agribusiness Uses Climate Predictions: Implications for Climate Research and Provision of Predictions. *Bull. Amer. Meteorol. Soc.*, **73**, 1999-2009.

Sperber, K.R., C. Brankovic, M. Deque, C.S. Frederiksen, R. Graham, A. Kitoh, C. Kobayashi, T. Palmer, K. Puri, W. Tennant and E. Volodin, 2001. Dynamical Seasonal Predictability of the Asian Summer Monsoon. *Mon. Wea. Rev.*, **129**, 2226-2248.

Staley, D.O., 1991. Baroclinic Instability and Isentropic Slope. *J. Atmos. Sci.*, **48**, 1133-1140.

Streten, N.A. and D.J. Pike, 1980. Indices of the mean monthly circulation over the Southern Hemisphere during FGGE. *Aust. Meteorol. Mag.*, **28**, 201-216.

Sutcliffe, R.C., 1953. The Formation of New Anticyclones. *Meteorol. Mag.*, **82**, 163-175.

Sutcliffe, R.C., 1966. *Weather and Climate*. Weidenfeld and Nicolson, London, 206 pp.

Taljaard, J.J., 1986. Change of rainfall distribution and circulation patterns over South Africa in summer. *J. Climatol.*, **6**, 579-592.

Taljaard, J.J., 1989. Climate and circulation anomalies in the South African region during the dry summer of 1982/3. *Tech. Paper No. 21*, Weather Bureau, Pretoria, 45 pp.

Taljaard, J.J. and P.C.L. Steyn, 1991. Relationships between atmospheric circulation and rainfall in the South African region. *Tech. Paper No. 24*, Weather Bureau, Pretoria, 62 pp.

Taljaard, J.J., 1996. Atmospheric circulation systems, synoptic climatology and weather phenomena of South Africa. Part 6: Rainfall in South Africa. *Tech. Paper No. 32*, Weather Bureau, Pretoria, p51-54.

Tennant, W.J., 1999. Numerical forecasting of monthly climate over South Africa, *Int. J. Climatol.*, **19**, 1319-1336.

Tennant, W.J., 2001. Evolutionary Associations between Rainfall and the General Circulation in Southern Africa. *Paper presented at SASAS conference, 6-7 September 2001, Cape Town.*

Tennant, W.J. and B.C. Hewitson, 2002. Intra-Seasonal Rainfall Characteristics and their Importance to the Seasonal Prediction Problem. *Accepted for publication in the Int. J. Climatol.*

Todd, M. and R. Washington, 1999. Circulation anomalies associated with tropical-temperate troughs in southern Africa and the south west Indian Ocean. *Climate Dynamics*, **15**, 937-951.

Trenberth, K.E., 1981. Observed Southern Hemisphere Eddy Statistics at 500 mb: Frequency and Spatial Dependence, *J. Atmos. Sci.*, **38**, 2585-2605.

Trenberth, K.E., 1991. Climate Diagnostics from Global Analyses: Conservation of Mass in ECMWF Analyses. *J. Climate*, **4**, 707-722.

Tyson, P.D., 1986: *Climatic Change and Variability in Southern Africa.* Oxford University Press, 220 pp.

Tyson, P.D. and R.A. Preston-Whyte, 2000. *The Weather and Climate of Southern Africa.* Oxford Univ. Press, Cape Town, 396 pp.

Ulbrich, U. and P. Speth, 1991. The Global Energy Cycle of Stationary and Transient Atmospheric Waves: Results from ECMWF Analyses. *Meteorol. Atmos. Phys.*, **45**, 125-138.

Vincent, D.G., A. Fink, J.M. Schrage and P. Speth, 1998. High- and Low-Frequency Intraseasonal Variance of OLR on Annual and ENSO Timescales. *J. Climate*, **11**, 968-986.

Vogel, C., 2000. Usable Science: An Assessment of Long-Term Seasonal Forecasts Amongst Farmers in Rural Areas of South Africa. *S. Afr. Geogr. J.*, **82**, 107-116.

Wallace, J.M. and P. Hobbs, 1977. *Atmospheric Science: An Introductory Survey.* Academic Press, San Diego, 467 pp.

Ward J.H., 1963. Hierarchical grouping to optimize an objective function. *J. Amer. Stat. Assoc.*, **58**, 236-244.

Watanabe, M. and M. Kimoto, 1999. Tropical-extratropical connection in the Atlantic atmosphere-ocean variability. *Geophys. Res. Lett.*, **26**, 2247-2250.

Wiin-Nielsen, A., 1962. On Transformation of Kinetic Energy between the Vertical Shear Flow and the Vertical Mean Flow in the Atmosphere. *Mon. Wea. Rev.*, **90**, 311-323

Xie, P. and P.A. Arkin, 1996. Analyses of Global Monthly Precipitation Using Gauge Observations, Satellite Estimates, and Numerical Model Predictions. *J. Climate*, **9**, 840 - 858.

Yanai, M. and T. Tomita, 1998. Seasonal and Interannual Variability of Atmospheric Heat Sources and Moisture Sinks as Determined from NCEP-NCAR Reanalysis. *J. Climate*, **11**, 463-482.

Yarnal, B., 1993. *Synoptic climatology in environmental analysis : a primer.* Belhaven Press, London, 195 pp.

Zheng, X. and E.A.B. Eltahir, 1998. The Role of Vegetation in the Dynamics of West African Monsoons. *J. Climate*, **11**, 2078-2096.

Zurbenko, I., P.S. Porter, S.T. Rao, J.Y. Ku, R. Gui and R.E. Eskridge, 1996. Detecting Discontinuities in Time Series of Upper-Air Data: Development and Demonstration of an Adaptive Filter Technique. *J. Climate*, **9**, 3548-3560.